

Fakultät Mathematik und Naturwissenschaften
der Technische Universität Dresden



Networks of delay-coupled delay oscillators

Dissertation

zur Erlangung des akademischen Grades

Doctor rerum naturalium
(Dr. rer. nat.)

vorgelegt von

Johannes Michael Höfener

geboren am 5. April 1982 in Wuppertal

Max-Planck-Institut für
Physik komplexer Systeme

Dresden, 2012

Abstract

The analysis of time-delayed dynamics on networks may help to understand many systems from physics, biology, and engineering, such as coupled laser arrays, gene-regulatory networks and complex ecosystems. Beside the complexity due to the network structure, the analysis is further complicated by the presence of the delays.

Delay systems are in general infinite dimensional and thus can display complex dynamics as oscillations and chaos. The mathematical difficulties related to the delays hinders the analysis of delay networks. Thus, little is known yet about basic relations between network structure and delay dynamics.

It has been shown that networks without delays can be studied efficiently with the generalized modeling approach, which analyzes the stability of an assumed steady state by a direct parametrization of the Jacobian matrix. In this thesis, I demonstrate the extension of the generalized modeling approach to delay networks and analyze networks of delay-coupled delay oscillators, with delayed auto-catalytic growth on the nodes and delayed transport between nodes.

For degree-homogeneous networks (DHONs), in which each node has the same number of links, the bifurcation lines that border the stable areas can be calculated analytically, where the topology of the network is described only by the eigenvalues of the adjacency matrix. For undirected networks, the stability pattern in the parameter space of growth and transport delay is governed by two periodic sets of tongues of instability, which depend on the largest positive and the smallest negative eigenvalue. The direct relation between the eigenvalue and the bifurcation lines allows us to predict stability patterns for networks with certain topological properties. Thus, bipartite networks display a characteristic periodicity of tongues.

In order to analyze the stability of degree-heterogeneous networks (DHENs), I apply a numerical sampling method based on Cauchy's Argument Principle. The stability patterns of these networks resembles the pattern of DHONs, which is governed by the two periodic sets. For networks with sufficiently many links, one set disappears, and the stability of DHENs can be approximates by the stability of a fully-connected network with the same average degree. However, random DHENs tend to be more stable than DHONs, and DHENs with a broad degree-distribution tend to be more stable than DHENs with a narrow distribution. Thus, such networks are more likely to give rise to amplitude death, i.e. the stabilization of an unstable steady state through diffusive coupling.

The stability pattern of DHENs can be qualitatively different than the pattern in DHONs. However, for small growth delays, close to the critical delay of the single node system, the bifurcation lines of all DHENs with the same average degree coincide. This, is particularly interesting, because there the stability depends on a global property of the network, which suggests a diverging interaction length.

In summary, the extension of generalized modeling to time-delay networks reveals basic relations between the delay dynamics and the topology. The generality of our model should allow to apply these results to a large class of real-world systems.

Nomenclature

ϕ_r An integer subscript r of an angle ϕ is defined as $\phi_r = \phi + 2\pi r$

$\overline{\phi_r}$ The overline operator combined with an integer subscript r is defined as $\overline{\phi_r} = 2\pi(r + 1) - \phi$

J^d Diagonal element of the Jacobian \mathbf{J}

J^o Off-diagonal element of the Jacobian \mathbf{J}

DHEN Degree-HEterogeneous Network

DHON Degree-HOMogeneous Network

EVP EigenValues with Positive real part

Contents

Nomenclature	v
1 Introduction	1
2 Introduction to time-delayed network dynamics	5
2.1 Introduction to dynamical systems	5
2.2 Delay differential equations	8
2.3 The Lambert W -function	9
2.4 Introduction to network science	11
2.5 Time-delays in network	13
3 The generalized flow model	19
3.1 Parametrization of the Jacobian	20
3.2 Comparison with other models	21
3.3 The single node	22
3.4 Networks without delays	24
3.5 A sufficient condition for instability	24
3.6 A sufficient condition for stability	25
3.7 Summary	27
4 Degree-homogeneous networks	29
4.1 Bifurcation lines in the delay space: Tongues of instability	30
4.1.1 Separated and merged tongues	33
4.1.2 Periodicity of the tongues	34
4.1.3 Tip positions of the tongues	37
4.1.4 Slopes of the tongue borders for large delays	38
4.1.5 Summary	41
4.2 Tongues and topology	42
4.2.1 The fully-connected network	42
4.2.2 General properties of undirected networks	44
4.2.3 Symmetries in spectra and delay space	46
4.3 Dynamical states inside tongues of instability	47
4.3.1 Synchronous dynamics	48
4.3.2 Multistability inside overlapping tongues	51
4.4 Stabilizing and destabilizing coupling	53

4.5	Bifurcation lines in the coupling space: Amplitude death	56
4.5.1	The limit of large coupling strength	64
4.5.2	Amplitude death in networks	64
4.5.3	Amplitude death for small coupling delays	69
4.6	Summary	71
5	Degree-heterogeneous networks	73
5.1	The numerical method	73
5.1.1	Comparison with analytical results	76
5.1.2	Test of the sufficient stability condition	78
5.1.3	Conclusions	81
5.2	Stability of ensembles of random networks	81
5.2.1	Stability transitions along sections through delay-plane	84
5.2.2	Influence of the degree distribution	88
5.3	Particularly stable and unstable topologies	90
5.3.1	Unstable networks above the bottom bifurcation line	98
5.3.2	Topology-independence of the bottom stability border	99
5.4	Amplitude death for small coupling delays	102
5.5	Summary	103
6	Discussion and Outlook	105
	Bibliography	109

1 Introduction

Complex systems can often be decomposed into similar interacting subsystems, which can be represented as nodes of a network. The nodes are connected by links, which symbolize the interaction between the subsystems. For instance, the nodes of the Internet are computers and routers, and the links describe the connections between them.

The purpose of a network is often related to dynamics on the network. For instance, the purpose of the Internet is the dynamical process of information transfer. For most of these networks, the analysis of the dynamics is essential for understanding and optimizing the function. Insights into the network dynamics can also help to prevent undesired processes such as the spreading of computer viruses.

Describing complex systems as networks allows to investigate the relation between the dynamics and the topology of the network. As an example we may consider the spreading of computer viruses on the Internet. If computers are connected randomly, the probability that an infected computer infects a neighbor needs to exceed a certain threshold to allow a virus to persist. However, in certain so-called scale-free networks, viruses can persist even if this probability is infinitely small [1]. This result also demonstrates the relevance of network science in the field of epidemiology [2].

In ecology, network models are used to study the population dynamics in complex ecosystems [3]. The networks visualize the interactions between populations. The diversity of these interactions can range from antagonistic to mutualistic. For instance, these networks may describe the interaction between herbivores and parasites as well as the interaction between pollinators and plants. Interaction networks of predators and prey, where predators themselves can be prey of other predators are called food-webs. A central question arising in ecology and in particular in food webs concerns the stability and the robustness of large ecosystems [4].

Other examples for dynamical processes on networks in biology are the spiking in neuronal networks, the activation and inhibition of genes in gene regulatory networks, the conversion of metabolites in metabolic networks, and the transmission of signal molecules of a signal transduction network [5]. Components of different networks interact with each other creating a network of networks that allows the cell to adapt to various environmental conditions. The processing of input information needed to adapt to a changing environment can be realized by appropriate network structures. Thus, recently synthetic genetic networks have been created that implement processing units such as toggle-switches [6] and basic logical operations [7].

The presented examples of dynamical processes on networks demonstrate the importance of analyzing the relations between topology and dynamics. Knowledge

about these relations may be used to maintain biodiversity, to prevent the spreading of diseases, and to understand the function of the complex networks in cells.

Beside empirical observations, dynamics on networks can be studied using mathematical models. As a first step to model a dynamical system, it is necessary to determine the structure of the system. That means, we have to identify all subsystems and their interactions that have a relevant impact on the dynamics. The information is captured by the network topology, which constitutes a structural model. Additionally, we need to model the dynamical processes on the nodes and the dynamical processes that mediate the interaction between nodes.

Usually, the dynamical processes are modeled by specific functions, which may include some parameters to fit the model to observations. This yields a set of ordinary differential equations (ODEs), which can be studied with the tools of dynamical systems theory. A central question in the analysis of dynamical systems deals with the stability of so-called steady states. Stable steady states do not change with time even if they are subject to small perturbations. If no stable steady states exist, the system won't rest but will display non-stationary dynamics such as oscillations and chaos. The stability of a steady state can be analyzed through the Jacobian matrix, which constitutes a local linear model.

Although the specific functions that model the dynamical processes can be modified through parameters, they are generally restricted to specific functional forms. Hence, the definition of a specific model already involves implicit assumptions. Even if the structure of a real-world system is known well, information about the dynamical processes is often hard to obtain. This is particularly true for systems from biology and ecology [8, 9]. Thus, it is possible that the implicit assumptions made by choosing specific functions to model the dynamical processes are invalid, so that the dynamics of the specific model can be qualitatively different from the dynamics of the real-world system. Hence, such unjustified implicit assumptions should be avoided if possible.

In generalized modeling, we do not restrict the dynamical processes to specific functions. Instead, we model the system by a direct parametrization of the Jacobian. This helps to avoid unnecessary assumptions because the Jacobian only contains local information of the system close to a steady state. Nonetheless, the parametrized Jacobian allows us to study the stability of steady states. The same Jacobian can describe steady states in many different specific models. Therefore, the parametrized Jacobian constitutes a more general model than the conventional. Generalized modeling already found applications in various disciplines, such as ecology [10–18], socio-economics [9] and cell biology, where this approach has been used to study cell signaling pathways [19], bone remodeling [20], and metabolic [8, 21, 22] and gene regulatory networks [23].

Beside the restriction on specific function, the generalized modeling approach also avoids the calculation of the steady state. This calculation can be computationally demanding, so that it might set limits to the investigation of large systems. But often the steady state itself is of little interest, so that the generalized modeling

approach can be used to study large systems with high numerical efficiency. The high efficiency also allows to study a large number of different networks so that the influence of topological properties can be studied statistically. In this context, the approach has successfully been used to investigate stability properties of food webs [15].

No matter if conventional or generalized modeling is used, all models simplify the real-world system they should describe. For instance, when studying the dynamics of gene-regulatory networks, the details of the complex processes that result in the activation and inhibition of genes are usually ignored. The time-delay caused by these processes, such as transcription, translation, and transport, can have an important influence on the systems dynamics [24]. When studying population dynamics within ecological models, delays arise naturally by processes such as growth, maturation, and regeneration. Hence, changes in the environment may have delayed effects on the population dynamics. These, examples demonstrate that delays arise frequently in models of complex systems. Therefore, the analysis of delays in networks may be crucial to understand the dynamics in many of these systems.

Mathematical models with time-delays have a long tradition in ecology going back to Volterra at around 1930 [25]. Later models incorporated delays in various intra- or interspecies interactions [26]. These early results suggested that large delays are in general destabilizing. More recently, it was shown that the effect of delays is more complex and that delays are not necessarily destabilizing [27]. In biological network models, delays have been introduced, for instance, into models of neuronal networks [28] and gene-regulatory networks [29]. However, usually delays have been introduced in specific models with only a small number of nodes.

In this thesis, I demonstrate the extension of generalized modeling to time-delay networks. I use this approach to investigate networks of delay-coupled delay oscillators. After I identify the parameter space for which the stability is topology independent, I analyze the topology dependence of the stability.

The systems display complicated stability patterns in the delay-space. For degree-homogeneous networks (DHONs), I provide an analytical description of the bifurcation lines that constitute the stability borders. For these networks, the topology dependence of the bifurcation lines is given by the eigenvalues of the networks adjacency matrix. Therewith, we find simple relations between symmetries of the topology, the stability pattern and the dynamical states. The more general class of degree-heterogeneous networks (DHENs) is analyzed with a numerical sampling method.

We find that major results for the DHONs can be extended to the DHENs. However, in general DHENs tend to be more stable than DHONs. Nonetheless, the stability borders of large random networks with sufficiently many links can be approximated by the bifurcation lines of a fully-connected network with the same mean degree. Even in small networks, we find that the topology dependence of the stability border for small coupling delays reduces to a dependence on the average degree. Above this stability border the identical oscillators silence each other to

death. This effect is called *amplitude death* and is commonly studied in so-called Stuart-Landau oscillators. For identical Stuart-Landau oscillators, amplitude death only occurs for finite coupling strength and coupling delays [30]. In contrast to this model, we find a simple relation between the critical delay and the coupling strength that shows that amplitude death occurs for infinitely small coupling delays as the coupling strength becomes infinitely large.

The results of this thesis relate dynamical properties of the delay-coupled delay oscillators to the topology of the network. Because of the generality of this model, these results might find applications in many real-world systems. Some results of this thesis have been published in Ref. [31].

This thesis is structured as follows: In chapter 2, I briefly discuss present results on time-delay networks. For this purpose, I first give a short introduction to dynamical systems theory, delay-differential equations and network science.

In chapter 3, I extend the generalized modeling approach to delay networks by applying it to a network with time-delays in the node dynamics and in the couplings between nodes. Further, I explore the parameter spaces in which the stability of these networks is governed by the single node system, so that the stability is topology independent. For instance, this is true for all systems with vanishing delays. Additionally, I provide sufficient conditions for stability and instability for arbitrary network topologies.

Chapter 4 deals with the analysis of degree-homogeneous networks. For these networks, I derive analytic expressions for the bifurcation lines in the parameter spaces of internal and coupling delay, and in the space of coupling strength and coupling delay. The bifurcation lines in the delay space are shaped like tongues and are periodic in the delays. We characterize these tongues by the tip positions and their asymptotic behavior for large delays. This facilitates the study of the parameter dependence of the bifurcation lines, which is discussed for a fully-connected network. By investigating small symmetric networks, we find a relation between certain topological properties and symmetries in the stability pattern. The different tongues in these patterns can be related to different synchronous dynamics. The calculation of the bifurcation lines in the coupling space allows us to study the effect of amplitude death.

In chapter 5, we investigate degree-heterogeneous networks. For this purpose, we introduce a numerical sampling method for the stability analysis of ensembles of random networks. This method is tested by comparing the results with the bifurcation lines for the DHONs. Further, we use it to verify the sufficient condition for instability from chapter 3, which has not been rigorously proved. By generating ensembles of random networks with the same average degree, we compare the results for DHENs to the results for DHONs. Additionally, we investigate the influence of the topology by comparing the stability patterns of different types of large random networks and by identifying particularly stable and unstable topologies.

In the final chapter, I summarize and discuss the main results and relate them to the findings made in other delay networks.

2 Introduction to time-delayed network dynamics

This chapter provides an overview of present results on time-delay networks. For this purpose, I first give a short introduction to dynamic systems theory, which is loosely based on the text book “Elements of Applied Bifurcation Theory” by Kuznetsov [32]. Further, I introduce some basic concepts of network science. This introduction is mostly based on the review “The structure and Function of Complex Networks” by M. Newman [33] and on the book “Modern Graph Theory” by B. Bollobás [34].

2.1 Introduction to dynamical systems

A Dynamical systems is the mathematical representation of a deterministic process [32]. These are processes in which the time-evolution of the system state is determined by certain rules. Thus, knowledge about the current state allows to predict future states of the system.

The state of the system is described by a set of state variables also denoted as state vector. The state variables need to contain enough information to predict the evolution of the variables. For instance, when describing the oscillation of a pendulum, it is insufficient to only consider the position of the pendulum, because the future position also depends on the velocity [32].

A dynamical system may describe the evolution of the state variables in discrete or continuous time [32]. For discrete time steps, we denote the state vector for each time-point t by \mathbf{x}_t . The time evolution is often given by a function or map \mathbf{f} that maps the state vector \mathbf{x}_t on the state vector \mathbf{x}_{t+1} , so that

$$\mathbf{x}_{t+1} = \mathbf{f}(\mathbf{x}_t). \quad (2.1)$$

In time-continuous systems, the evolution of the state variables is most commonly given by a set of ordinary differential equations, which often express the velocities $\dot{\mathbf{x}}$ of the state variables in dependence of the state variables, so that

$$\dot{\mathbf{x}} = \frac{d\mathbf{x}}{dt} = \mathbf{f}(\mathbf{x}), \quad (2.2)$$

where $\frac{d}{dt}$ is the time-derivative operator.

The analysis of dynamical systems usually begins with the identification of the so-called steady states, which do not change with time. Thus, for discrete time, steady

states satisfy $\mathbf{x}_t = \mathbf{x}_{t+1} = \mathbf{f}(\mathbf{x}_t)$, and for continuous time, they satisfy $\dot{\mathbf{x}} = \mathbf{f}(\mathbf{x}) = 0$ for all times t . These states are also called fix points or equilibria [32].

Real systems are always affected by fluctuation, which perturb the state variables. Thus, a system is never exactly at a steady state and the time-evolution at a steady state is determined by the dynamics in the vicinity of the steady state. The local stability describes the response of the system close to the steady state. A steady state is asymptotically stable if all states in a sufficiently small neighborhood of the steady state evolve to the steady state as time goes to infinity [32]. If the steady state is unstable, small perturbations from the steady state grow and the system leaves the steady state.

Considering a system of N ordinary differential equations, we can determine the dynamics close to a steady state \mathbf{x}^* by a linearization of the ODEs, which gives

$$\dot{\mathbf{y}} = \mathbf{J}\mathbf{y} \quad (2.3)$$

with $\mathbf{y} = \mathbf{x} - \mathbf{x}^*$ and the Jacobian matrix

$$J_{ij} = \frac{\partial \dot{x}_i}{\partial x_j}, \quad (2.4)$$

with $i, j = 1 \dots N$. By rewriting Eq. (2.3) in the basis of the eigenvectors \mathbf{v}_i of the Jacobian \mathbf{J} , we obtain the N independent differential equations

$$\dot{c}_i = \lambda_i c_i, \quad (2.5)$$

with $c_i = \mathbf{y} \cdot \mathbf{v}_i$ and the eigenvalue λ_i of \mathbf{J} that corresponds to the eigenvector \mathbf{v}_i [35]. For given initial conditions $c_i^0 = c_i(t=0)$, Eq. (2.5) has a unique solutions

$$c_i(t) = c_i^0 e^{\lambda_i t}. \quad (2.6)$$

Hence, if the eigenvalue λ_i has a positive real-part, perturbations along the eigenvector \mathbf{v}_i grow exponentially. If the eigenvalue has a negative real-part, the perturbations decline exponentially.

The eigenvectors of the Jacobian can be obtained from the eigenvalue equation

$$\lambda \mathbf{v} = \mathbf{J}\mathbf{v}. \quad (2.7)$$

Non-trivial solutions for \mathbf{v} can only be found if λ is a root of the characteristic polynomial

$$P(\lambda) = \det(\lambda \mathbf{I} - \mathbf{J}). \quad (2.8)$$

These roots are the eigenvalues λ_i of the Jacobian. Therewith, the Jacobian can be factorized as

$$P(\lambda) = (\lambda - \lambda_1)(\lambda - \lambda_2) \dots (\lambda - \lambda_N). \quad (2.9)$$

In this thesis, we only consider characteristic polynomials with real coefficients. In this case, the eigenvalues need to be either real or they appear in pairs of complex conjugated numbers [36].

If eigenvalues with zero real-part exist, the system dynamics close to the steady state depends on higher order terms. Such steady state are called *non-hyperbolic*. If the real parts of all eigenvalues are either positive or negative the steady state is *hyperbolic* [32].

By calculating the eigenvalues of the Jacobian, we can determine the stability of the steady state. If the Jacobian has eigenvalues with positive real-part, the according perturbations grow exponentially. If all eigenvalues have a negative real-part, all perturbations decline and the system approaches the steady state [37]. Hence, the stability is determined by the *leading eigenvalue*, which has the largest real-part. If it's real-part is positive, the system is unstable. If the real-part is negative, the system is stable.

Bifurcations

Now, we consider a parameter dependent dynamical system such as an ordinary differential equation

$$\dot{\mathbf{x}} = \mathbf{f}(\mathbf{x}, \mathbf{p}), \quad (2.10)$$

that depend on a set of parameter $\mathbf{p} \in \mathbb{R}^m$. Changing the parameters can change the topological type of the system [32], giving rise to qualitatively different dynamics. The points in parameter space, where such qualitative changes occur are called bifurcations.

Bifurcations are often classified into *local* and *global* bifurcations. In this thesis, we only consider local bifurcations that can be analyzed by studying the system close to a steady state [37].

Bifurcations are also classified by their *codimension*, which is “the difference between the parameter space and the dimension of the corresponding bifurcation boundary” [32]. Thus, the border of a codimension 2 bifurcation is a point in a three dimensional parameter space and a line in a four dimensional space. A more practical definition states that the codimension is “the smallest dimension of a parameter space which contains the bifurcation in a persistent way” [37]. Thus, a system can be tuned to a codimension 1 bifurcation by changing a single parameter. In order to tune a system to a codimension 2 bifurcation, two parameters need to be changed.

Two hyperbolic steady states are locally topological equivalent if and only if both steady states have the same number of eigenvalues with positive and the same number of eigenvalues with negative real-part [32]. Hence, a steady state undergoes a local bifurcation if eigenvalues cross the imaginary axis. There are only two generic types of codimension 1 bifurcations. Either a single real eigenvalue or a pair of complex conjugated eigenvalues cross the imaginary axis. The first type is called saddle-node or fold bifurcation, the second type is called Hopf bifurcation. At a saddle node bifurcation a stable and an unstable steady state collide and disappear. At a Hopf bifurcation a limit cycle arises around the steady state. Thus, a Hopf bifurcation can give rise to oscillatory dynamics.

2.2 Delay differential equations

Now, we consider an ordinary differential equation in which the derivatives not only depend on the current system state but also on the system state at a time τ in the past. Thus, we obtain a delay differential equation (DDE)

$$\dot{\mathbf{x}} = \mathbf{f}(\mathbf{x}, \mathbf{x}^\tau), \quad (2.11)$$

with $\mathbf{x}^\tau(t) = \mathbf{x}(t - \tau)$. The delay turns the ODE into a functional differential equation, because the future evolution of the system state depends on the time-dependent function of the system state $\mathbf{x}(t)$ [36]. In order to calculate a future state of the system, we need to specify initial conditions that provide the function values $\mathbf{x}(t)$ for all times between $-\tau$ and 0. Thus, the delay system is infinite dimensional, because we have to provide an infinite set of numbers to specify the initial conditions [38]. As infinite dimensional systems, DDEs can show complex high dimensional dynamics such as oscillations, multistability and chaos [39–44]. Further, it was observed that the dimension of chaotic attractors of DDEs are proportional to the delay [38, 45].

Similarly to ODEs, we analyze the system by investigating the stability of steady states. A steady state \mathbf{x}^* is not affected by the delays because $\mathbf{x}^*(t - \tau) = \mathbf{x}^*(t)$. Therefore, we can replace the delayed variable in the DDE by the undelayed variable, so that we obtain the undelayed ODE. A linearization of Eq. (2.11) results in

$$\dot{\mathbf{y}}(t) = \mathbf{A}\mathbf{y}(t) + \mathbf{B}\mathbf{y}(t - \tau), \quad (2.12)$$

with $A = \frac{\partial f}{\partial \mathbf{x}}$ and $B = \frac{\partial f}{\partial \mathbf{x}^\tau}$. Considering that the linear ODE system has exponential solutions, we assume that the linear DDE has exponential solutions as well [36]. Inserting the ansatz $\mathbf{y}(t) = \mathbf{v} \exp(\lambda t)$ into Eq. (2.12) provides $P(\lambda) = 0$ with the characteristic polynomial

$$P(\lambda) = \det(\lambda - \mathbf{J}(\lambda)), \quad (2.13)$$

and

$$\mathbf{J}(\lambda) = \mathbf{A} + \mathbf{B} \exp(-\lambda \tau), \quad (2.14)$$

which we denote as the Jacobian of the delay system.

It can be shown that the steady state is asymptotically stable if all roots of $P(\lambda)$ have negative real parts and that the steady state is asymptotically unstable if at least one root has a positive real part [46].

Without time-delays the eigenvalues λ of the Jacobian can be calculated straightforwardly by standard algorithms from linear algebra. But with delays, the Jacobian itself depends on the eigenvalues of the Jacobian. Additionally, calculating the eigenvalues by finding the roots of the characteristic polynomial is more complicated because the delays turn the characteristic polynomial into a transcendental equations with infinitely many roots. However, the number of roots with positive real-part is still finite.

Calculation and continuation of eigenvalues

In order to calculate an eigenvalue of the system, we can use the following procedure. First, we calculate the Jacobian $\mathbf{J}(\lambda^{\text{in}})$, with an initial guess for λ^{in} . Then, we use standard methods of linear algebra to calculate the eigenvalue λ^{out} of the Jacobian. In general λ^{in} and λ^{out} differ, but by applying minimization algorithms to the difference $|\lambda^{\text{in}} - \lambda^{\text{out}}|$ a valid eigenvalue can be found.

This method can be used to obtain a continuation of an eigenvalue through parameter space. But we cannot use this method to show that a system is stable, because the system has an infinite number of eigenvalues, so that we cannot be sure that the computed eigenvalue is the largest one.

2.3 The Lambert W -function

For some simple delay systems, it is possible to represent the eigenvalues by the Lambert W function [47], which is defined to satisfy the equation

$$W(z)e^{W(z)} = z. \quad (2.15)$$

Let's consider a scalar system of the type of Eq. (2.12). The linearization provides the equation

$$\dot{y}(t) = Ay(t) + By(t - \tau), \quad (2.16)$$

with scalar coefficients A and B . The roots of the characteristic polynomial are given by

$$\lambda = A + Be^{-\lambda\tau}. \quad (2.17)$$

By subtracting A and multiplying $\exp(\lambda - A)\tau$ on both sides of Eq. (2.17) [48], we obtain

$$(\lambda - A)e^{(\lambda - A)\tau} = Be^{-A\tau}. \quad (2.18)$$

A comparison with the definition of the Lambert function from Eq. (2.15) yields

$$\lambda = A + \frac{1}{\tau}W(B\tau e^{-A\tau}). \quad (2.19)$$

The Lambert function has infinitely many branches $W_n(z)$ indexed by the integer n , with $n = 0, \pm 1, \pm 2, \dots$, which provide the infinitely many solutions of Eq. (2.17) (Fig. 2.1(a,b)).

For real-valued $z \in [-1/e, \infty)$ the principle branch of the Lambert function $W_0(z)$ is real and increasing. For $z \in [-1/e, 0)$, the branch $W_{-1}(z)$ is real as well [47]. If z decreases from 0 to $-1/e$, $W_{-1}(z)$ increases from $-\infty$ to -1 , where it collides with $W_0(z)$ (Fig. 2.1(c)). For $z < -1/e$, the two branches are complex conjugates. This explains the different indexing in the figures 2.1(b) and (c).

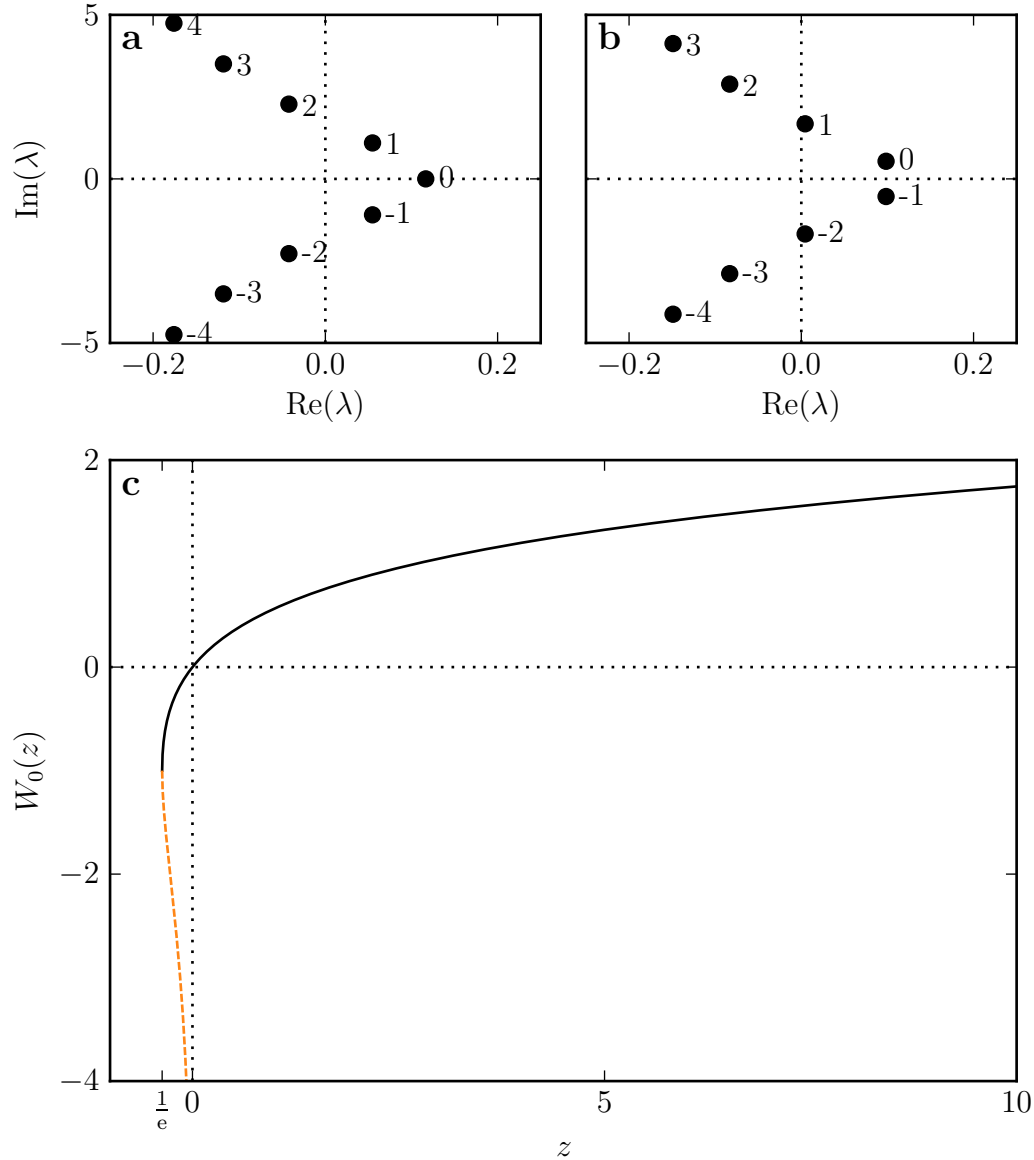


Figure 2.1: The Lambert W function and the solutions of Eq. (2.17). (a,b) Solutions λ of Eq. (2.17) with $B = 2$ (a) and $B = -2$ (b). The solutions can be expressed with the Lambert function W (Eq. (2.19)), which has infinitely many branches n . The other parameters are $A = -1$ and $\tau = 5$. Thus, the argument of the Lambert function is larger 0 for $B = 2$ (a) and smaller $-1/e$ for $B = -2$ (b). (c) The principle branch, $n = 0$, (solid black line) and the branch $n = -1$ (dashed orange line) of the Lambert function $W(z)$ are real for $z \in [-1/e, \infty)$ and $z \in [-1/e, 0]$, respectively. For $z < -1/e$, the two branches are complex conjugates. Note that the principle branch is increasing for real $z > -1/e$.

2.4 Introduction to network science

A network is defined by a set of nodes and a set of links. A link is defined by a pair of nodes, which are connected by the link. In graph theory, networks are usually denoted as graphs, nodes as vertices and links as edges [33]. This thesis focuses on undirected networks, in which all links are bidirectional. The number of links connected to a node i is denoted as the degree d_i of the node. Thus, the average degree of an undirected network is given by $\langle d \rangle = 2K/N$. Further, we denote the number of nodes in a networks with N and the number of links with K . Even though we focus on undirected networks, most of our results are also valid for directed networks for which the number of incoming and outgoing links is identical for each node.

We only consider connected networks, i.e. each pair of nodes is connected by a path through the network. In order to be connected, an undirected network needs at least $N - 1$ links. Such networks are denoted as trees and do not contain any loops, because a loop would allow to remove a link without disconnecting a node. All trees are bipartite. This means that all nodes can be assigned one of two colors so that links only exist between nodes of different colors [33].

The network structure is often represented by the adjacency matrix \mathbf{A} , which is a $N \times N$ matrix with elements A_{ij} . If the network contains a directed link from node j to node i , the element $A_{ij} = 1$, otherwise $A_{ij} = 0$. The eigenvalues of the adjacency matrix are called the spectrum of the network [34]. For undirected networks, the adjacency matrix is symmetric and the eigenvalues are purely real.

The following list reviews some basic properties of the spectra of certain networks which are used throughout this thesis [34]:

- For degree homogeneous networks, in which all nodes have the same degree d , the largest eigenvalue is d and the corresponding eigenvector is $(1, 1, \dots, 1)$.
- Bipartite networks have a symmetric spectra, i.e. for each non-zero eigenvalue λ there exists an eigenvalue $-\lambda$.
- If H is a subgraph of G , then $\lambda^{\min}(G) \leq \lambda^{\min}(H) \leq \lambda^{\max}(H) \leq \lambda^{\max}(G)$, where λ^{\min} and λ^{\max} are the smallest and the largest eigenvalues of the adjacency matrix. Therewith, we can follow that the smallest eigenvalue of any connected node needs to be smaller or equal to -1 , because every connected network contains the subgraph consisting of only two connected nodes, which has the eigenvalue -1 . Hence, the fully-connected network, which has one eigenvalue $N - 1$ and $N - 1$ eigenvalues -1 , has the largest possible smallest eigenvalue.

Instead of the adjacency matrix, the network structure can also be described by the Laplacian matrix \mathbf{L} , which is defined as $\mathbf{L} = \mathbf{D} - \mathbf{A}$, where \mathbf{D} is a diagonal matrix with elements $D_{ii} = d_i$. The Laplacian is often normalized for instance by dividing each element L_{ij} by $\sqrt{d_i d_j}$ [34] or by d_i [49, 50]. Thus, the diagonal elements of the normalized Laplacian matrices are 1. Both, normalized and unnormalized Laplacian,

have an eigenvalue 0, which belongs to the eigenvector $(1, 1, \dots, 1)$, whereas all other eigenvalues are larger or equal to 0 [34, 49].

Random networks

When investigating the influence of the topology on the dynamics on a network, the interest is usually focused on classes of networks that share certain properties rather than studying individual network realizations. However, numerical methods often requires the construction of an actual network. Therefore, it is necessary to construct random networks with desired properties such as networks with a fixed number of links or a certain degree-distribution.

Probably the simplest way of constructing random networks is the Erdős-Rényi model [51]: In a network of N nodes, K out of the $N(N - 1)/2$ possible links are chosen randomly. For this purpose, we start from a network without links and randomly draw two nodes to be connected. If the same node is drawn twice or if two nodes are already connected, another pair of nodes is drawn. This procedure is repeated until K links are added. In order to increase the numerical efficiency for $K > N(N - 1)/4$, we start from a fully-connected network and use the same procedure to delete $N(N - 1)/2 - K$ links.

The node degree of Erdős-Rényi networks is distributed according to a binomial distribution, which approaches a Poisson distribution for large N . However, many real-world networks have been found to follow a much broader distribution, which resemble the so-called scale-free distribution. In scale-free networks, the probability to find a node with degree d is proportional to $d^{-\gamma}$ and hence, the majority of nodes have only a few neighbors, whereas a few nodes have a large number of neighbors [33, 52].

In order to generate random scale-free networks, we use the Barábasi-Albert model [53]: Starting from m disconnected nodes, we add one node after another connecting each node to m nodes already present. The probability that a present node i is connected to the added node j is given by $d_i / \sum_j d_j$. Hence, the probability to obtain a new connection is approximately proportional to the degree of the node.

Whereas the networks that are analyzed in this thesis are too small to be considered scale-free, we use the Barábasi-Albert model to generate networks with a broad degree-distribution. Thus, by comparing the dynamics of Erdős-Rényi and Barábasi-Albert networks, we can study the influence of the degree distribution.

Collective network dynamics

The interaction between nodes can give rise to phenomena of collective dynamics, such as synchronization and amplitude death. Perhaps the most studied phenomena is the *synchronization* of coupled chaotic or oscillating systems. Already in the 17th century, Christiaan Huygens reported that two clock pendulums which he mounted to the same frame swung with the same frequency at a phase difference of 180° . Further, he reported that these anti-phase oscillations are restored after perturbing

the pendulums [54, 55]. Synchronization in networks might play an important role for neuronal communication [56] and the coordination of oscillating dynamics on genetic networks in interacting cells [57]. For instance, synchronization has been found in the transcription of genes across hundreds of neurons, governing the circadian rhythm in animals [58]. The circadian rhythm has a period of around 24 hours and can thus help the organism to adjust to the daily variations of sunlight. In ecological systems, the synchronization of oscillating population dynamics at different locations may result in simultaneous extinction events at distant habitats, which might dramatically increase the risk for a species to go extinct [59].

The terms *amplitude death* and *oscillator death*, describe the phenomena that the coupling of dynamical systems can quench oscillations that are present in the uncoupled systems [46]. An early report of this phenomena has been made by Lord Rayleigh in the 19th century, who observed that two organ pipes standing close to one another almost suppressed each other to silence [60]. Later amplitude death was observed in chemical oscillators [61], electronic circuits [62], thermo-optical oscillators [63], coupled lasers [64], and even in an living coupled oscillator system made of a plasmodial slime mold [65]. It has been proposed to utilize amplitude death in order to realize stabilizing feedback controls for engineering applications [66]. However, amplitude death can also be detrimental, if it suppresses oscillations that are important for the proper function of the system. In this context, it has been argued that amplitude death may be “critical for living systems, as one can easily be convinced by considering the possibility of cessation of oscillations in a group of interacting cardiac cells” [50]. These examples show that amplitude death might play an important role in many real-world systems [67].

Most mathematical models study amplitude death by investigating the conditions under which an unstable steady state is stabilized by diffusive coupling. Such studies showed that amplitude death occurs either if the frequencies of the oscillators are sufficiently disparate [68–72] or if the coupling is time-delayed [30].

2.5 Time-delays in network

The following survey of time-delayed dynamics on networks focus on communication delays, which appear in the coupling terms. Delayed self-feedback is usually considered by allowing self-loops in the network, which are realized by non-zero diagonal elements in the adjacency matrix.

The survey starts with coupled maps and continues with DDE models beginning from the famous Kuramoto model of coupled phase oscillators. The Kuramoto model is particularly suited to study synchronization but ignores the amplitude of the oscillators. In order to study amplitude death, we need to study more complex models such as the Stuart-Landau oscillator. In fact, the Kuramoto model can be derived from a system of coupled Stuart-Landau oscillators if the coupling is so weak that it does not affect the amplitude [46]. The Stuart-Landau oscillator is a two

dimensional system that can be described by a single complex state variable. Higher dimensional system, such as the three-dimensional Lorenz and Rössler oscillators, allow us to study synchronization and amplitude death in system with potentially chaotic dynamics. The delay coupling of infinite dimensional system is studied by delay models, such as the Mackey-Glass and Ikeda model.

Delay-coupled maps

In time-discrete systems, even simple models such as the logistic map [73],

$$f(x) = \rho x(1 - x), \quad (2.20)$$

can give rise to chaotic dynamics. The logistic map has been used to describe the dynamics of seasonally breeding populations with non-overlapping generations. Later, it became prominent as a prototype model displaying chaotic dynamics. In order to study delay-coupled chaotic systems, it is common to choose $\rho = 4$ and analyze models of the type of

$$x_i(t+1) = f(x_i(t)) + \frac{k}{d_i} \sum_j A_{ij} (f(x_j(t-\delta)) - f(x_i(t))), \quad (2.21)$$

where k is the coupling strength. For the sake of consistency, we denote the coupling delay by δ .

Both, synchronization and amplitude death in time-delay systems have been studied with chaotic maps. It has been shown that the stability of synchronized chaotic solutions in identical chaotic maps without time-delays depends on the eigenvalues of the coupling matrix [49] and random networks synchronize better than networks with spatial structures such as rings. These results have been extended for time-delay coupling with identical delays, and it was concluded that time-delays in general increases the synchronizability [74]. Stability conditions for a homogeneous steady state, which gives rise to amplitude death, show that the topology dependence is governed only by the largest eigenvalue of the network Laplacian [75]. Further, stabilization is not possible for bipartite networks or for networks with only even delays. Considering the bipartite networks, similar results have been found for time-continuous systems [50].

For random delays, amplitude death becomes more probable, and except for the mean degree, the topology has only a minor influence [76]. For sufficiently large globally connected networks with random delays, the stability is similar to the stability of a single map with multiple feedbacks with the same delay distribution [77]. In the same work, it has been shown that networks with only even delays do not give rise to amplitude death but stabilize a periodic orbit. Recently, conditions for amplitude death for homogeneous and distributed delays have been found, which confirmed the results for homogeneous delays from [74] and explained that for heterogeneous delays, the stability is governed by the distribution of delays, whereas the topology has a minor influence [78].

A detailed analysis of synchronization and amplitude death in dependence of the network topology and delay distribution is given in [79]. The authors of this work also analyzed the effect of self-feedbacks. The self-feedbacks was chosen to be of the same strength as the coupling to a single neighbor. Hence, it is not surprising that the influence decreases for large and highly connected networks. For small networks, the self-feedback may enhance or degrade synchronization dependent on the topology and on the delay distribution.

The Kuramoto model with delays

Synchronization in time-continuous time-delay networks is often studied using the Kuramoto model with delayed coupling,

$$\dot{\phi}_i(t) = \omega_i + \frac{k}{d_i} \sum_j A_{ij} \sin(\phi_j(t - \delta) - \phi_i(t)), \quad (2.22)$$

where each oscillator i has an own natural frequency ω_i . It has been shown that a system of two delay-coupled oscillators has multiple synchronized solutions with different common frequencies, unlike the undelayed system that has at most one solution [80]. The phase differences between the two systems are usually close to 0 or π . In a later work, multistability between synchronized and desynchronized states has been found in fully-connected networks [81]. In the desynchronized state, the phases are almost uniformly distributed, while in the synchronous state all oscillators are in phase. As for two coupled oscillators, there exist several synchronized solutions with different collective frequencies.

The stability of the desynchronized state displays a delay-periodic “resonance”-pattern in the coupling delay [82], which vanishes for heterogeneous delays [83]. Such a periodicity has been found also for the stability of in-phase, anti-phase and other out-of-phase synchronization modes in small network motifs [84]. The stability of the in-phase solution for a general coupling function $f(\phi_j(t - \delta) - \phi_i(t))$ can be determined by a simple criterion [85], which holds for all degree-homogeneous networks and is independent of the topology.

Further, works on synchronization in Kuramoto models with communication delays studied nonidentical oscillators in two-dimensional grids [86], bimodal frequency distributions, spatially non-local coupling in rings [87], and distance dependent delays [88, 89]. Recently, it has been demonstrated that for certain systems finite differential equations can be derived which describe the macroscopic evolution of these system [90]. This approach has already been applied to study the effect of heterogeneous coupling delays [83].

Delay-coupled Stuart-Landau oscillators

The first publications on delay induced amplitude death analyzed systems of globally and diffusively delay-coupled Stuart-Landau oscillators [30, 91], described by

$$\dot{z}_i(t) = (1 + i\omega_i - |z_i(t)|^2)z_i(t) + \frac{k}{d_i} \sum_j A_{ij}(z_j(t - \delta) - z_i(t)). \quad (2.23)$$

These works demonstrate that time-delays can induce amplitude death even if the frequencies of the oscillators are identical. In these systems, amplitude death occurs inside separate islands in the (k, δ) -plane. Between these islands, there are delay values for which no amplitude death can occur. Distributed delays enlarge these islands [92] and if the width of the distribution exceeds a threshold, islands merge so that amplitude death can occur for any delay value.

For ring topologies, the size of the stability islands decreases with increasing system size N and approaches the stability area of rings with even N , which is independent of the system size [93]. For a similar system, it has been shown that amplitude death is less likely for gradient instead of diffusive coupling [94].

For both topologies, the globally coupled network and the ring, there exists a maximum coupling strength for which amplitude death is possible. Partial and complete amplitude death in rings with distributed delays, as well as the transient between the regimes, have been studied by numerical simulations [95].

Also in a single Stuart-Landau oscillator, delayed feedbacks can stabilize an otherwise unstable steady state [96]. However, this phenomena is usually not referred to as amplitude death, because this term is usually restricted to systems with diffusive coupling. Feedbacks have also been investigated in a systems of two coupled oscillators but only feedbacks with coupling strength and delays identical to the mutual couplings have been considered [97].

Time-continuous chaotic systems with delays

Whereas synchronization and amplitude death in limit-cycle oscillators can be studied with the two-dimensional Stuart-Landau oscillator, higher dimensional systems allow to study chaotic systems. In such systems, the m -dimensional system variables $\mathbf{x} \in \mathbb{R}^m$ can be coupled by a function $\mathbf{H} : \mathbb{R}^m \rightarrow \mathbb{R}^m$, so that

$$\dot{\mathbf{x}}_i = \mathbf{F}(\mathbf{x}_i) + \frac{k}{d_i} \sum_j A_{ij} \mathbf{H}(\mathbf{x}_j), \quad (2.24)$$

where the function $\mathbf{F} : \mathbb{R}^m \rightarrow \mathbb{R}^m$ governs the internal node dynamics. Without delays, a master stability function for the complete synchronous state can be calculated numerically. This function governs the stability for any coupling strength k and any coupling topology, where the effect of the topology is given by the eigenvalues of the adjacency matrix \mathbf{A} [98].

Delay-coupled chaotic systems have been investigated with the three-dimensional Lorenz and Rössler oscillators. Depending on the parameter values for k and δ , the coupled systems can display chaotic or regular dynamics such as periodic cycles and amplitude death [99]. For general m -dimensional system, the so-called odd number rule has been proved in rings [100] and globally connected networks [101]. This rule states that amplitude death never occurs for any diffusive time-delayed coupling if the Jacobian of the isolated system has an odd number of real positive eigenvalues. A similar rule also holds for a single systems with delayed feedbacks [102]. Further, analytical works provided necessary and sufficient conditions for synchronization and amplitude death in m -dimensional systems with time-delayed coupling [50, 60, 103, 104]. There is evidence that chaotic systems cannot be synchronized if the coupling delay is much larger than the characteristic time scale of the isolated system [105].

Even though some of the models discussed above include feedbacks, the main focus of these works is on the influence of the delayed interaction between the autonomous systems. However, after Pyragas demonstrated that a delayed feedback can stabilize periodic orbits in chaotic systems [106], this Pyragas control attracted a lot of attention [102, 107–109]. The amplitude death related stabilization of a chaotic system by delayed feedbacks has first been demonstrated experimentally in a NH_3 laser [110]. Later, this effect has been analyzed numerically in Lorenz and Rössler oscillators [111, 112]. Similarly to the Stuart-Landau oscillators, amplitude death occurs inside death islands in the (k, δ) -plane.

Coupled delay systems

In the previous section, we already discussed delayed feedbacks in chaotic systems. This sections deals with systems in which an internal time-delay of the node gives rise to complex dynamics. It was already noted that even scalar equations with time-delays can display high-dimensional dynamics. Maybe the most prominent examples for such equations are the Mackey-Glass [38, 39],

$$\dot{x} = \frac{ax^\tau}{1 + (x^\tau)^c} - bx, \quad (2.25)$$

and the Ikeda model [40],

$$\dot{x} = -x + a \sin(x^\tau - b). \quad (2.26)$$

The Mackey-Glass model was introduced to describe the blood production in patients suffering from leukemia and the Ikeda model has been used to describe an optical bistable resonator. Both models are famous for exhibiting delay-induced chaos.

In unidirectional, undelayed coupled delay systems with identical delays, different forms of synchronization have been found, such as complete (CS) [113–115], anticipating (AS) [116], lag (LS) [117] and phase synchronization (PS). In systems with different delays, general synchronization (GS) has been observed [115, 118, 119].

Here, we denote the dynamical variable of the responding system, which receives the signal from the driving system, by y and the variable of the driving system by x . Then CS refers to states $y(t) = x(t)$, AS to $y(t) = x(t + \tau)$, LS to $y(t) = x(t - \tau)$, where τ is the internal node delay. PS means that the phases are in synchrony, but the amplitudes are still chaotic, and GS means that the dynamic of the responding system is completely determined by the driving system, but the relation between the two dynamic variables might be arbitrarily complicated. Hence, synchrony is not observed between driving and responding systems, but two responding system would display completely synchronized dynamics.

All these studies only considered the undelayed coupling of two delay systems. A model of two delay-coupled delay systems is discussed in the next section. However, non of these works considered the effect of network structures.

Delay-coupled delay systems

Studies on delay-coupled delay systems are rare. Amplitude death has been studied in two delay-coupled delay systems [66]. The death regions in the (k, δ) -plane has been obtain numerically, where δ refers to the coupling delay and τ to the internal delay of the node dynamics. However, the interplay between the two different kinds of delays τ and δ is not studied. Further, only two systems are coupled, so that relations between network topology and dynamics is not studied as well.

Systems with multiple delays are known to display complex stability patterns in the delay parameter space. Such patterns have been observed in chaotic system with multiple delayed feedbacks [111, 120, 121] and in networks of coupled oscillators, where both delays appear in each connection [122]. A common finding in all these works is that multiple delays allow the stabilization of a steady state even for large delays, whereas large delays usually prohibit amplitude death in systems with a single delay. Further, the stability patterns are symmetric in both delays, because both delays are of the same type, so that exchanging the delays does not change the system. When considering the internal and the coupling delay in delay-coupled delay oscillators, this symmetry is broken and we might expect more complex relations between the stability patterns and the network topology as compared to the model in which both delays appear in the coupling. Such a model is studied in the following.

3 The generalized flow model

In this thesis, we analyze a generalized network model with delayed flows between nodes and delayed production on nodes. For simplicity, we assume that the number of incoming links d_i^{in} and the number of outgoing links d_i^{out} are identical for each node i such that $d_i^{in} = d_i^{out} = d_i$. Note that this includes all undirected networks.

Each node is described by an internal dynamical variable X_i , which for instance might represent the number of individuals in an ecological system or the number of RNA molecules in a gene regulatory network. In the following, we refer to the variables X_i as the load on node i . The load may increase due to an auto-catalytic process which involves a growth delay τ and is described by the growth function G . For instance, in an ecological system, the increase of the population size depends on the number of sexually mature individuals, which is represented by the load X . However, the increase of sexually mature individuals is delayed by the time τ needed for the development and maturation of the fertilized egg. In contrast, we assume that loss due to mortality, which is described by the function L , only depends on the actual number of mature individuals. We now assume that there are separate populations on different patches represented by the nodes of the network. If there is a link from node j to node i , a certain fraction F of the individuals from patch j moves to patch i . However, moving between patches takes a travel-time δ . Hence, the number of mature individuals on patch i changes by

$$\dot{X}_i = G(X_i^\tau) - L(X_i) + \sum_j (A_{ij}F(X_j^\delta) - A_{ji}F(X_i)), \quad (3.1)$$

where $X^\tau = X(t - \tau)$, and G , L and F are positive functions. As long as the functions are not specified, we refer to Eq. (3.1) as the generalized or the structural model.

We assume that the flow function $F(X)$ is increasing, so that unequal loads on two bidirectionally coupled nodes generate an equilibrating net flow. For networks with $d_i^{in} = d_i^{out}$, nodes with a comparable small load receive net inflows, whereas the outflows are larger than the inflows for nodes with a comparable large load. Thus, if the functions G and L are identical for all nodes, it is reasonable to consider a homogeneous steady state, in which all node loads X_i^* are identical, with X^* satisfying the steady state condition for the isolated node, so that $G(X^*) = L(X^*)$. The rest of this thesis deals with the stability analysis of such a homogeneous steady state of Eq. (3.1), where we avoid further restrictions on G , L and F by applying the generalized modeling approach.

3.1 Parametrization of the Jacobian

In the generalized modeling approach, a structural model such as in Eq. (3.1) is analyzed by a direct parametrization of the Jacobian. In order to obtain interpretable parameters, the model equations are normalized to an assumed steady state. The normalized equations depend on characteristic rates, which provide the first set of parameters. Furthermore, the Jacobian depends on the derivatives of the normalized functions, which provide the second set of parameters [9].

We have seen that it is reasonable to assume that the system described by Eq. (3.1) has a homogeneous steady state with $X_i^* = X^*$ for all nodes i and that $G(X^*) = L(X^*)$. Using $X^* = X^{\tau*} = X^{\delta*}$, we normalize Eq. (3.1) by introducing the normalized variables $x_i = X_i/X_i^*$ and the functions

$$g(x) = \frac{G(xX^*)}{G(X^*)}, \quad l(x) = \frac{L(xX^*)}{L(X^*)}, \quad f(x) = \frac{F(xX^*)}{F(X^*)}, \quad (3.2)$$

so that we obtain

$$\dot{x}_i = \alpha(g(x_i^\tau) - l(x_i)) - d_i\beta f(x_i) + \beta \sum_j A_{ij}f(x_j^\delta), \quad (3.3)$$

where $\alpha = G^*/X^* = L^*/X^*$ and $\beta = F^*/X^*$ are constant parameters that describe characteristic turnover and flow rates, respectively. The turnover rate is defined by the ratio of the steady state growth and loss rates to the steady state load. And the flow rate is defined by the ratio of the steady state flow to the steady state load. Thus, both parameters α and β are positive quantities that have a direct interpretation in terms of the unnormalized system.

The Jacobian of the normalized system depends on the derivatives of the normalized functions with respect to the normalized loads, which are introduced as the second set of parameters

$$g' = \left. \frac{\partial g}{\partial x} \right|_{x=1}, \quad l' = \left. \frac{\partial l}{\partial x} \right|_{x=1}, \quad f' = \left. \frac{\partial f}{\partial x} \right|_{x=1}. \quad (3.4)$$

Here, we follow a terminology from metabolic control theory and denote these quantities as *elasticities* [123]. Alternatively, we might denote them as *exponent parameters*, because the elasticity of a power law function $F(X) = X^p$ is given by the exponent p . Even for general functions, the elasticities can be interpreted in the context of the original system, because they are the logarithmic derivatives of the unnormalized quantities, as can be seen from the equation

$$g' = \left. \frac{\partial g}{\partial x} \right|_{x=1} = \left. \frac{X^*}{G^*} \frac{\partial G}{\partial X} \right|_{X=X^*} = \left. \frac{\partial \log G}{\partial \log X} \right|_{X=X^*}. \quad (3.5)$$

With the parameters obtained above, the elements of the Jacobian \mathbf{J} are given by

$$\begin{aligned} J_{ii} &= \alpha(g'e^{-\lambda\tau} - l') - d_i\beta f' & =: J_i^d, \\ J_{ij} &= \beta f'e^{-\lambda\delta} A_{ij} & =: J^o A_{ij}. \end{aligned} \quad (3.6)$$

Note that the Jacobian only depends on the product of f' and β , so that both quantities do not appear independently in the equations. Therefore, we introduce the effective coupling strength $k := \beta f'$, which we assume to be positive. Also, the loss elasticity l' is assumed to be positive. Further, we normalize the time-scale by setting $\alpha = 1$.

In the following sections, we study the stability of some simple special cases by utilizing properties of the Laplacian matrix. For this purpose, we rewrite \mathbf{J} in matrix form,

$$\mathbf{J} = (g'e^{-\lambda\tau} - l')\mathbf{I} - k(\mathbf{D} - \mathbf{A}e^{-\lambda\delta}), \quad (3.7)$$

where \mathbf{I} is the identity matrix and \mathbf{D} is the diagonal matrix with $D_{ii} = d_i$. We define $\mathbf{L}(\lambda) := \mathbf{D} - \mathbf{A}e^{-\lambda\delta}$ and note that $\mathbf{L} = \mathbf{L}(0)$ is the graph Laplacian. In order to calculate the roots of the characteristic polynomial $P(\lambda) = \det(\lambda\mathbf{I} - \mathbf{J}(\lambda))$, we substitute $\lambda - (g'e^{-\lambda\tau} - l')$ with z , so that $P(z) = \det(z\mathbf{I} + k\mathbf{L}(\lambda))$. Thus the roots of $P(z)$ are given by $-k\text{Ev}(\mathbf{L}(\lambda))$, where $\text{Ev}(\mathbf{L}(\lambda))$ denotes the eigenvalues of $\mathbf{L}(\lambda)$. The back-substitution yields

$$\lambda = (g'e^{-\lambda\tau} - l') - k\text{Ev}(\mathbf{L}(\lambda)). \quad (3.8)$$

This equation relates the dynamics of the system to the structure of the network, where the structural information is captured by the eigenvalues of the matrix $\mathbf{L}(\lambda)$. However, this matrix depends on the eigenvalue λ and the coupling delay δ , so that a complete decoupling of structure and dynamics is not possible in general.

3.2 Comparison with other models

The coupling in our model differs from the coupling in most other models. Comparing our model, described by Eq. (3.1), with Eq. (2.21),

$$x_i(t+1) = f(x_i(t)) + \frac{k}{d_i} \sum_j A_{ij}(f(x_j(t)) - f(x_i(t))), \quad (3.9)$$

we note that in the latter case the coupling strength is divided by the degree of the node. Hence, in these models only the average of the inputs of all incoming signals influences the node dynamics, whereas the inputs are added in our model. Thus, in our model a node that has two identical neighbors behaves differently than a node that is connected only to one of them. In most other models, the node behaves identically in both cases. Modifying our model accordingly results in

$$\mathbf{J} = (g'e^{-\lambda\tau} - l' - k)\mathbf{I} + k\mathbf{A}'e^{-\lambda\delta}, \quad (3.10)$$

with $A'_{ij} = A_{ij}/d_i$. This Jacobian has the same structure as Eq. (3.7) for a degree-homogeneous network. Thus, all networks of the type of Eq. (3.9) can be studied accordingly to degree-homogeneous networks in our model. In chapter 4, we see

that for our model, the analysis of degree-homogeneous networks is easier than the analysis of degree-heterogeneous networks. However, in chapter 5, we also study degree-heterogeneous networks.

The more common models of the type of Eq. (3.9) might be suitable to describe signal transmission. In order to describe systems in which matter is transported between nodes, we should assume a conservation of flow, which is violated in the common models. Hence, such systems are better described by our model.

3.3 The single node

In order to be able to compare the stability of networks with the stability of isolated nodes, we first study a single isolated node by considering the case of vanishing coupling strength, $k = 0$. Thus, Eq. (3.8) becomes

$$\lambda = g'e^{-\lambda\tau} - l'. \quad (3.11)$$

Without delay, the system is stable for $g' < l'$ and unstable otherwise. The system with delay can be analyzed by expressing Eq. (3.11) with the Lambert function (Sec. 2.3) as

$$\lambda = \frac{1}{\tau} W(g'\tau e^{l'\tau}) - l'. \quad (3.12)$$

For $g' = l'$, we see that $\lambda = 0$, because $W(xe^x) = x$ by definition. Further, we see that at least one eigenvalue λ is positive for $g' \geq l'$, because the principle branch of W is increasing for positive arguments. Hence, as the system without delay, the delay system is unstable for all $g' > l'$.

Below, I show that systems with $|g'| < l'$ are stable for all network topologies, including the single isolated node¹. Thus, in both cases, $|g'| < l'$ and $g' > l'$, the stability of a single node is independent of the delay τ . By contrast, the stability is delay dependent for $g' < -l'$.

For $g' < -l'$, the system is stable for $\tau = 0$, because $\lambda = g' - l' < 0$. However, if τ increases above a bifurcation point τ^* , the system becomes unstable. The calculation of this critical delay τ^* is demonstrated in the book “From Clocks to Chaos” by Leon Glass and Michael Mackey [125]². The stability changes if the leading eigenvalue crosses the imaginary axis. In order to find such bifurcations, Eq. (3.12) is separated into its real part κ and its imaginary part ω , so that $\lambda = \kappa + i\omega$. By setting $\kappa = 0$, we obtain the bifurcation condition

$$0 = g' \cos(\phi) - l', \quad (3.13)$$

$$\omega = -g' \sin(\phi), \quad (3.14)$$

¹This stability condition can also be obtained from a more general result from Hale et al.[124].

²In the book by Mackey and Glass the parameters g' and l' are replaced by B and $-A$, respectively. However, the stability conditions are lacking the restriction $A + B < 0$.

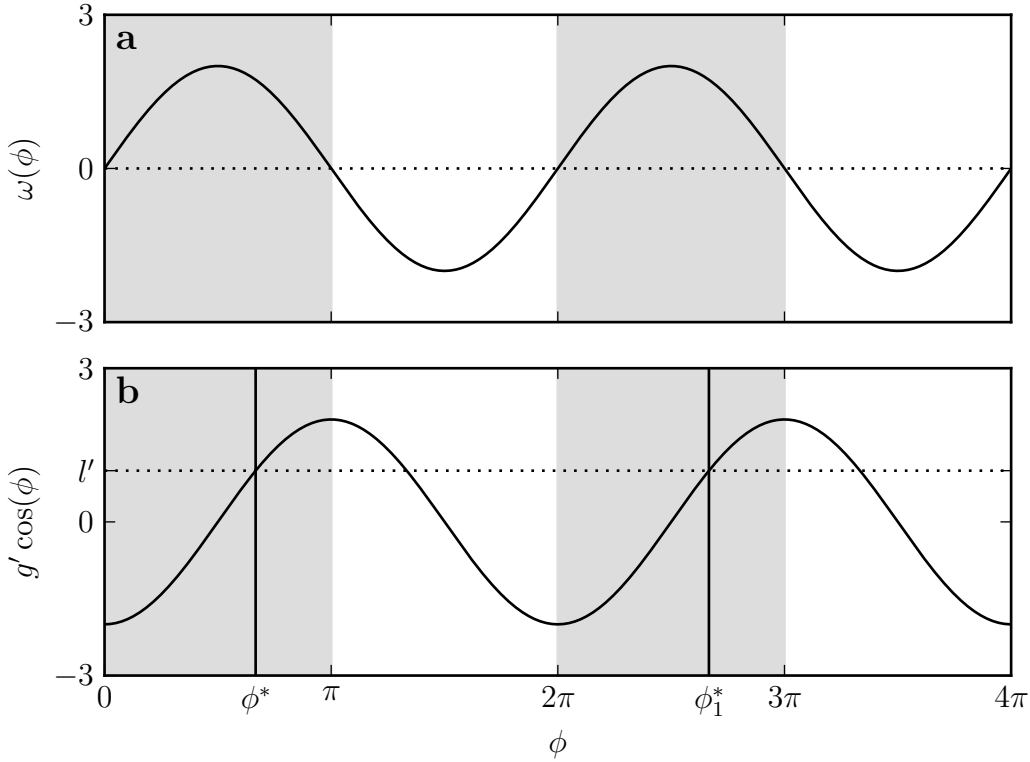


Figure 3.1: Calculating the bifurcation points for an isolated node with $g' < -l' \leq 0$. We are only interested in solutions for which Eq. (3.14) provides $\omega > 0$ (a). Therefore, we only consider solutions of Eq. (3.13) (intersections of $g' \cos(\phi)$ and l' in (b)), which are inside the light gray area. We find infinitely many solutions ϕ_r^* with $\phi_r^* = \phi^* + 2\pi r$, $\phi^* = \cos^{-1}(l'/g')$ and an integer r .

with $\phi = \omega\tau$. We are only interested in solutions of Eq. (3.13) for which Eq. (3.14) provides $\omega > 0$. Noting that we only consider $g' < 0$, the corresponding solutions of ϕ lie inside the intervals $[2r\pi, (2r+1)\pi]$, with an integer r (Fig. 3.1). Thus, they are given by $\phi_r^* = \cos^{-1}(l'/g') + 2\pi r$. Inserting ϕ_r^* into Eq. (3.14) provides $\omega = \sqrt{g'^2 - l'^2}$, and we find the bifurcation delays

$$\tau_r^* = \frac{\cos^{-1}(l'/g') + 2\pi r}{\sqrt{g'^2 - l'^2}}. \quad (3.15)$$

The system becomes unstable if τ increases above the smallest τ_r^* . Hence, the stability border of the isolated single node is given by $\tau^* = \tau_0^*$.

In summary, an isolated node is unstable for $g' > l'$ and stable for $|g'| < l'$. For $g' < -l'$, the node is stable for $\tau < \tau^*$ and unstable otherwise.

3.4 Networks without delays

Now, we consider a network of coupled delay systems, described by Eq. (3.7). However, here we restrict our analysis to networks without coupling delays, so that $\delta = 0$. For $\delta = 0$, equation (3.8) becomes

$$\lambda = g'e^{-\lambda\tau} - l' - k\text{Ev}(\mathbf{L}). \quad (3.16)$$

Recall that the smallest eigenvalues of the graph Laplacian \mathbf{L} is 0 and all other eigenvalues are larger or equal to 0. In order to obtain the leading eigenvalue from Eq. (3.16), we need to choose $\text{Ev}(\mathbf{L}) = 0$. Hence, the leading eigenvalue of networks with $\delta = 0$ is identical to the leading eigenvalue of the single node. Thus, the stability of the network is given by the stability of the single isolated node, which has been discussed in the previous section.

Choosing the eigenvalue $\text{Ev}(\mathbf{L}) = 0$, we see that all eigenvalues of the single node systems are also eigenvalues of the network with $\delta = 0$. However, the opposite is not true, because the other eigenvalues of $\text{Ev}(\mathbf{L})$ give rise to additional eigenvalues in the network system. Hence, without coupling delay, the network system can only be less stable than the isolated node.

If $\tau = \delta = 0$, the leading eigenvalue of a network is given by $g' - l'$. Therefore, the systems are stable for $g' < l'$ and unstable otherwise. Thus, the stability of all undelayed networks is identical to the stability of the undelayed isolated node.

3.5 A sufficient condition for instability

After, we discussed the special cases of networks with vanishing delays, this section deals with a sufficient condition for instability of networks with non-vanishing delays.

Lacking a rigorous proof, I formulate the conjecture that all networks that are described by Eq. (3.7) are unstable for $g' > l'$. In order to motivate this proposal, I present numerical results showing that the leading eigenvalue of an isolated node, which is real and positive, remains real and positive if several of these nodes are coupled in a network. Admitting that numerical results are only obtained for a small number of different networks and parameters, I refer to section 5.1.2, where the proposal is tested for a much larger number of different configurations.

By setting the coupling strength k to zero, any network decomposes into isolated nodes. For $g' > l'$, the leading eigenvalue of the isolated node is real and positive and can be calculated with Eq. (3.12) by using the principle branch of the Lambert function. While increasing k from 0 to 10, we follow this eigenvalue by a numerical continuation. The parameters of the isolated node are fixed to study the effect of different network topologies and coupling delays. Therefore, all lines collide at $k = 0$. However, other choices of g' , l' and τ provide qualitatively the same results. We observe that the eigenvalue approaches 0 faster for networks with large numbers of links (Fig. 3.2(a)). Topological differences between random networks with the same

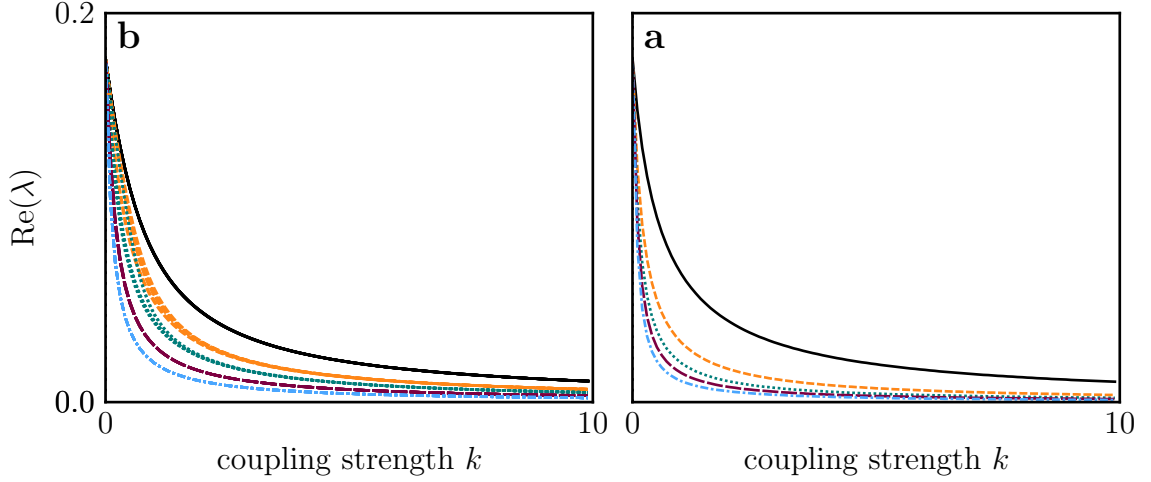


Figure 3.2: Continuation of the leading eigenvalue of the isolated node as the coupling strength k increases from 0 to 10. (a) Results for random networks with $N = 10$ nodes and $K = 9, 15, 20, 30$ and 45 links (from top to bottom), and a coupling delay $\delta = 3$. For each K , 10 random networks are generated. However, lines for different networks with the same K can only be distinguished for small non-zero k , and $K = 15$ and $K = 20$. (b) Results for fully-connected networks with $\delta = 1, 3, 5, 7$ and 10 (top to bottom). In all cases, the eigenvalue remains real and positive. The initial value for $k = 0$ is calculated with Eq. (2.19). Other parameters are: $g' = 2, l' = 1$ and $\tau = 3$.

number of links seem to have only a minor influence on the eigenvalue, which is only visible for small k . Eigenvalues also approach 0 faster for large coupling delays δ (Fig. 3.2(b)). In all cases, we observe that the eigenvalue remains real and does not change its sign. This has also been observed in much more general networks, such as in weighted networks with randomly distributed delays. These results confirm our conjecture that the network coupling cannot stabilize nodes with $g' > l'$.

3.6 A sufficient condition for stability

Finally, I prove that all networks described by the Jacobian from Eq. (3.7) are stable for $|g'| < l'$. For this purpose, I apply the Gershgorin circle theorem that states that all eigenvalues of a complex matrix \mathbf{M} lie inside circles in the complex plane, where each row or each column of the matrix gives rise to one circle. The center of the circle of row i is given by the diagonal element M_{ii} ; The radius is given by the sum of the absolute values of the off-diagonal elements in the row: $R_i^G = \sum_{j \neq i} |M_{ij}|$ [126].

Applying the theorem to the Jacobian from Eq. (3.7) and considering only the row i , the radius of the Gershgorin circle is $R_i^G = |kd_i \exp(-\lambda\delta)| = kd_i \exp(-\kappa\delta)$, with $\kappa = \text{Re}(\lambda)$. The center of the circle is at $D_i^G = g' \exp(-\lambda\tau) - l' - kd_i$. For complex λ with unknown imaginary part ω , the center itself lies on a circle around

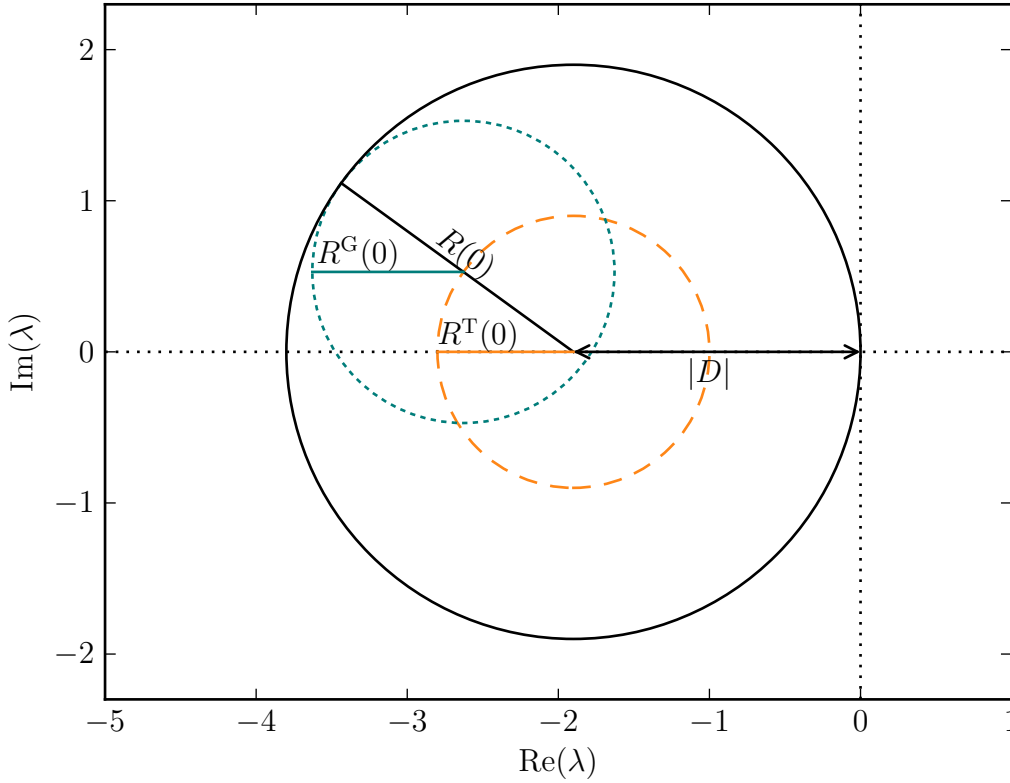


Figure 3.3: Sufficient stability condition for delay systems. All eigenvalues of a matrix \mathbf{M} have to lie inside Gershgorin Circles with radii R^G around points C (dotted green). For delay systems the Jacobian matrix depends on the unknown eigenvalue λ with real-part κ . Therefore, the radii depend on κ and the centers C themselves lie on circles with radii $R^T(\kappa)$ around points D (dashed orange). Thus, all eigenvalues lie inside circles with radii $R(\kappa) = R^T(\kappa) + R^G(\kappa)$ around points D (solid black). The radii $R(\kappa)$ is decreasing with respect to κ . Hence, if D is negative and $R(0) < D$, no eigenvalues with positive real-part can exist and the system is stable.

$D_i = -l' - kd_i$ with radius $R^T = |g'| \exp(-\kappa\tau)$. We denote the sum of this radius and the radius from the Gershgorin theorem by $R_i = R_i^G + R_i^T$. Hence, all eigenvalues have to lie inside circles around D_i with radii $R_i(\kappa)$ (Fig. 3.3). Note, that $R_i(\kappa)$ is strictly decreasing.

In order to show that all network are stable for $|g'| < l'$, we assume that an unstable network exists. An unstable network has a leading eigenvalue with positive real-part κ . But then, the radius $R_i(\kappa) < R_i(0)$ and no eigenvalues with real-parts larger than $D_i + R_i(0) = |g'| - l' < 0$ can exist. Hence, all eigenvalues must have negative real-parts. This contradicts the assumption that the leading eigenvalue has a positive real-part and thus shows that all networks are stable for $|g'| < l'$.

3.7 Summary

In this chapter, I demonstrated the extension of generalized modeling to delay networks by applying it to a system of delay-coupled delay oscillators (Sec. 3.1). The nodes are coupled by conserved flows between them. However, the more common case that only the average input of a node influences the node dynamics, results in a similar model. Such models can be analyzed analog to the case of degree-homogeneous networks in our model (Sec. 3.2).

By studying our model, we justified a conjecture that all networks are unstable for $g' > l'$ (Sec. 3.5). Further we found that all networks are stable for $|g'| < l'$ (Sec. 3.6). In contrast, we will see that the stability depends on the topology and on the delays for $g' < -l'$. However, for vanishing coupling delays, $\delta = 0$, the stability of the network is given by the stability of the single node system (Sec. 3.4), which is stable for $\tau < \tau^*$ and unstable otherwise (Sec. 3.3). In the following, we study the topology and delay dependent stability of networks with $g' < -l'$.

4 Degree-homogeneous networks

In this chapter, we restrict our analysis to degree-homogeneous networks, i.e. networks in which all nodes have the same number of links, so that $d_i = d_j$ for all nodes i and j . For these networks, it is possible to decompose the Jacobian from Eq. (3.7) into N independent equations. This allows to calculate the bifurcation lines analytically. The analysis of degree-heterogeneous networks is postponed to chapter 5, where we apply a numerical method to determine the number of eigenvalues with positive real part.

In the previous chapter, we found that all networks with $g' > l'$ are unstable (Sec. 3.5) and that all networks with $|g'| < l'$ are stable (Sec. 3.6). Thus, we can restrict our analysis to the case $g' < -l'$. We recap that the diagonal and off-diagonal elements of the Jacobian from Eq. (3.7) are given by

$$J^d = g'e^{-\lambda\tau} - l' - d_i k, \quad (4.1)$$

$$J^o = ke^{-\lambda\delta}. \quad (4.2)$$

For degree-homogeneous networks, all diagonal elements of \mathbf{J} are identical. Hence, we can substitute all terms $\lambda - J^d$ that occur in the characteristic polynomial by z , so that $P(z) = \det(z\mathbf{I} - J^o\mathbf{A})$. Thus, the roots of $P(z)$ are given by $c_i J^o$, with the N eigenvalues c_i of the adjacency matrix. The back-substitution gives N independent scalar equations,

$$\lambda = J^d(\lambda) + c_i J^o(\lambda). \quad (4.3)$$

In order to distinguish the eigenvalues of the adjacency matrix from the eigenvalues of the Jacobian, we refer to them as *topological eigenvalues*. These are in general complex. Therefore, we rewrite the eigenvalues as $c = |c|e^{i\psi_c}$, where we denote ψ_c as complex phase of the topological eigenvalue and chose the domain as $[0, 2\pi)$.

Note that for $c = 0$, the system reduces to the single node system with $l' \rightarrow l' - dk$. This case is qualitatively different from the generic case of $c \neq 0$ but won't be treated below because it has already been discussed in section 3.3.

We study systems with topological eigenvalues $c \neq 0$ by calculating the bifurcation points. At a bifurcations point, the eigenvalue λ becomes purely imaginary, so that $\lambda = i\omega$ and the exponential functions in Eq. (4.1) can be replaced by cosine and sine functions. By separating Eq. (4.3) into it's real and imaginary part, we obtain

$$0 = g' \cos(\phi) - l' - dk + |c|k \cos(\psi), \quad (4.4)$$

$$\omega = -g' \sin(\phi) - |c|k \sin(\psi). \quad (4.5)$$

where $\psi := \omega\delta - \psi^c$.

In the following, we restrict our study to two independent parameters, where all other parameters are kept fixed. In this case, the bifurcation points constitute lines in the two-dimensional parameter space. First, we derive the bifurcation lines in the (τ, δ) -plane to study resonance between the two delays. Then, we investigate the effect of amplitude death that has been studied for undelayed oscillators. In order to be able to compare the results for our model of delay-coupled delay oscillator to known results for other delay-coupled systems, we calculate the bifurcation lines in the (k, δ) -plane.

4.1 Bifurcation lines in the delay space: Tongues of instability

In order to calculate the bifurcation lines in the (τ, δ) -plane, we start from the Eqs. (4.4,4.5), which contain the three independent variables ϕ , ψ and ω . Given a solution triplet (ϕ, ψ, ω) , there exists another solution triplet $(-\phi, -\psi, -\omega)$. Hence, it is sufficient to calculate the solutions with positive ω . Further, we see that the equations are 2π -periodic in ϕ and ψ . Thus, we can restrict ϕ and ψ to an interval of size 2π . With a given solution triplet (ϕ, ψ, ω) from this interval, we find other solutions at $(\phi + 2\pi r, \psi + 2\pi s, \omega)$, with integers r and s enumerating the solutions branches. In contrast to the topological branches arising from the different eigenvalues of the adjacency matrix, we denote the r - and s -branches as delay branches. In the following, we use the notation: $\phi_r = \phi + 2\pi r$ and $\bar{\phi}_r = 2\pi(r + 1) - \phi$. For $r = 0$, the index is omitted.

In order to calculate the solutions for a single delay branch, we treat ϕ as a free parameter, solve Eq. (4.4) for ψ and insert the result into Eq. (4.5). Thus, we obtain

$$\psi^{L,R} = \pm \cos^{-1}(p(\phi)) \quad (4.6)$$

$$\omega^{L,R} = -g' \sin(\phi) \mp |c|k\sqrt{1 - p(\phi)^2}, \quad (4.7)$$

with

$$p = \frac{d}{|c|} + \frac{l' - g' \cos(\phi)}{|c|k}, \quad (4.8)$$

and the co-domain of \cos^{-1} is $[0, \pi]$. The two solution branches L and R are denoted as left and right branch.

With the back-substitutions

$$\tau = \frac{\phi + 2\pi r}{\omega(\phi)} \quad (4.9)$$

$$\delta = \frac{\psi(\phi) + \psi_c + 2\pi s}{\omega(\phi)} \quad (4.10)$$

the Eqs. (4.6-4.8) provide a parametric representation of the bifurcation lines in the delay-plane. But in order to obtain real-valued solutions with $\omega > 0$, we have to restrict the domain of ϕ and choose the according solution branch.

Real solutions with positive ω

In order to obtain real-valued solutions from the Eqs. (4.6,4.7), we need to restrict the domain of $p(\phi)$, so that $|p(\phi)| \leq 1$ (Fig. 4.1(a,c)). For the considered parameter space, $g' < -l'$ and $|c| \leq d$, we see from Eq. (4.8) that $p(0) > 1$ and has a minimum at $\phi = \pi$. We denote the values of g' for which this minimum becomes 1 and -1 by g^t and g^b , with

$$g^{t,b} = -(d \mp |c|)k - l'. \quad (4.11)$$

For $g' > g^t$, $p(\phi) > 1$ for all ϕ and no bifurcation lines arise. For smaller g' , $p(\phi) \leq 1$ inside $[\phi^p, \overline{\phi^p}]$ and for $g' < g^t$, $p(\phi) < -1$ inside $(\phi^q, \overline{\phi^q})$, with

$$\phi^{p,q} = \cos^{-1} \left(\frac{l' + (d \mp |c|)k}{g'} \right). \quad (4.12)$$

Hence, for $g' > g^t$ no bifurcation lines arise, for $g^b < g' < g^t$, ϕ needs to be restricted to the interval $I^p = [\phi^p, \overline{\phi^p}]$ (Fig. 4.1(a)) and for $g' < g^b$, ϕ needs to be restricted to the two interval $I^{q,1} = [\phi^p, \phi^q]$ and $I^{q,2} = [\overline{\phi^q}, \overline{\phi^p}]$ (Fig. 4.1(c)).

Restricting ϕ as described above only ensures that the solutions of the Eqs. (4.6,4.7) are real. In order to find solutions with positive ω , we need to further restrict ϕ (Fig. 4.1(b,d)).

For $g^b < g' < g^t$, $\omega(\phi)$ is positive for $\phi = \phi^p$ and changes sign at ϕ^ω and $\overline{\phi^\omega}$ for the left and the right branch, respectively, where

$$\phi^\omega = \cos^{-1} \left(\frac{l'}{g'} + \frac{g'^2 - l'^2 + (d^2 - |c|^2)k^2}{2g'(l' + dk)} \right). \quad (4.13)$$

Therefore, we restrict the domain of ϕ to $I^L = [\phi^p, \phi^\omega]$ for the left branch and to $I^R = [\phi^p, \overline{\phi^\omega}]$ for the right branch (Fig. 4.1(b)).

For $g' < g^b$, the interval $I^{q,2}$ only provides solution with negative ω , whereas ω is positive inside $I^{q,1}$ for both branches. Hence, for both branches, we restrict the domain of ϕ to the interval $I^q = [\phi^p, \phi^q]$ (Fig. 4.1(d)).

The two conditions $g^b < g' < g^t$ and $g' < g^b$ on g' can be translated into conditions on the topological eigenvalue c . For this purpose, we introduce the quantity

$$c^* = d + \frac{g' + l'}{k}, \quad (4.14)$$

and obtain the two conditions $-|c| < c^* < |c|$ and $c^* < |c|$. Therewith, we also see that only those topological eigenvalue that satisfy $|c| > c^*$ give rise to bifurcation lines.

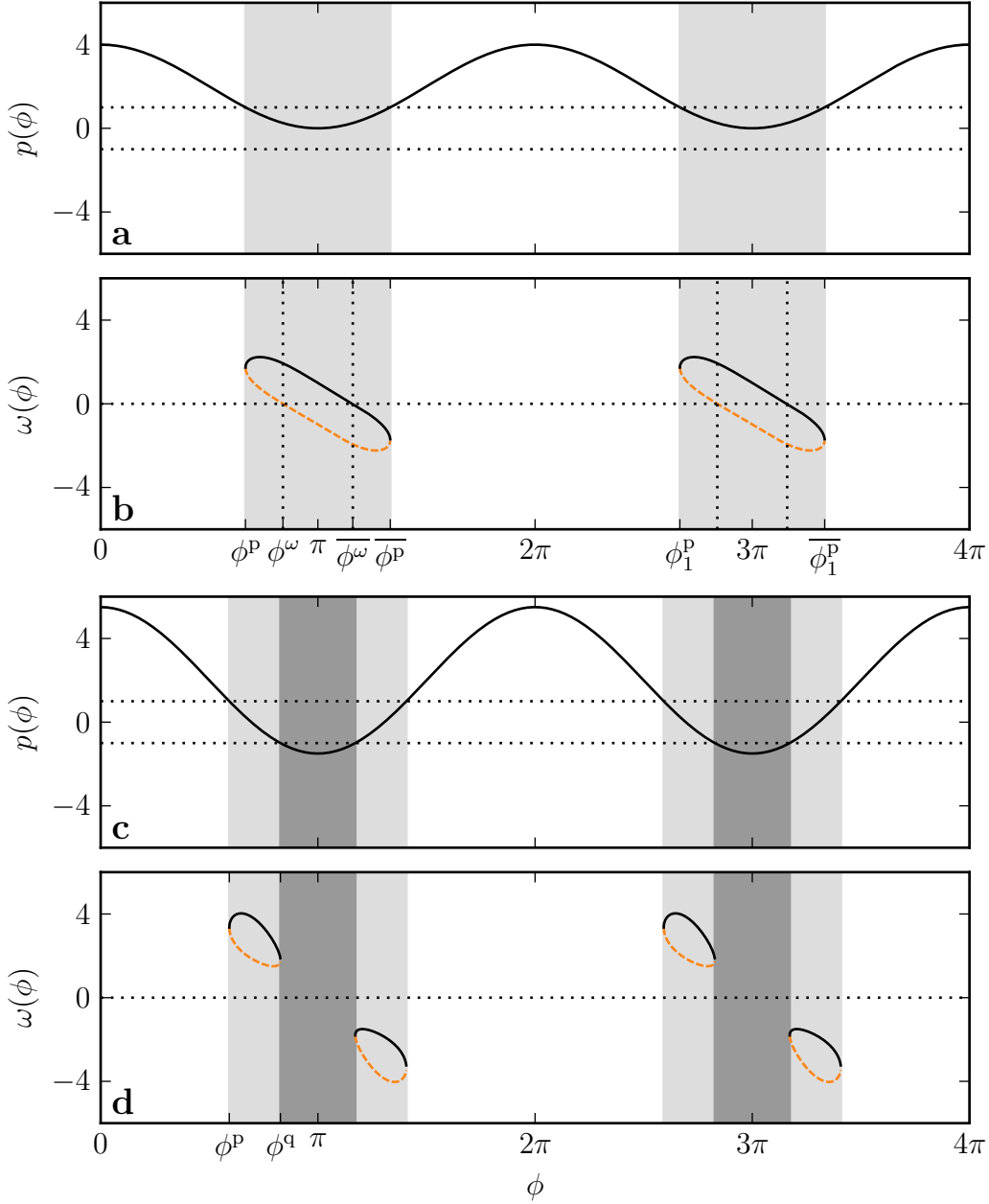


Figure 4.1: Functions $p(\phi)$ (a,c) and $\omega(\phi)$ (b,d) for $g' = -2$ (a,b) and $g' = -3.5$ (c,d). Valid solutions of the Eqs. (4.6,4.7) only exist if $|p(\phi)| < 1$. For $g' < g^t = -1$, $p(\phi) < 1$ inside $[\phi^P, \bar{\phi}^P]$ (gray areas). For $g' < g^b = -3$ (c,d), $p(\phi) < -1$ inside $[\phi^a, \bar{\phi}^a]$ (dark gray area) and $\omega > 0$ inside $I^a = [\phi^P, \phi^a]$. For $g^b < g' < g^t$ (a,b), $\omega > 0$ inside $I^L = [\phi^P, \phi^\omega]$ for the L-branch (dashed orange lines) and inside $I^R = [\phi^P, \bar{\phi}^\omega]$ for the R-branch (solid black lines). Other parameters: $l' = 0, k = 1, d = 2, c = 1$.

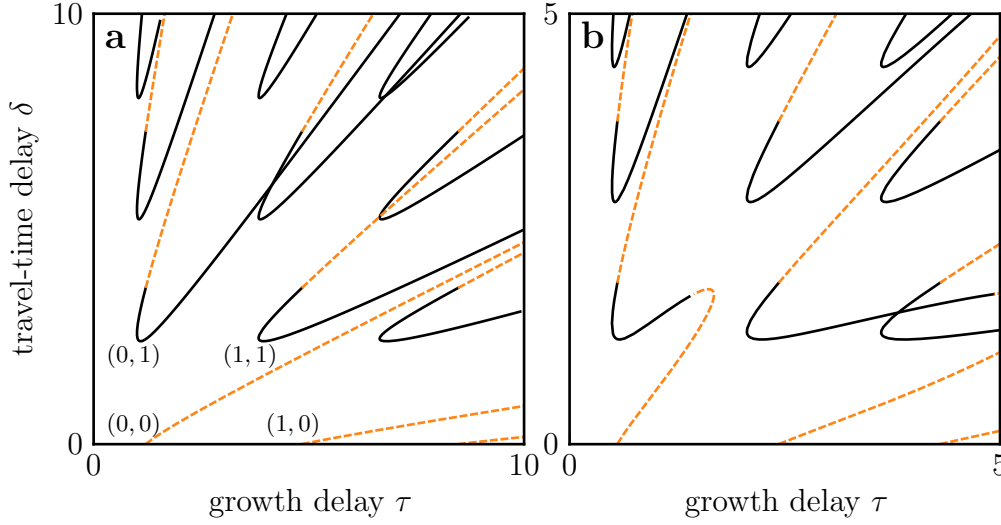


Figure 4.2: Bifurcation lines in the delay plane (Parameters as in Fig. 4.1). (a) For $-|c| < c^* < |c|$, the bifurcation lines give rise to tongues of instability, where the upper left border of a tongue is described by the L-branch of the Eqs. (4.6,4.7) (dashed orange lines) and the tips and the right part of the border are described by the R-branch (solid black lines). The tongues are enumerated by the indexes (r, s) from Eqs. (4.9,4.10). (b) For $c^* < -|c|$, bifurcation lines for different s merge.

4.1.1 Separated and merged tongues

From the Eqs. (4.6,4.7), we see that at the left domain border of ϕ , where $p(\phi = \phi^P) = 1$, both branches of ψ and ω are identical. Thus, the two branches are connected, and we obtain only a single bifurcation line for each pair of indexes (r, s) .

For $-|c| < c^* < |c|$, the right domain borders are given by ϕ^ω and $\overline{\phi^\omega}$, respectively. There, ω becomes 0. Hence, according to the Eqs. (4.9,4.10), τ and δ get infinitely large. In this case, the bifurcation lines for different (r, s) are separated and constitute borders of tongues (Fig. 4.2(a)). The upper left part of a border is described by the L-branch, whereas the tip and the right part of a border are described by the R-branch. The bifurcation lines at the bottom of figure 4.2(a) are described by the L-branch with $s = 0$. The according R-branch provides solutions with $\delta < 0$.

From section 3.4, we know that the system is stable for $\tau = \delta = 0$. Thus, the number of eigenvalues with positive real-part is zero, there. At a bifurcation line, two eigenvalues cross the imaginary axis, one with $\omega_1 > 0$ the other with $\omega_2 = -\omega_1$. Thus, whenever entering a tongue the number of eigenvalues with positive real-part increases. Hence, the system is unstable inside tongues. Between tongues there might be stable channels as such in figure 4.2(a) at the resonant delays $\tau = n\delta$, where n is an integer.

For $c^* < -|c|$, the right domain border of ϕ is ϕ^a , where $p(\phi) = -1$. There, ω is identical for both branches, but $\psi^L = \pi$ whereas $\psi^R = -\pi$. Thus, for tongues

with the same index r , the left branch with index s is connected with the right branch with index $s + 1$. Hence, all tongues with the same index r compose a single connected bifurcation line. Therefore, no stable channels can exist between these lines (Fig. 4.2(b)).

In summary, we found that a topological eigenvalue c gives rise to bifurcation lines only if $|c| > c^*$. For $-|c| < c^* < |c|$, each delay branch, which is indexed by (r, s) , provides a separate bifurcation line bordering a tongue of instability (Fig. 4.2(a)). Stable channels can exist between these tongues. For $c^* < -|c|$, bifurcation lines of the same index r are connected, so that they constitute a single bifurcation line going from $\delta = 0$ to infinity (Fig. 4.2(b)). Thus, the tongues are merged and no stable channels can exist between them.

4.1.2 Periodicity of the tongues

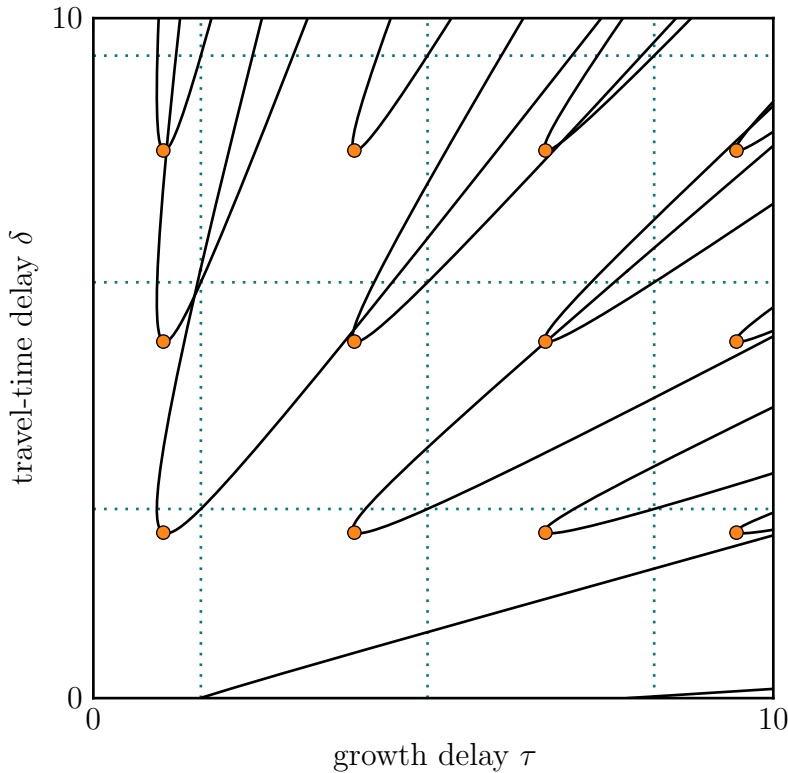


Figure 4.3: Tips and periodicity of the bifurcation lines (solid black lines) in the delay plane. The tip of a tongue is defined as the point on the bifurcation line at which ω becomes maximal (orange circles). Not only the tips but any bifurcation point lies on a rectangular grid that connects corresponding points on different tongues (dotted green lines). However, except for the tips, this periodicity is hard to see because the grid constant depends on ω and changes along the bifurcation line. Other parameters: $c = d = 2, g' = -1, l' = 0, k = 1$.

We already noted that every solution triplet (ϕ, ψ, ω) can be mapped to another solution by shifting ϕ and ψ by multiples of 2π . For a bifurcation point, which is characterized by a triplet (τ, δ, ω) , this means that we find further bifurcation points at $(\tau + 2\pi/\omega, \delta + 2\pi/\omega, \omega)$. Hence, all these points lie on rectangular grids, best visible at the tip of the tongues (Fig 4.3). The periodicity is not that apparent at other points, because ω and thus the grid constant changes along the bifurcation line.

Even though we restricted our analysis to degree-homogeneous networks, this periodicity is more general and also applies to degree-heterogeneous networks. Usually, a time delay τ enters a Jacobian only through the function $\exp(-\lambda\tau)$ that becomes $2\pi/\omega$ periodic if the real-part of the eigenvalue vanishes. Hence, by shifting the delays by multiples of $2\pi/\omega$ we obtain the same Jacobian and hence the same self-consistent eigenvalues.

The periodicity of the bifurcation points is a general property of delay systems that can be explained by the existence of periodic orbits at a bifurcation. At a bifurcation point (τ, δ, ω) there exists a purely imaginary eigenvalue $\lambda = i\omega$. The eigenfunction y of this eigenvalue, describes a perturbation of the steady state, where the time evolution of the perturbation is given by $y(t) = ye^{i\omega t}$. Hence, this solution describes a periodic orbit with period $T = 2\pi/\omega$. It has been shown that a periodic orbit of a system with time delay $\tau = \tau_0$ reappears at time delays $\tau = \tau_0 + nT$, where n is an integer [127]. Thus, when shifting the delays τ and δ by multiples of $T = 2\pi/\omega$, we find the same periodic orbit. That means, we find the same eigenfunction and eigenvalue and thus another bifurcation point.

In Figure 4.3, only the topological eigenvalues $c = d$ gives rise to a set of tongues of instability. Therefore, it is sufficient to calculate only one tongue border, whereas the others borders can be obtained by the above mapping. However, in general, each topological eigenvalue can give rise to such a set of tongues.

The transformation that maps one tongue onto another deforms the tongue by stretching some parts and squeezing others. This phenomena has been described in detail for the mapping of a periodic orbits in a single delay system [127]. Here, we are interested in the consequences of this transformation for the stable channels between the tongues. Figure 4.4(a) shows the bifurcation lines for a large range of τ . The light gray areas mark those values of τ for which the system is unstable for $\delta = 2$. Apparently, the unstable areas expand with τ , whereas the stable areas shrink. The unstable areas are bordered by the two intersections of the line $\delta = 2$ with the tongues $(r, 1)$. The positions of the two intersections are denoted as τ_r^L and τ_r^R . Hence, the unstable area of the tongue r ranges from τ_r^L to τ_r^R and the stable area between the tongues r and $r + 1$ ranges from τ_r^R to τ_{r+1}^L . By applying the mapping, we can calculate the positions τ_r^L from the position τ_0^L : $\tau_r^L = \tau_0^L + 2\pi r/\omega^L$, where ω^L is the imaginary-part of the eigenvalue that becomes purely imaginary at $(\tau_0^L, \delta = 2)$. In the same way, $\tau_r^R = \tau_0^R + 2\pi r/\omega^R$. Hence, the width W_r of the stable

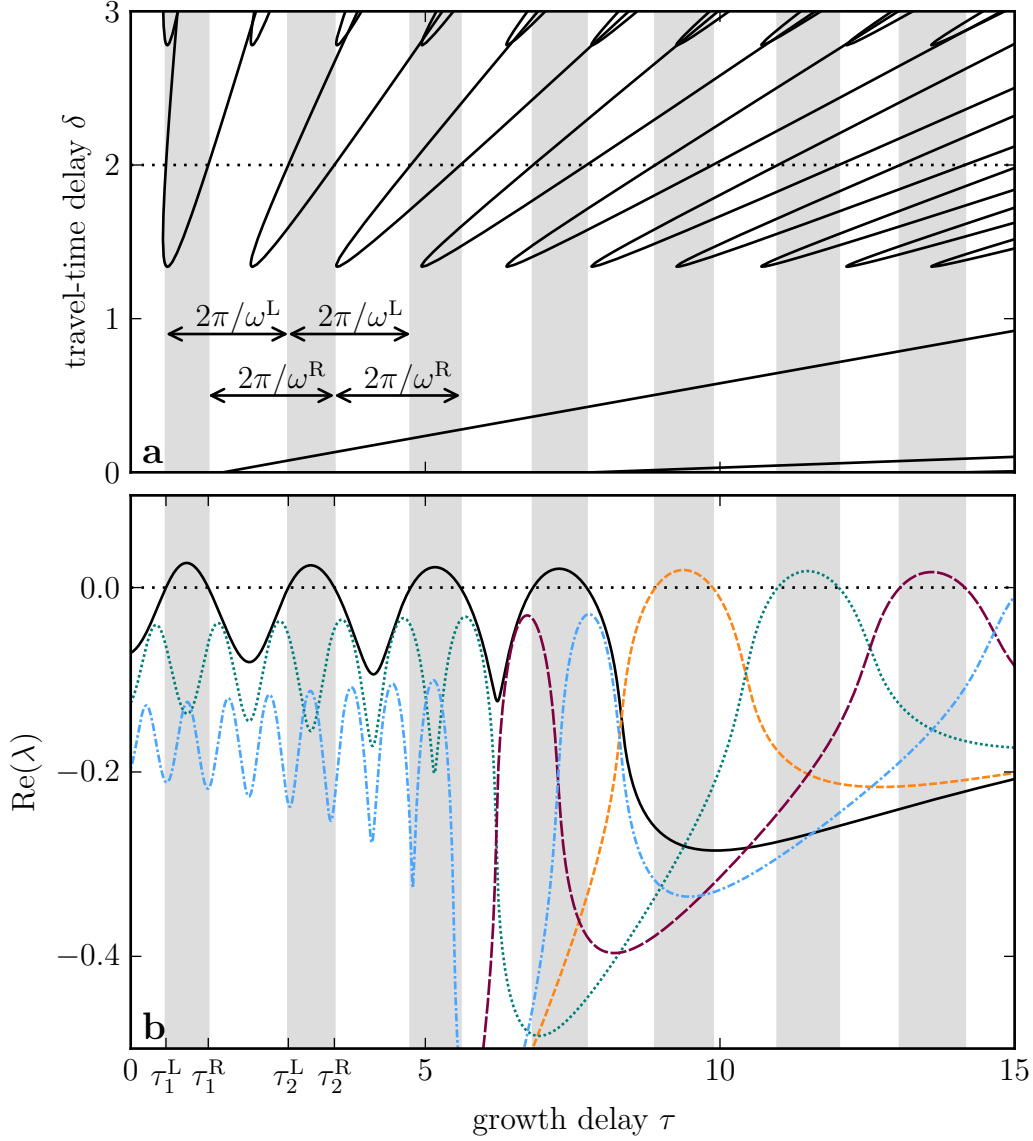


Figure 4.4: Comparison of the periodic bifurcation lines with the corresponding eigenvalues. (a) Bifurcation lines for a fully-connected network with $N = 10$ nodes ($d = 9, c = 9$). For $\delta = 2$, the system is unstable between τ_r^L and τ_r^R (gray areas). There, the leading eigenvalue is purely imaginary, and we denote the imaginary parts by ω^L and ω^R , respectively. Both sets of delays $\tau^{L,R}$ are periodic in τ with periods $2\pi/\omega^{L,R}$. Because $\omega^L > \omega^R$, the width of the unstable area increases with τ , whereas the width of the stable area decreases. (b) Real part of the eigenvalues that give rise to the unstable areas (obtained by numerical continuation). Whereas the intersections between eigenvalues and the zero-axis occur periodically, the eigenvalues show no periodicity for non-vanishing real-parts. Other parameters: $g' = -1, l' = 0, k = 1$.

area between the neighboring tongues r and $r + 1$ is given by

$$W_r = \tau_1^L - \tau_0^R + r \left(\frac{2\pi}{\omega^L} - \frac{2\pi}{\omega^R} \right) = W_0 + r\Delta W. \quad (4.15)$$

We see from the first few tongues that the stable area decreases. Therefore, we know that ΔW is negative. Hence, for $r > -W_0/\Delta W$, the tongues $(r, 1)$ and $(r + 1, 1)$ overlap at $\delta = 2$, so that no stable area exist between these tongues.

The periodicity of the bifurcation lines, at which eigenvalues cross the imaginary axis, does not imply that the eigenvalues show a similar periodicity for non-vanishing real-parts. Figure 4.4(b) shows the real-parts of the eigenvalues that give rise to the first 7 tongues. The irregular behavior of the eigenvalues is best seen by the fact that the first four tongues are caused by a single eigenvalue branch, whereas there are new eigenvalue branches giving rise to the following tongues. This shows that the eigenvalues with non-vanishing real-part cannot be mapped as easily as the bifurcation lines.

4.1.3 Tip positions of the tongues

In order to investigate the stability for small delays, it is useful to calculate the position of the tongue tips. Further, we will see that the tip position provides information about the underlying topological eigenvalue. Instead of defining the tip as the point of the bifurcation line with the largest curvature, we define the tip as the position where ω becomes maximal (Fig. 4.3). The maximum of ω (Eq. (4.7)) lies on the R-branch at

$$\phi^{\text{tip}} = \cos^{-1}(q), \quad (4.16)$$

$$\omega^{\text{tip}} = (|c|k - g)\sqrt{1 - q^2}, \quad (4.17)$$

with

$$q = -\frac{l' + dk}{|c|k - g}. \quad (4.18)$$

Inserting Eq. (4.16) into the Eqs. (4.9,4.10) gives

$$\tau^{\text{tip}} = \frac{\cos^{-1}(q) + 2r\pi}{(k|c| - g')\sqrt{1 - q^2}}, \quad (4.19)$$

$$\delta^{\text{tip}} = \frac{\cos^{-1}(q) + (2s - 1)\pi + \psi^c}{(k|c| - g')\sqrt{1 - q^2}}. \quad (4.20)$$

For the parameter considered here, the first factor in the denominator is always larger than one. However, the second factor $\sqrt{1 - q^2}$ only provides real values for $|q| < 1$. We obtain the same restriction on q if we consider that q is the argument of the arcus cosine function in the nominator. Because q is negative for the considered parameters, we only need to discuss the condition $q > -1$. We can rewrite this

condition as $|c| > c^*$, which is the condition for the existence of bifurcation lines. Thus, the Eqs. (4.19,4.20) tell us how the bifurcation lines vanish. If q approaches -1 from above, the denominator approaches 0, so that τ^{tip} and δ^{tip} become infinitely large¹. Hence, the tongues move to infinitely large delays before they finally disappear.

If we compare the functions for τ^{tip} and δ^{tip} , we note that both are identical for $r = s$ and $\psi^c = \pi$. The condition $\psi^c = \pi$ means that the topological eigenvalue c is real and negative. Hence, real negative topological eigenvalue give rise to tongues with tips on the diagonal of the delay plane.

4.1.4 Slopes of the tongue borders for large delays

We have seen that for $-|c| < c^* < |c|$, the bifurcation lines for different (r, s) constitute separate tongues of instability, and stable channels can exist between them. The left and the right border of these tongues approach straight lines. The slope of these lines can provide information about the existence of stable channels for large delays. By expressing the bifurcation lines in the delay-plane as functions $\delta(\tau)$, the slopes of the tongue borders are given by the derivatives

$$\frac{d}{d\tau}\delta(\tau) = \frac{\delta'(\phi)}{\tau'(\phi)} = \frac{\frac{\psi'(\phi)}{\omega(\phi)} - \frac{\psi(\phi) + \psi^c + 2\pi s}{\omega(\phi)^2}\omega'(\phi)}{\frac{1}{\omega(\phi)} - \frac{\phi + 2\pi r}{\omega(\phi)^2}\omega'(\phi)}, \quad (4.21)$$

where we used the Eqs. (4.9,4.10).

In order to obtain the slopes of the left and the right part of the bifurcation lines for large delays, we need to choose ϕ so that ω from Eq. (4.7) approaches 0, which results in τ and δ from the Eqs. (4.9,4.10) diverging towards infinity. Thus, we have to calculate the slope of the L-branch at $\phi = \phi^\omega$ and the slope of the R-branch at $\phi = \overline{\phi^\omega}$. For these ϕ , the values of $\psi(\phi)$, $\psi'(\phi)$ and $\omega'(\phi)$ are finite, whereas ω approaches 0. Therefore, the second terms in the nominator and in the denominator of Eq.(4.21) dominate the other terms, which can be neglected. Hence, the slope of the left and right branch are given by

$$S_{r,s}^{\text{L}} = \frac{2\pi s + \psi^\omega + \psi^c}{2\pi r + \phi^\omega}, \quad (4.22)$$

$$S_{r,s}^{\text{R}} = \frac{2\pi s - \psi^\omega + \psi^c}{2\pi(r+1) - \phi^\omega}, \quad (4.23)$$

with

$$\psi^\omega = \psi^{\text{L}}(\phi^\omega) = -\psi^{\text{R}}(\overline{\phi^\omega}) = \cos^{-1}\left(\frac{d}{|c|} - \frac{g'^2 - l'^2 + (d^2 - |c|^2)k^2}{2|c|k(l' + dk)}\right). \quad (4.24)$$

Considering that ϕ^ω and ψ^ω are restricted to $[0, \pi)$, we find that $S_{r,s}^{\text{R}} \leq S_{r,s}^{\text{L}}$ for all parameters. Hence, the L-branch is left of the R-branch at least for sufficiently large delays .

¹For $s = 0$ and $\psi^c = 0$, only τ^{tip} approaches infinity, while δ^{tip} approaches a finite value.

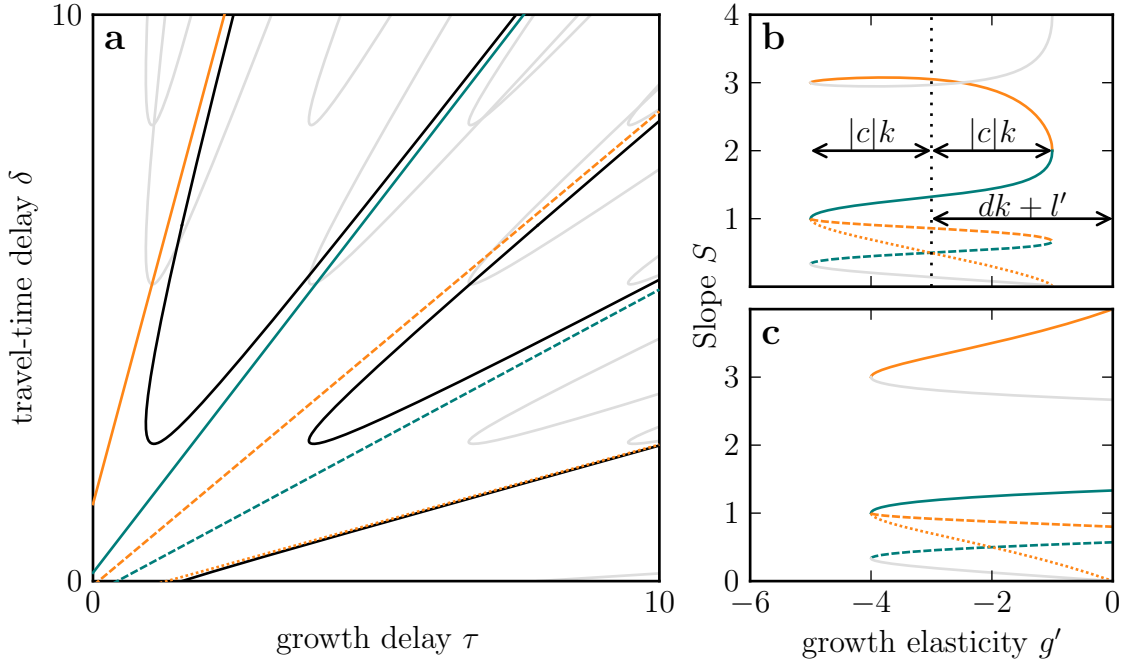


Figure 4.5: Bifurcation lines in the (τ, δ) -plane for $g' = -1$ and $l' = 0$ (a) and their asymptotic slopes in dependence of g' for $l' = 1$ (b) and $l' = 0$ (c). For large delays, the two ends of the tongue borders approach straight lines. The conditions for emergence and merging of tongues, $c^* < \pm|c|$, are equivalent to $g' < -(dk + l') \pm |c|k$. (b) The tongues emerge at $g' = -1$, where they are infinitely narrow, and they merge at $g' = -5$. (c) For $l' = 0$, the tongues emerge with a finite width at $g' = 0$, and they disappear at $g' = -4$. The light gray lines show the slopes of other tongues. Note that not all tongues are considered. Other parameters are $c = d = 2, k = 1$.

In order to find a stable channel between two tongues for large delays, the right slope of one tongue needs to be smaller than the left slope of the other tongue (Fig. 4.5), whereas the offsets of the lines is only important if both slopes are identical. However, the offsets used in the figure 4.5(a) are calculated with

$$A_{r,s}^{L,R} = \delta_s^{L,R}(\phi) - S_{r,s}^{L,R} \tau_r^{L,R}(\phi), \quad (4.25)$$

by choosing $\phi = \phi^\omega - 10^{-8}$ for $A_{r,s}^L$ and $\phi = \overline{\phi^\omega} - 10^{-8}$ for $A_{r,s}^L$.

Now we want to discuss the behavior of the slopes when the parameters approach the critical condition for vanishing tongues, $c^* = |c|$, and for merging tongues, $c^* = -|c|$. For this purpose, we recap that we only obtain valid solutions for the bifurcation lines if ϕ is between ϕ^p and $\overline{\phi^p}$, where $p(\phi) \leq 1$ (Fig. 4.1(a,c)). Considering the case $c^* = |c|$, we find from Eq. (4.8) that in general, $p(\phi) > 1$ except for $\phi = \pi$, where $p(\phi) = 1$. An exception is the case $l' = 0, |c| = d$ and $c^* = |c|$, for which $p(\phi) = 1$ for all ϕ . For $c^* = -|c|$, $p(\phi)$ becomes -1 at $\phi = \pi$ and solutions with $\omega > 0$

are only found for $\phi < \pi$. With these information, we can calculate the quantities ϕ^ω and ψ^ω for the two cases $c^* = |c|$ and $c^* = -|c|$. Thus, we are able to calculate the slopes of the tongue borders for large delays when tongues are emerging and merging.

In general, if $c^* \rightarrow |c|$, $p(\phi)$ becomes 1 at $\phi = \pi$ and is above 1 otherwise. Inserting $\phi = \pi$ into the Eqs. (4.6,4.7) and using $p = 1$, we find that $\omega = 0$ and $\psi_L = 0$. Hence, for $g' < 0$ and $c^* \rightarrow |c|$, $\phi^\omega \rightarrow \pi$ and $\psi^\omega \rightarrow 0$. Inserting $\phi^\omega = \pi$ and $\psi^\omega = 0$ into Eqs. (4.22,4.23), we find that $S_{r,s}^L = S_{r,s}^R$. This means that if parameters are changed so that c^* approaches $|c|$, the width of a tongue becomes infinitely narrow before the tongue finally disappears (Fig. 4.5(b)).

For $l' = 0$, $|c| = d$ and $c^* \rightarrow |c|$, i.e. g' approaches 0 from below, the function $p(\phi)$ becomes 1 for all ϕ . In this case, Eq. (4.13) can be simplified to

$$\phi^\omega = \cos^{-1} \left(\frac{g'}{2dk} \right). \quad (4.26)$$

Hence, for $g' \rightarrow 0$, $\phi^\omega \rightarrow \pi/2$, whereas $\psi^\omega \rightarrow 0$ as in the general case. Inserting $\phi^\omega = \pi/2$ and $\psi^\omega = 0$ into the Eqs. (4.22,4.23), we find that $S_{r,s}^L > S_{r,s}^R$, so that the width of the tongues is finite when the tongues disappear (Fig. 4.5(c)). However, because the tips move to infinitely large delays as c^* approaches $|c|$, the width of tongues has no influence on the stability for finite delays.

If c^* decreases down to $-|c|$, tongues merge. For $c^* = -|c|$, $\phi^q = \phi^\omega = \pi$, so that $p(\phi) = -1$ and $\omega(\phi) = 0$ for $\phi = \pi$ (Fig. 4.1). Inserting $p(\pi) = -1$ into Eq. (4.6) provides $\psi^\omega = \pi$. Therewith, the Eqs. (4.22,4.23) tell us that the slope of the left branch of the tongue (r, s) is equal to the slope of the right branch of the tongue $(r + 1, s)$. Thus, when tongues merge, the merging branches are parallel.

Note that the values of the slopes at the critical points, $c^* = |c|$ and $c^* = -|c|$, only depend on the tongue indexes (r, s) and the complex phase of the topological eigenvalues ψ^c and do not depend on the values of g', l', k, d or $|c|$. Hence, there is an easy relation between the slopes and the underlying topological eigenvalue.

The figures 4.5(b,c) show the slopes of the two branches of different tongues for $l' = 0$ and $l' = 1$. The conditions $-|c| < c^* < |c|$ are equivalent to $-(dk + l') - |c|k < g' < -(dk + l') - |c|k$. For $l' = 1$, this gives $-5 < g' < -1$. Hence, for $g' > -1$, no tongues exist and the system is stable for all delays. Tongues emerge at $g' = -1$, but we see that the left and the right slopes are identical, i.e. the tongues are infinitely narrow (Fig. 4.5(b)). When decreasing g' , tongues become broader and different tongues may overlap as it happens for the tongues $(0, 0)$ and $(1, 1)$ at $g' = -3$. There, the stable channel between these tongues is closed. For $g' = -5$, tongues with the same index s merge to a single bifurcation line, so that all remaining stable channels are closed. However, note that not all tongues of the network are shown in the figure and that most stable channel are closed earlier by other tongues. For $l' = 0$, the critical values for g' are shifted right by 1 (Fig. 4.5(c)). In contrast to the case $l' > 0$, the tongues are of finite size before they disappear at $g' = 0$.

The channel at slope 1 is particularly interesting because it gives the stability on the diagonal of the delay plane at $\tau = \delta$. This channel is bordered by the right branch of the tongues ($r = i, s = i + 1$) and by the left branch of the tongues ($r = i, s = i$), with positive integers i (Fig. 4.5(a)). For c^* close to $|c|$, $S_{i,i+1}^R = (i + 1)/(i + 1/2) > 1$, and $S_{i,i}^L = i/(i + 1/2) < 1$. For c^* approaching $-|c|$ from above, $S_{i,i+1}^R$ and $S_{i,i}^L$ approach 1, so that the channel is closed. However, considering all topological eigenvalues of a network, the channel vanishes earlier due to negative or complex eigenvalues.

Here, we have seen that the calculation of the slopes of the tongue borders allows us to study the presence of stable channels between tongues. This is particularly useful if several topological eigenvalues need to be considered.

4.1.5 Summary

We derived a parametric representation of the bifurcation lines in the (τ, δ) -delay space for degree-homogeneous networks. For these networks, the topology dependence is given by the eigenvalues of the adjacency matrix and each eigenvalue can in principle give rise to bifurcation lines, which are independent of the other eigenvalues. However, only those eigenvalues c give rise to bifurcation lines that satisfy the condition $|c| > c^*$, where c^* depends on the parameters of the system.

Each bifurcation line is part of a set of bifurcation lines that is $2\pi/\omega$ -periodic in the τ and in the δ delay, where ω is the imaginary part of the eigenvalue that is purely imaginary on the bifurcation line (Sec. 4.1.2). We enumerate the bifurcation lines of such a set by the integers r and s , so that the bifurcation line (r, s) can be obtained by shifting the bifurcation line $(0, 0)$ by $2\pi r/\omega$ along the τ -axis and by $2\pi s/\omega$ along the δ -axis.

For $c^* < -|c|$, bifurcation lines of the same index r constitute a connected bifurcation line ranging from $\delta = 0$ to infinity. Thus these lines are vertically aligned in the (τ, δ) -plane. Right to the leftmost of these lines, networks are unstable. For $-|c| < c^* < |c|$, each bifurcation line (r, s) borders a tongue of instability, whose two ends approach infinitely large delays τ and δ . Between these tongues, stable channels can exist (Sec. 4.1.1).

The tongues of instability can be characterized by the slopes of the two ends of the bordering bifurcation line and by the tip, which we define to be the point on the bifurcation line for which ω becomes maximal. The tips provide us information about the stability for small delays, whereas the slopes of the tongue borders provide us information about the stability for large delays. Thus, the slopes of the tongue borders tell us if stable channels between tongues are possible (Sec. 4.1.4).

The tip position also provides us information about the underlying topological eigenvalue. The complex phase ψ^c of the eigenvalue c is given by the tip position (τ, δ) through $\psi^c = (\delta - \tau)/\omega$. Thus, all tongues with tips on the diagonal $\tau = \delta$ arise because of real negative eigenvalues (Sec. 4.1.3).

This section dealt with the relation between a single topological eigenvalue and the corresponding bifurcation lines in the delay-space. But the stability of a network

can in principle depend on the full eigenvalue spectra. However, we already saw that eigenvalues violating the condition $|c| < c^*$ do not give rise to bifurcation lines. Further, some eigenvalues may give rise to bifurcation lines but may not influence the stability of the network. In order to get some basic insights into the stability of networks, we study the bifurcation lines of full eigenvalue spectra of some networks in the following sections.

4.2 Tongues and topology

In the previous sections, we studied the properties of the bifurcation lines for a given topological eigenvalue c . However, the adjacency matrix of networks has more than just one eigenvalue. Even though the bifurcation lines of different eigenvalues are independent of each other and thus can be studied separately, all bifurcation lines need to be considered to determine the stability of the system. In this section, we start with the stability analysis of a fully-connected network, including a discussion about the influence of the growth elasticities g' , which can be easily extended to other parameters. Next, by considering some special networks, we see that symmetric spectra of the topological eigenvalues give rise to symmetric stability patterns in the delay space. Finally, we discuss general stability properties of undirected networks.

4.2.1 The fully-connected network

The stable areas of a fully-connected network are bordered by the bifurcation lines of the topological eigenvalues $c = d = N - 1$ and $c = -1$, which is $N - 1$ times degenerated. But all degenerated eigenvalue give rise to the same bifurcation lines. Thus, we only need to consider the two different eigenvalues $c = d$ and $c = -1$. In order to investigate the parameter dependence of the tongues of instability, we calculate the slopes of some tongue borders for large delays.

Figure 4.6(a) shows the slope of some tongues of a fully-connected network with $N = 3$ nodes. Further, the bifurcation lines are shown for four different values of g' . The topological eigenvalues of a fully-connected network with $N = 3$ nodes are $c = d = 2$ and $c = -1$. The tongues of the eigenvalue $c = d$ emerge for $g' \leq l' = -1$, but are not visible for $g' = -1$, because they are shifted towards infinitely large delays and they are infinitely narrow. Analogously, the diagonal $\tau = \delta$ is stable (Fig. 4.6(b)) for $g' = -2$, even though figure 4.6(a) suggest that a tongue of the eigenvalue $c = -1$ exist, whose borders have the slope 1 and should therefore cover parts of the diagonal.

When further decreasing g' below $g' = -2$, the tongue $(0, 0)$ of the eigenvalue -1 broadens and moves to smaller delays (Fig. 4.6(c)). We already discussed that the tip of this tongue lies on the diagonal. Further, we see from (Fig. 4.6(a)) that this tongue opens around the diagonal and hence quickly closes the stable channel. For $g' = -4$ (Fig. 4.6(d)), the tongues for the eigenvalue $c = -1$ start to merge.

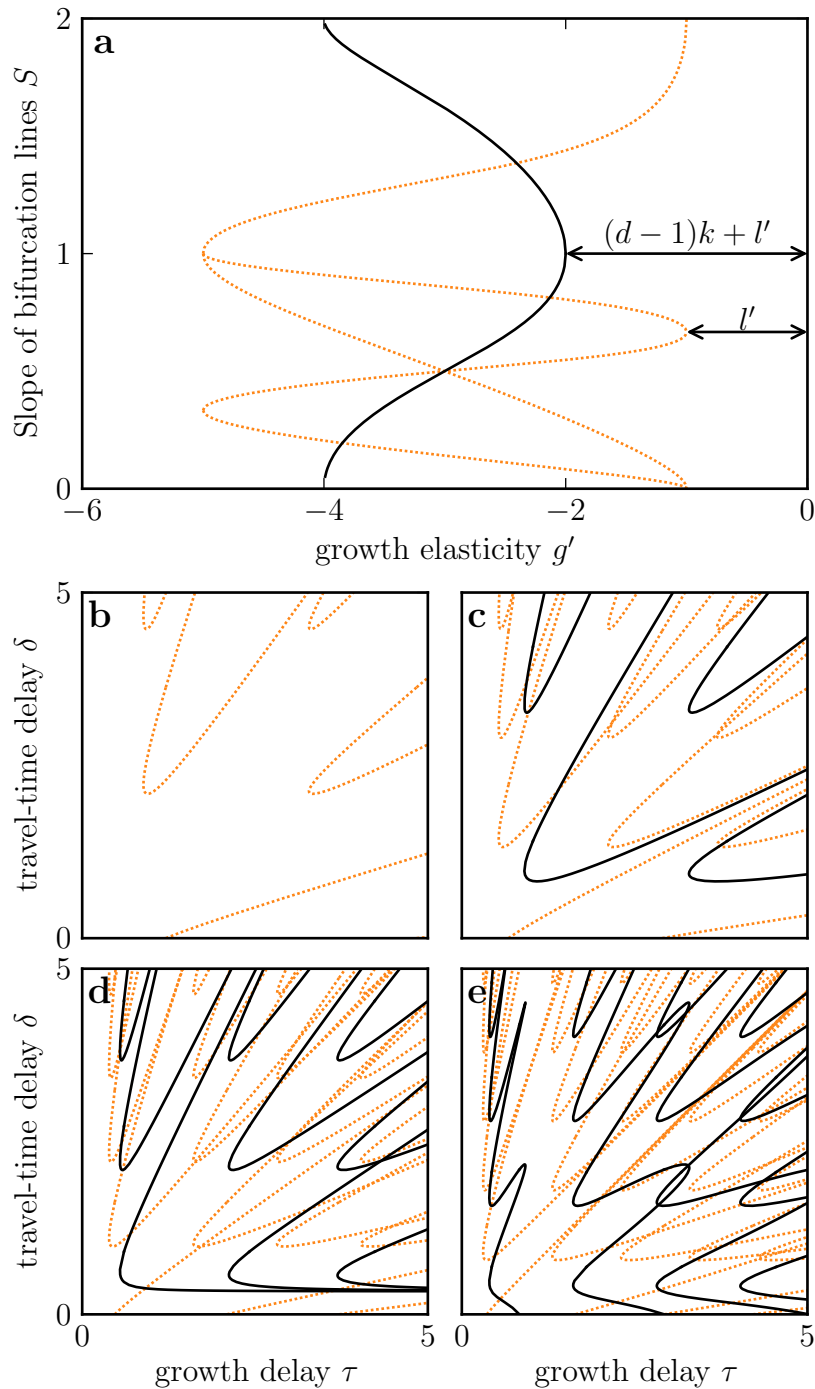


Figure 4.6: Bifurcation lines in the delay space ($g' = -2, -3, -4, -5$ (b-e)) and their asymptotic slopes (a) for a fully-connected network with $N = 3$ nodes. The slopes show when tongues emerge (at $g' = -1$ and $g' = -2$ for $c = d$ (dashed orange line) and $c = -1$ (solid black line)), when they merge (at $g' = -5$ and $g' = -4$), and when they close stable channels between them (e.g. $g' = -3, S = 0.5$). Other parameters are $l' = 1, k = 1$.

But stable channels might still exist, because the borders of neighboring tongues are parallel. However, all these channels are already covered by the tongues of the eigenvalue $c = 2$. For $g' = -5$ (Fig. 4.6(e)), the tongues of eigenvalue -1 already merged and constitute connected bifurcation lines, so that no stable channels are possible. Also the tongues of the eigenvalue 2 start to merge. But without the eigenvalue $c = -1$, there would be a stable channel around $\tau = \delta$.

In this example, it seems like stable channels may only appear in a narrow parameter window. The range in g' from the emergence to the merging of the tongues of the eigenvalue $c = 2$ is 4 and most stable channels are covered by the emerging tongues of the eigenvalue $c = -1$. However, the range in g' between emergence and merging of tongues of an eigenvalue c is $2|c|k$ (Fig. 4.5(b)). The center of this area is at $g = -dk - l$ and hence independent of c (Fig. 4.6(a)). For a fully-connected network this means that the range in g' between the first emergence of the tongues of the positive eigenvalue d and the emergence of tongues of the negative eigenvalue $c = -1$ is given by $(d - 1)k$. Thus, the parameter range in which stable channels can exist increases with the degree d .

We have seen that the analysis of the slopes of tongue borders allows us to study the exists of stable channels between tongues. Even if several topological eigenvalues give rise to bifurcation lines, the parameter regions in which stable channels exist can be easily obtained from figures plotting the slopes against the parameters. Further, even eigenvalues that give rise to bifurcation lines often do not influence the stability of the network and can therefore be neglected. This is discussed in more detail in the following sections.

4.2.2 General properties of undirected networks

Most networks that are studied throughout this thesis are undirected. This sections discusses some general properties of the spectra, the bifurcation lines, and the stability of undirected networks.

For unidirectional networks, the adjacency matrix is symmetric and the topological eigenvalues are real. In this case, the condition $|c| > c^*$ constitutes a separation of positive and negative eigenvalues. Because the tips of the tongues (i, i) of negative eigenvalues are always located at the diagonal $\tau = \delta$, we refer to these sets of tongues as diagonal sets (DS), whereas the sets of tongues arising from positive eigenvalues are referred to as off-diagonal sets (OS).

The complex phase is either 0 for positive or π for negative eigenvalues. Thus, different OS and different DS only differ in the absolute values of c . Therefore, it is interesting to study the influence of different absolute values of c while the complex phase ψ^c is fixed to 0 or π .

Figure 4.7(c) shows the tongues of instability of the network shown in figure 4.7(a). For the chosen parameters, only two positive and two negative eigenvalues give rise to tongues of instability, because the other eigenvalues violate the condition $|c| > c^* = 1$ (Fig. 4.8(b)). Note that the eigenvalue -1 appears twice, so that the

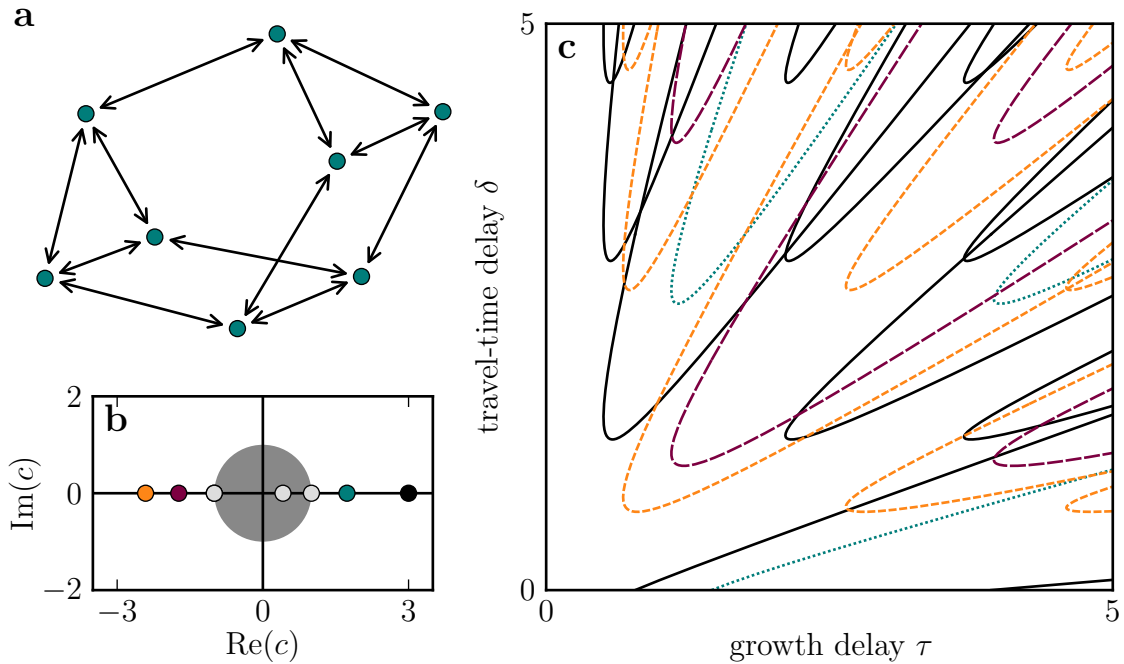


Figure 4.7: Topological eigenvalues (b) and tongues of instability (c) of the undirected network shown in (a). The parameters used in (c) are $g' = -2, l' = 0, k = 1$. For these parameters, there are only two positive and two negative eigenvalues that give rise to tongues (outside the unit circle). The two positive eigenvalues give rise to the off-diagonal sets of tongues (solid black and dotted green lines). The two negative eigenvalues to the diagonal sets (dashed orange and long dashed violet lines). The tongues of the eigenvalues with the smaller absolute value (dotted green and long dashed violet lines) lie inside the tongues of the other eigenvalue with the same sign. Thus, only the largest positive and the smallest negative eigenvalue govern the stability of the network.

total number of eigenvalues equals the number of nodes $N = 8$. The tongues of the smaller positive eigenvalue lie completely inside the tongues of the larger positive eigenvalue. Similarly, the tongues of the larger negative eigenvalue lie inside the tongues of the smaller negative eigenvalue. Thus, only the largest positive and the smallest negative eigenvalue determine the stability border.

From figure 4.7(c), we followed that the bifurcation lines of an eigenvalue c_1 , which has the same complex phase ψ^c but a smaller absolute value than another eigenvalue c_2 , lie inside the unstable area bordered by the bifurcation lines of the eigenvalue c_2 . In section 4.5.2, we will see that this is not true in general. Nevertheless, when considering that each undirected degree-homogeneous network has at least one positive eigenvalue, $c = d$, and at least one negative eigenvalue that is smaller or equal to -1, the final conclusion that the stability is only governed by the largest positive and the smallest negative eigenvalue seems to be true in general.

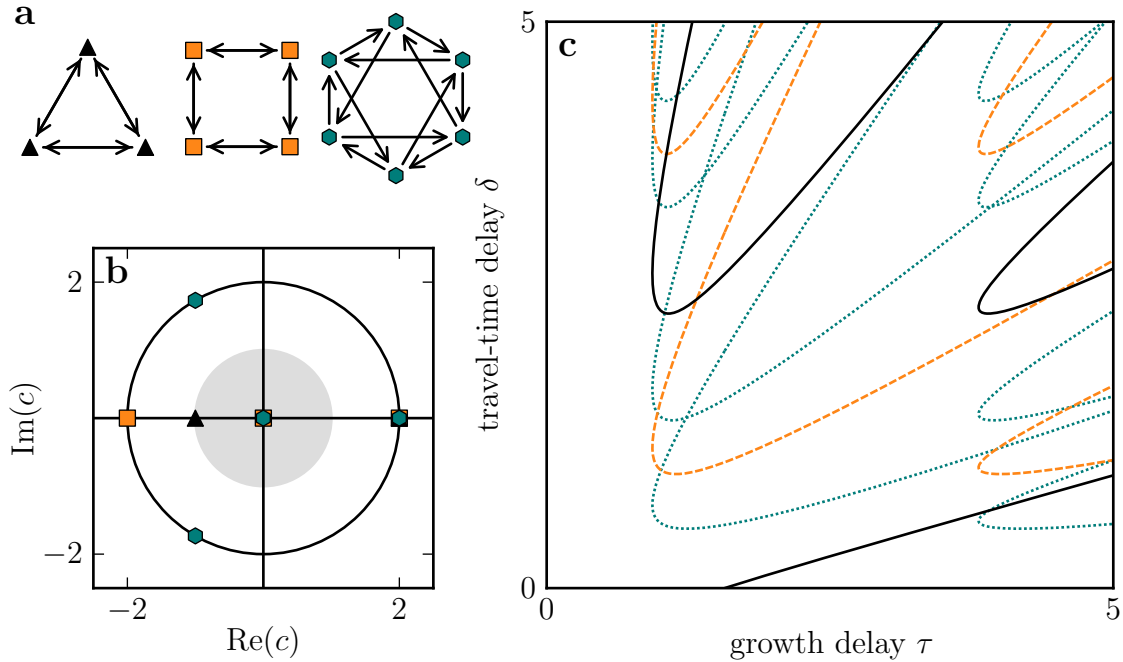


Figure 4.8: Symmetries in the spectra and in the delay space. The symbols in (b) represent the topological eigenvalues of the corresponding networks in (a). All networks share the eigenvalue $c = d = 2$. Eigenvalues inside the gray circle don't give rise to tongues. (c) The tongues of the eigenvalue $c = d$ (solid black line) appears in all networks. The second set of tongues of the square network is shifted by π/ω (dashed orange lines) along the δ -axis. The two other sets of the hexagon network are shifted by $2\pi/3\omega$ and $4\pi/3\omega$ (dotted green lines) with respect to the $c = d$ set. The complex phase ψ^c shifts the tongues along the δ -axis. Other parameters are $g' = -1, l' = 0, k = 1$.

In undirected networks, the stability seems to be governed only by the largest positive and the smallest negative eigenvalue. Thus, we may ignore all but these two eigenvalues. Similarly, we may ignore complex topological eigenvalues as they arise in directed networks, if there exists another eigenvalue with the same complex phase ψ^c but a larger absolute value. However, in directed networks, the complex phase of the eigenvalues is not restricted to two values. Thus, we may have to consider more than just two eigenvalues to study the stability. An example of such a situation can be found in the next section.

4.2.3 Symmetries in spectra and delay space

We already noted that there is a direct connection between the topological eigenvalues of a network and the tongues of instability. Therefore, we expect that symmetries in the eigenvalue spectra give rise to symmetries in the tongue pattern. Here, we want to demonstrate this by comparing the eigenvalue spectra with the tongue patterns

for the three small networks shown in figure 4.8(a), which we denote as triangle, square and hexagon.

All three networks are degree-homogeneous and share the eigenvalue $c = d = 2$. The triangle network is a fully-connected network with $N = 3$ nodes. Beside of the eigenvalue $c = 2$ this network has two degenerated eigenvalue $c = -1$. However, these eigenvalues violate the condition $|c| > c^*$ and can be ignored. The square network is bipartite, and hence has a symmetric spectra with an eigenvalue $c = -2$. The other two eigenvalues are zero and do not give rise to bifurcation lines. The hexagon has three zero eigenvalues. The other three eigenvalues are at $2, 2 \exp\left(\frac{2\pi}{3}i\right)$ and $2 \exp\left(\frac{4\pi}{3}i\right)$. Thus, all eigenvalues of the three networks that give rise to bifurcation lines lie on a circle with radius 2 around the origin of the complex plane (Fig. 4.8(b)). Therefore, the eigenvalues only differ in the complex phase ψ^c .

As we have seen from the Eqs. (4.6-4.10), the complex phase ψ^c only shifts the bifurcation lines by ψ^c/ω along the δ -axis. Hence, the bifurcation lines of the eigenvalues $c = -2$ are shifted by π/ω with respect to the lines of the eigenvalue $c = 2$. Because tongues of a single topological eigenvalue already give rise to $2\pi/\omega$ -periodic bifurcation lines, the two eigenvalues 2 and -2 give rise to a π/ω -periodicity along the δ -direction. Similarly, the three eigenvalues with $|c| = 2$ of the hexagon network give rise to the $2\pi/3\omega$ -periodicity (Fig. 4.8(c)).

Note that the symmetries of the networks chosen in Fig. 4.8(a) are not the cause for the symmetries of the spectra. For instance, even non-symmetrical bipartite networks have a symmetric spectra and thus give rise to corresponding symmetries in the tongue patterns.

The symmetry of the spectra of degree-homogeneous bipartite networks give rise to an eigenvalue $c = -d$. Thus, we can expect that the dynamics emerging inside the corresponding tongues are related to the bipartite topology. A similar relation should exist for the complex eigenvalues of the hexagonal network. In contrast, the dynamics arising in tongues of the eigenvalue $c = d$ should not be related to any topological property except for the homogeneous degree. The dynamical states emerging inside individual tongues and inside overlapping tongues of different eigenvalues are studied in the following sections.

4.3 Dynamical states inside tongues of instability

The tongues of instability are related to the eigenvalues of the networks adjacency matrix. The corresponding eigenvectors point along the direction of the unstable perturbation. Therefore, an eigenvector of the adjacency matrix may provide information about the dynamical states arising if delays are chosen inside the corresponding tongues. In this section, we investigate the relation between the dynamical states and the corresponding tongues for a specific model of coupled Mackey-Glass systems. This also allows us to compare the analytical results for the generalized model to numerical simulations of a specific model.

It should be noted that once the steady state under investigation lost its stability other bifurcations that are not related to the steady state can change the dynamics of the system. Such bifurcations are not considered here. Thus, when changing parameters inside a tongue, we cannot expect the dynamics to remain qualitatively the same even if we do not cross any bifurcation line of the steady state. Therefore, in order to analyze the dynamics that is related to a certain tongue, we should choose delays close to the bifurcation line bordering the tongue. However, for the Mackey-Glass model we use here, we have not observed qualitative changes of the dynamics inside tongues.

In order to analyze the dynamical states arising inside tongues of instability, we simulate networks of delay-coupled Mackey-Glass systems described by the differential equations

$$\dot{X}_i = \frac{aX_i^\tau}{1 + (X_i^\tau)^b} - cX_i + \epsilon \sum_j (A_{ij}X_j - A_{ji}X_i), \quad (4.27)$$

with $a = 2, b = 10, c = 1, \epsilon = 10$. For these parameters and small delays τ , the isolated Mackey-Glass system has a stable steady state at $X = 1$. At $\tau = 0.471$, the steady state becomes unstable and the system evolves to a stable limit cycle. A sequence of period doubling bifurcation occurs for $1.33 < \tau < 1.68$. For most larger delays τ , the system shows chaotic attractors [113].

We want to study the homogeneous steady state of the network, for which $X_i = 1$. Thus, the normalization of the generalized modeling approach keeps the system unchanged and the elasticities are given by the derivatives of the functions with respect to X at $X = 1$, so that we obtain $g' = -4, l' = 1, k = \epsilon$.

4.3.1 Synchronous dynamics

Here, we study the case that the delays lie inside a single tongue, whereas the case in which the delays lie inside overlapping tongues is discussed in the next section.

Figures (4.9,4.10) show results for the bipartite square and the hexagonal network from figure 4.8(a). For each figure, subfigure (a) shows the bifurcation lines in the delay space and subfigures (b-d) show simulation results for some selected delay values marked in the delay space. The simulations are performed using the *pydelay* python tool [128]. In order to set the initial conditions, we need to define the history of the node loads X_i for $t < 0$. For this purpose, we set each point in the history to $1 + \xi$, where ξ is a uniform distributed random number between -0.5 and 0.5. Choosing the delays τ and δ outside tongues, the loads approach the steady state at $X_i = 1$ (Fig. 4.9(d)). Inside tongues, oscillatory dynamics emerge.

The tongues of the eigenvalue $c = d = 2$ are present in the square and in the hexagon network. The corresponding eigenvectors are of the form $(1, \dots, 1)$. They describe perturbations in which all nodes behave identical. Because all other possible perturbations decrease, we expect the system to show in-phase synchronization. In fact, choosing the delay pair $\tau = 0.25, \delta = 0.55$, which lie inside the tongue $(0, 1)$ of

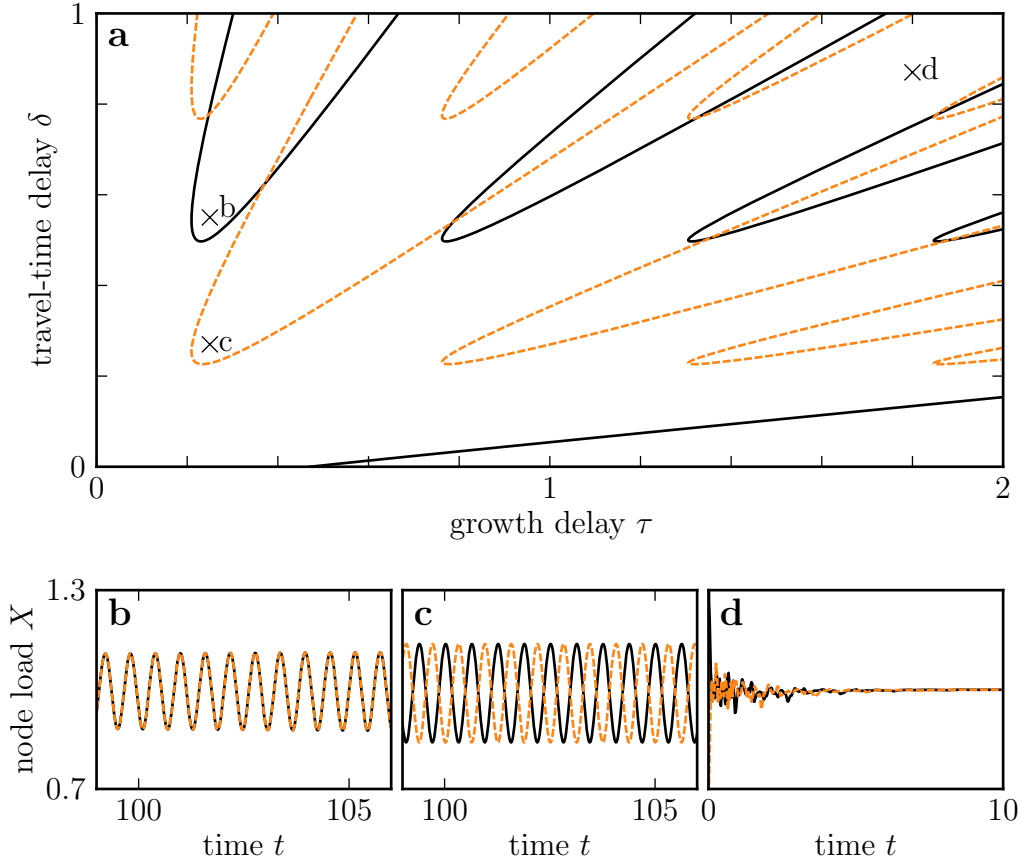


Figure 4.9: Dynamical states inside tongues of the bipartite square network from Fig. 4.8(a). (a) Tongues of instability of the topological eigenvalues $c = 2$ (solid black lines) and $c = -2$ (dashed orange lines). (b-d) Time-evolution of the square network of delay-coupled Mackey-Glass systems. Shown are the loads X_i for two neighboring nodes and the delays $\tau = 0.25, \delta = 0.55$ (b), $\tau = 0.25, \delta = 0.27$ (c) and $\tau = 1.8, \delta = 0.87$ (d). The three delay-tuples are marked in (a). The first two lie inside the tongues of the eigenvalue $c = d$ and $c = -d$, respectively. The last tuple lies outside tongues and the system evolves to the steady state (d). For the other delays, we observe in-phase (b) and anti-phase (c) synchronization.

the eigenvalue $c = d$, the simulation results show that the node loads oscillate in phase (Fig. 4.9(b), Fig. 4.10(b)).

Now we consider tongues of the eigenvalue $c = -d$ of the bipartite square network. Enumerating the nodes of the square network counter-clockwise, the corresponding eigenvector $(1, -1, 1, -1)$ hints to a dynamical state in which neighboring nodes oscillate in anti-phase. Indeed, we observe such oscillations for the delays $\tau = 0.25, \delta = 0.27$, which lie inside the tongue $(0, 0)$ of the eigenvalue $c = -2$ (Fig. 4.9(c)).

We already noted that the symmetric spectra, and therefore the eigenvalue $c = -d$, is related to the bipartite topology of the network. In bipartite networks, we can

mark the nodes with two different colors so that there are only links between nodes of different colors. In-phase synchronization is likely to appear in all topologies, because in such a state, all nodes get the same input from their neighbors and should therefore react in the same way. Similarly, anti-phase synchronization is likely to appear in bipartite networks. In such an anti-phase state, the nodes with the same color oscillate in synchrony. So, all nodes of the same color get the same input from their neighbors, which share the other color. Therefore, nodes of the same color should react identical to the identical input from their neighbors. In order to obtain self-amplifying oscillations, the phase shift between nodes of different colors should be either a full period, resulting in the in-phase state that occurs in all topologies, or half a period, resulting in the anti-phase state that is typical for bipartite networks. In the anti-phase state, the nodes of one color, let's say green, reinforce the anti-phase oscillations of the nodes of the other color, for instance red. The red nodes then reinforce the anti-phase oscillations of the green nodes, so that there is a positive feedback.

In the same way, we can explain the π/ω -periodicity of the tongues. Considering the in-phase synchronized state, the travel-time delay δ needs to be close to $2n\pi/\omega$, where n is an integer. Then the inflow and the internal oscillation of the nodes add up at least partially. If δ is reduced by π/ω , the inflow and internal oscillation partially cancel each other. However, if neighboring nodes are oscillating in anti-phase the inflow adds to the internal oscillation again.

For bipartite networks, in-phase and anti-phase oscillations are similarly likely in some sense. However, when adding links between nodes of the same color, these links damp the oscillations of the connected nodes in the anti-phase state but will support the oscillations in the in-phase state. Hence, we expect the tongues causing the anti-phase oscillations to vanish.

Finally, we want to discuss the dynamical states emerging at the two sets of tongues of the hexagonal network that arise because of the eigenvalues $c = d \exp\left(\frac{2\pi}{3}i\right)$ and $c = d \exp\left(\frac{4\pi}{3}i\right)$. The corresponding eigenvectors are given by \mathbf{v} with $v_n = \exp\left(\frac{2\pi}{3}ni\right)$ and $v_n = \exp\left(\frac{4\pi}{3}ni\right)$, respectively. Again, the nodes of the networks are enumerated counter-clockwise. Thus, nodes i and $i + 3$ are in synchrony, whereas neighboring nodes are separated by a phase shift of $2\pi/3$. The two different synchronous states can be interpreted as clockwise and counter-clockwise traveling waves (Fig. 4.10(c,d)).

The δ -shift of the tongues of the eigenvalues $c = d \exp\left(\frac{2\pi}{3}i\right)$ and $c = d \exp\left(\frac{4\pi}{3}i\right)$ with respect to the tongues of $c = d$, and the phase shifts between nodes can be explained in a similar way as for the bipartite network, by noting that the nodes of the hexagonal network can be marked by three different colors, so that nodes of one color only get inflow from nodes of a certain other color.

We have seen that symmetries in the topological eigenvalues are related to certain network properties, which can give rise to characteristic dynamics. For instance, anti-phase oscillations are likely to appear in bipartite networks. Since, we can relate tongues of instability to the different eigenvalues, we can also relate characteristic dynamics as in-phase and anti-phase synchronized states to the different tongues.

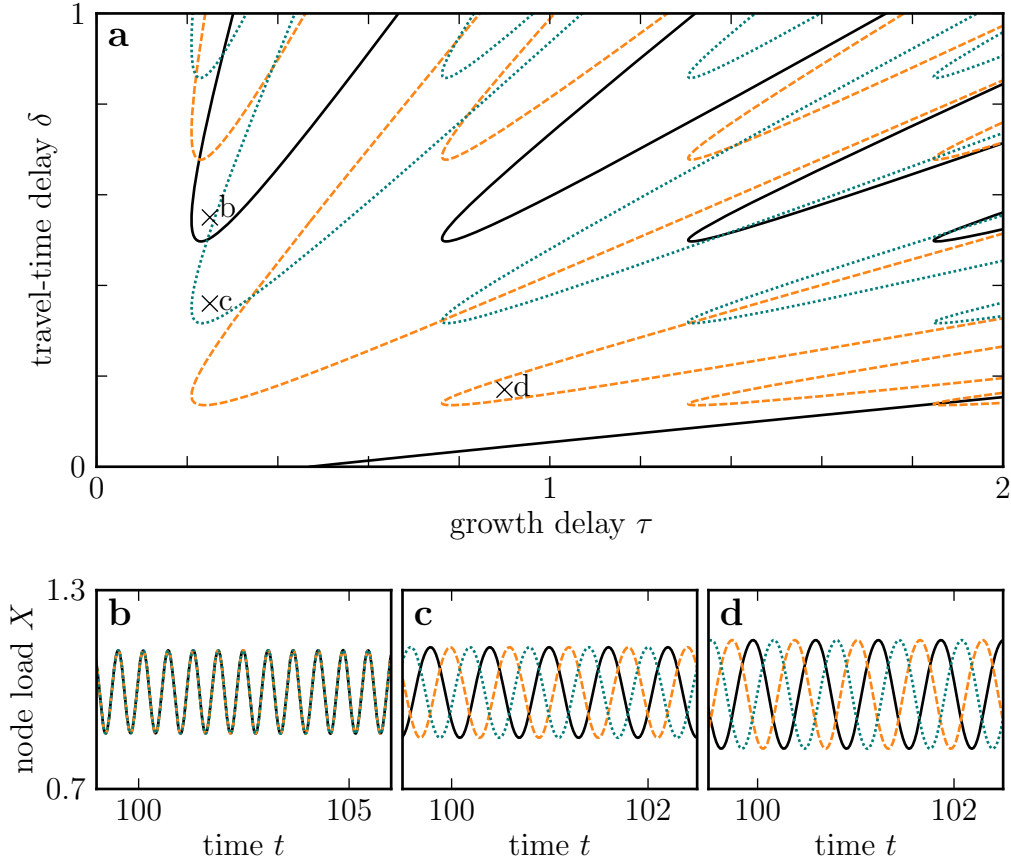


Figure 4.10: Dynamical states inside tongues of the hexagon network from Fig. 4.8(a). (a) Bifurcation lines of the topological eigenvalues $c = 2$ (solid black lines), $c = 2 \exp(2\pi i/3)$ (dashed orange lines) and $c = 2 \exp(4\pi i/3)$ (dotted green lines). (b-d) Time-evolution of a hexagonal network of delay-coupled Mackey-Glass systems. Shown are the loads X_i for three neighboring nodes and the delays $\tau = 0.25, \delta = 0.55$ (b), $\tau = 0.25, \delta = 0.36$ (c) and $\tau = 0.9, \delta = 0.17$ (d). The three delay values are marked in (a). Again the eigenvalue $c = d$ gives rise to synchronized dynamics. For the other two eigenvalues, neighboring nodes oscillate with a phase shift of $2\pi/3$, resembling clockwise and counter-clockwise traveling waves.

4.3.2 Multistability inside overlapping tongues

In the previous section, we studied the dynamical states evolving inside a single tongue. Here, we study the dynamical states for delays inside overlapping tongues. For this purpose, we consider the bipartite square network from the previous section and choose the delays $\tau = 0.46, \delta = 0.75$, so that they lie inside a tongue of the eigenvalue $c = 2$ and inside a tongue of the eigenvalue $c = -2$ (Fig. 4.11(a)).

Choosing random initial conditions such as in the previous section, we may observe irregular oscillations as shown in (Fig. 4.11(b)). However, for different simulations

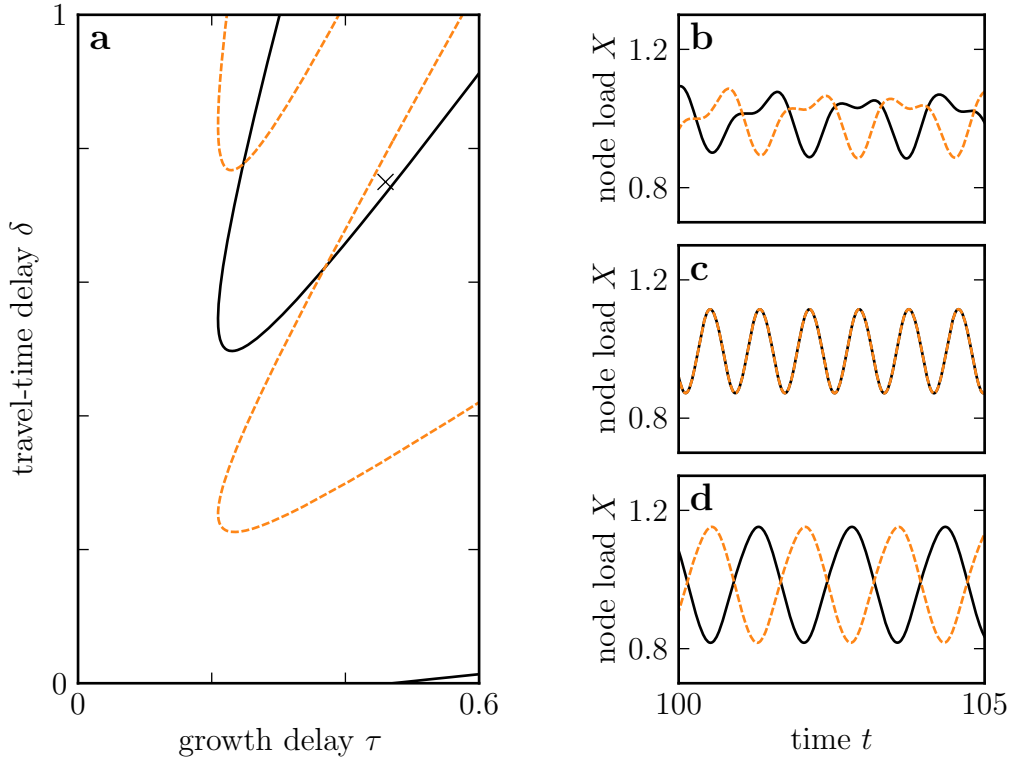


Figure 4.11: Dynamical states inside overlapping tongues. (a) Bifurcation lines of the topological eigenvalues $c = 2$ (solid black lines) and $c = -2$ (dashed orange lines). (b-d) Time-evolution of a square network of delay-coupled Mackey-Glass systems for three different initial conditions. Shown are the loads X_i for two neighboring nodes and the delays $\tau = 0.46, \delta = 0.75$, which lie inside the tongue $(0, 1)$ of the eigenvalue $c = 2$ and inside the tongue $(0, 0)$ of the eigenvalue $c = -2$ (a). (b) Noisy initial conditions such as for figures (4.9, 4.10). (c) In-phase initial conditions. (d) Anti-phase initial conditions. Initializing the system with in-phase or anti-phase synchronized states, the synchronization remains unchanged. For noisy initial conditions more irregular dynamics can emerge.

runs, we can observe various dynamics that may resemble in-phase or anti-phase synchrony. Initializing the node history with in-phase (Fig. 4.11(c)) and anti-phase (Fig. 4.11(d)) oscillations, we find that the phase relations are maintained. For figure 4.11(c), we defined the history of the node with $X_i = 1 + 0.5 \sin(t)$. For figure 4.11(d) we redefined the history of the even nodes with $X_i = 1 - 0.5 \sin(t)$. Both figures show stable oscillatory dynamics, which differ in the phase relation between nodes. Thus, depending on the initial conditions, we find multiple stable dynamical states.

If delays are shifted so that they are close to a tongue border, the two corresponding eigenvalues of the Jacobian have a real-part close to 0. Hence, the positive eigenvalues of the other tongue will dominate the dynamics. For instance, if the delays are

chosen close to the border of the in-phase tongue of the eigenvalue $c = d$ but well inside the anti-phase tongue of the eigenvalue $c = -d$, we can expect the emergence of anti-phase synchronization when starting with random initial conditions.

If the real-parts of all eigenvalues of the Jacobian are similar, it is more likely to observe irregular dynamics such as in figure 4.11(b). Close to the intersection of two tongue borders, we may even expect chaotic behavior, because it is known that chaotic dynamics are generically present close to double Hopf bifurcations [11, 32].

Here, we studied dynamical states for delays which lie inside overlapping tongues. Depending on the initial conditions, we may observe dynamical states that are characteristic for the one or the other tongue. However, we may also observe more irregular dynamics, which may also include chaotic dynamics.

4.4 Stabilizing and destabilizing coupling

At the end of our analysis of the bifurcation lines in the delay space for degree-homogeneous networks, we want to compare the stability of a network with the stability of a single node system. Thus, we can investigate under which conditions the coupling has a stabilizing or destabilizing effect.

The stability of an isolated node has been studied in section 3.3. The bifurcation lines in the (τ, δ) -plane are straight vertical lines at τ_r^* (Eq. (3.15)). The stability transition occurs at $\tau^* = \tau_0^*$. Bifurcations only exist for $g' < -l'$, which is identical to the condition for the existence of bifurcation lines, $c^* < |c|$, for a topological eigenvalue with $|c| = d$.

Figure 4.12 compares the bifurcation lines of a fully-connected network with $N = 3$ nodes with the bifurcation lines of a single node. For the chosen parameters, only the topological eigenvalue $c = d = 2$ gives rise to tongues of instability, whereas the two times degenerated eigenvalue $c = -1$ of the fully-connected network violates the condition $|c| > c^*$.

We know from section 3.4 that all bifurcation points of the single node system are also bifurcation points for networks with $\delta = 0$. Therefore, each point $(\tau_r^*, 0)$ must be crossed by a bifurcation line of the network system. Here, we see that in degree-homogeneous networks, these points are crossed by the bifurcation lines $(r, 0)$ of the eigenvalue $c = d$. However, corresponding bifurcation lines also have to exist in degree-heterogeneous networks. We denote the lines that cross the points $(\tau_r^*, 0)$ as *bottom bifurcation lines*. The line crossing $(\tau^*, 0)$ is also denoted as *bottom stability border*.

Since bifurcation lines are $2\pi/\omega$ -periodic in the delay space, degree-heterogeneous networks not only give rise to bottom bifurcation lines that correspond to the lines in the degree-homogeneous networks but they give rise to a whole set of tongues that corresponds to the tongues of the eigenvalue $c = d$. All these tongues need to obey the condition for existence of bifurcation lines for the single node system $g' < -l'$.

Beside the fact that the bifurcation delays τ_r^* of the single node system are identical

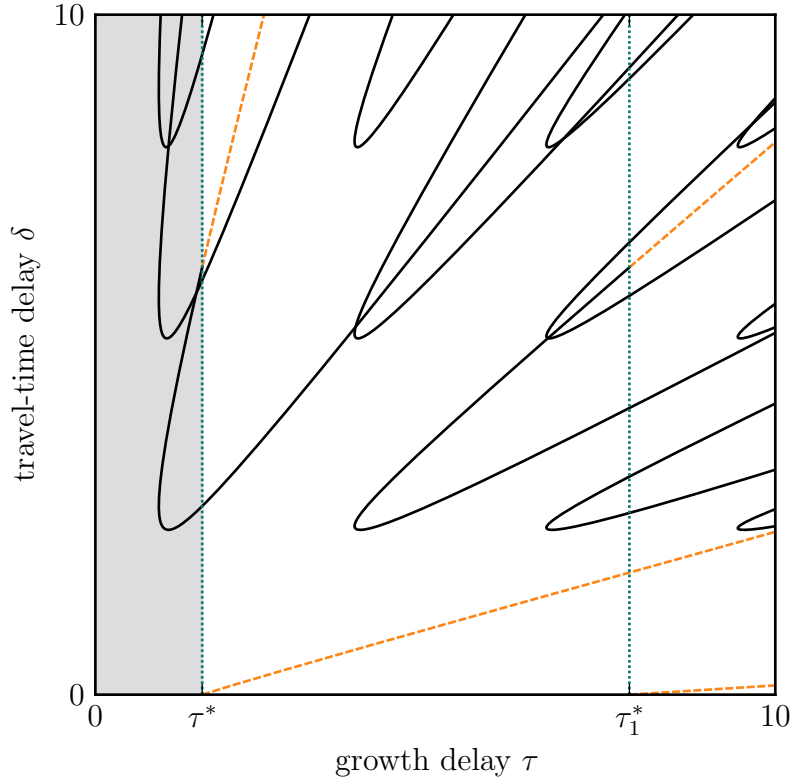


Figure 4.12: Comparison of the stability of a fully-connected network with $N = 3$ nodes (solid black lines for R-branch and dashed orange lines for L-branch) and a single node system (dotted green lines). The light gray area mark parameter values for which a single node system is stable, otherwise it is unstable. The bifurcation delays τ_r^* of the uncoupled system are identical to the delays for which the bottom tongues $(r, 0)$ of the eigenvalue $c = d$ cross the x-axis. Further, these delays separate the L- and the R-branch of tongues (r, s) connect. Even though, each topological eigenvalue gives rise to destabilizing tongues, the parameter space in which the coupling destabilizes otherwise stable nodes (inside tongues in gray area) is small compared to the areas in which the coupling is stabilizing (outside tongues in white area). Other parameters: $g' = -1, l' = 0, k = 1$.

to the delays at which the bifurcation lines $(r, 0)$ of the eigenvalue $c = d$ cross $\delta = 0$, τ_r^* also marks the border between the L- and the R-branch for the tongues (r, s) . Whereas the right border of the tongue is always described by the R-branch, the left border is described by the R-branch for $\tau < \tau_r^*$ and by the L-branch for $\tau > \tau_r^*$.

Finally, we want to compare the stability of the uncoupled system with the stability of the network system. The comparison of the stability areas in figure 4.12 shows that there are only small areas where the coupling destabilizes otherwise stable nodes. In contrast, the coupling stabilize unstable nodes in a comparable large area. The phenomena of the stabilization of an unstable steady state by diffusive coupling is known as amplitude death and is studied more intensely in the next sections.

When choosing an appropriate ratio between the delays τ and δ , stable systems can be found for arbitrarily large delays. However, for δ much larger than τ unstable nodes cannot be stabilized by the coupling. This might be related to the finding that chaos synchronization can never occur when the transmission delay is much larger than the characteristic time scale of the single node [105], which might be identified with the growth delay τ .

4.5 Bifurcation lines in the coupling space: Amplitude death

In mathematical models, amplitude death usually refers to the stabilization of an unstable steady state due to diffusive coupling [66]. This effect was first observed in coupled non-identical oscillators. Later, it was shown that amplitude death can occur in identical oscillators if the coupling is delayed [30]. In this section, we study amplitude death in systems of identical delay-coupled delay oscillators described by the Jacobian from Eq. (3.7). For this purpose, we calculate the stability borders in the (k, δ) -plane, while the growth delay τ is chosen so that the uncoupled subsystems are unstable.

In order to calculate the bifurcation lines in the (k, δ) -plane, we start with the Eqs. (4.4,4.5),

$$0 = g' \cos(\phi) - l' - dk + |c|k \cos(\psi), \quad (4.28)$$

$$\omega = -g' \sin(\phi) - |c|k \sin(\psi). \quad (4.29)$$

For $c = 0$, the equations are independent of ψ . Otherwise, Eq. (4.29) yields

$$\cos^2(\psi) = 1 - \frac{(\phi + g'\tau \sin(\phi))^2}{|c|^2 k^2 \tau^2} \quad (4.30)$$

By subtracting $|c|k \cos(\psi)$ from Eq. (4.28), squaring the resulting equation, and inserting Eq. (4.30), we obtain

$$(d^2 - |c|^2)k^2 \tau^2 - 2dhk\tau + f^2 + h^2 = 0, \quad (4.31)$$

with

$$f = \phi + g'\tau \sin(\phi), \quad (4.32)$$

$$h = (g' \cos(\phi) - l')\tau. \quad (4.33)$$

From Eq. (4.31), we see that the case $|c| = d$ needs to be treated separately from the case $0 < |c| < |d|$. The calculation of k for the three cases $c = 0$, $|c| = d$ and $0 < |c| < |d|$ is demonstrated below.

Once k is known, we can calculate δ by using the Eqs. (4.6,4.8,4.10), which provide the two branches

$$\delta^{\text{L,R}} = \frac{\psi^{\text{L,R}} + \psi_c + 2\pi s}{\phi} \tau, \quad (4.34)$$

with

$$\psi^{\text{L,R}} = \pm \cos^{-1} \left(\frac{d}{|c|} + \frac{l' - g' \cos(\phi)}{|c|k} \right). \quad (4.35)$$

By considering that $\psi^{\text{L}} > 0$, $\psi^{\text{R}} < 0$ and $k > 0$, we see from Eq. (4.29) that we need to apply the L-branch for $f < 0$ and the R-branch otherwise.

The topological eigenvalue $c = 0$

For $c = 0$, the Eqs. (4.28,4.29) are independent of ψ , respectively δ . Hence, the bifurcation lines in the (k, δ) -plane are vertical lines, so that we only need to calculate k . For this purpose, we set $c = 0$ in both equations and multiply Eq. (4.29) by τ and use $\phi = \omega\tau$. This provides

$$k = (g' \cos(\phi) - l')/d, \quad (4.36)$$

$$\phi = -g'\tau \sin(\phi) =: \Phi(\phi), \quad (4.37)$$

which is equivalent to

$$k = \frac{1}{\tau} \frac{h}{d}, \quad f = 0. \quad (4.38)$$

We are only interested in solutions with $k > 0$. Therefore, we restrict ϕ to the intervals $I_r^k = [\phi_r^k, \bar{\phi}_r^k]$, with $\phi^k = \cos^{-1}(l'/g')$ (Fig. 4.13(a)). Further, ϕ needs

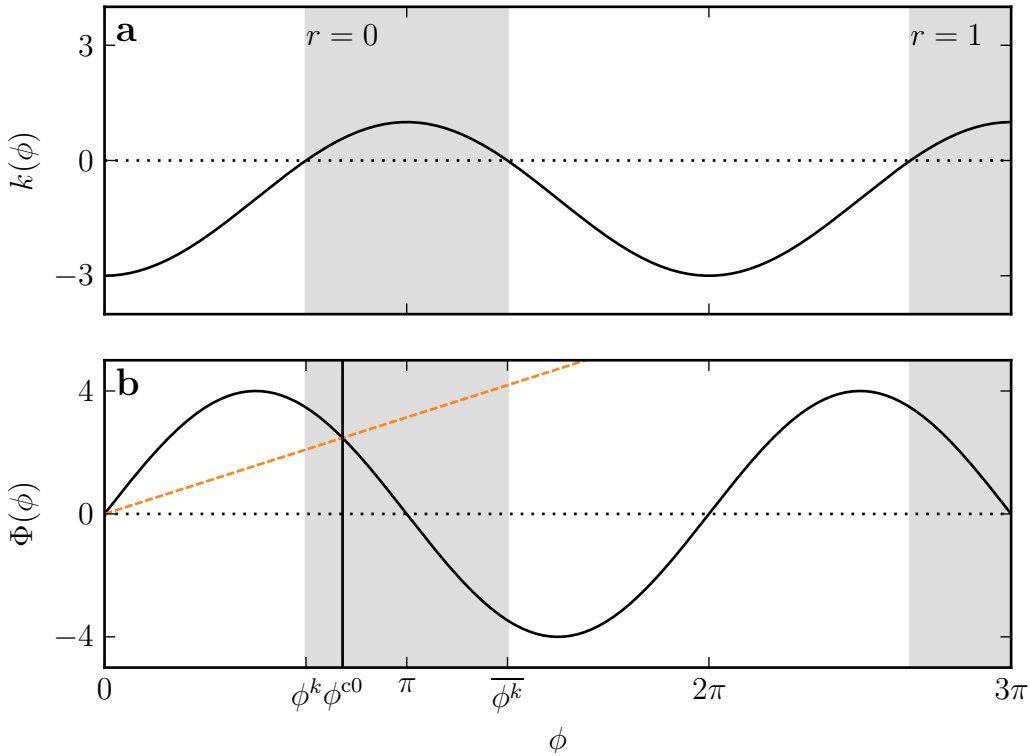


Figure 4.13: Calculation of the bifurcation lines in the (k, δ) -plane for $c = 0$. (a) According to Eq. (4.36), solutions with positive k only exist inside the interval $I_r^k = [\phi_r^k, \bar{\phi}_r^k]$, where $g' \cos(\phi) > l'$ (light gray areas). (b) The solutions $\phi^{c0,r}$ need to satisfy Eq. (4.37): $\Phi(\phi) = \phi$ (Φ : solid black, ϕ : dashed orange line). In order to find a solution inside an interval I_r^k , $\Phi(\phi_r^k)$ needs to be larger than ϕ_r^k . The value of ϕ_r^k can also be used as initial guess to obtain the solution numerically. Parameters: $g' = -2, l' = 1, k = 1, d = 1, \tau = 5$.

to satisfy the self-consistency condition from Eq. (4.37). $\Phi(\phi)$ is monotonically decreasing inside all intervals I_r^k (Fig. 4.13(b)). Thus, the largest value inside I_r^k is given by $\Phi(\phi_r^k) = \tau\sqrt{g'^2 - l'^2}$. Hence, valid solution inside I_r^k exist only if

$$\phi_r^k < \tau\sqrt{g'^2 - l'^2}. \quad (4.39)$$

By using $\tau^* = \phi^k / \sqrt{g'^2 - l'^2}$ (Eq. (3.15)), we see that an index r only provides a solution if

$$r < \frac{1}{2\pi}\sqrt{g'^2 - l'^2}(\tau - \tau^*). \quad (4.40)$$

Thus, in order to obtain at least one solution, τ needs to be larger than the critical delay τ^* that gives the stability border of a single node system. Hence, if the single node system is stable, topological eigenvalues $c = 0$ do not give rise to bifurcation lines and thus do not influence the stability in a network.

The solutions $\phi^{c0,r}$ can be found by applying a numerical root-finding algorithm to $\phi + g'\tau \sin(\phi)$ with the initial guess ϕ_r^k . Inserting $\phi^{c0,r}$ into Eq. (4.36) provides the solution k_r^{c0} .

In order to discuss the effect of amplitude death, we are most interested in the bifurcation line separating the stable and the unstable parameter space. A system can be stable for large k and is unstable if k is reduced below the largest k_r^{c0} .

In order to find the index r for which k_r^{c0} is maximal, we note that the functions $\Phi(\phi)$ and $k(\phi)$ are 2π -periodic. Thus, we can substitute $\phi^{c0,r}$ by $\phi^{c0,r} - 2\pi$ in the argument of the functions of Eq. (4.36,4.37), so that we obtain $\phi^{c0,r} = \Phi(\phi^{c0,r} - 2\pi r)$ and $k_r^{c0} = k(\phi^{c0,r} - 2\pi r)$. The arguments $\phi^{c0,r} - 2\pi r$ all lie inside I^k . Because $\Phi(\phi)$ is decreasing inside I^k and $\phi^{c0,r}$ is increasing with r , we find that $\phi^{c0,r} - 2\pi r$ is decreasing with r . Further, $k(\phi)$ is increasing inside I^k , so that k_r^{c0} also decreases with increasing r . Hence, the largest k_r^{c0} , which provides the stability border, is given by $k^{c0} = k_{r=0}^{c0}$.

In section 4.2.2, we suggested that the stability of an undirected degree-homogeneous network is governed only by the largest positive eigenvalue $c = d$ and the smallest negative eigenvalue, which is smaller than -1 . Thus, the eigenvalue $c = 0$ does not affect the stability of the network (see Sec. 4.5.2).

Topological eigenvalues with $|c| = d$

The case $|c| = d$ includes the particularly important eigenvalue $c = d$, which is present in all degree homogeneous networks. Further, eigenvalues $c = d \exp(i\psi^c)$ appear in degree homogeneous networks with special properties, such as in the square and the hexagonal network from figure 4.8.

For $c = |d|$, Eq.(4.31) yields

$$k = \frac{1}{\tau} \frac{f^2 + h^2}{2dh}. \quad (4.41)$$

In order to obtain positive solutions for k , h must be positive. Therefore, we need to choose $\phi \in I_r^k = [\phi_r^k, \bar{\phi}_r^k]$, with $\phi^k = \cos^{-1}(l'/g')$. Hence, as for the (τ, δ) -plane,

we find bifurcation lines for each index r . For every branch r , Eq. (4.34) provides infinitely many branches s and the different branches (r, s) can be identified with the tongues in the (τ, δ) -plane.

Figure 4.14(a) shows the bifurcation lines for the topological eigenvalue $c = d = 2$ in the (k, δ) -plane with $\tau = 5$. In the following, we denote the delay τ used for a (k, δ) -figure by T . By indexing the bifurcation lines with (r, s) , we can relate them to the tongues in the (τ, δ) -plane (Fig. 4.14(b,c)).

In section 4.1, we found that the tongues of the same index r and different indexes s are connected if $c^* < -|c|$. This condition can be translated into $k < k^m$, with

$$k^m = -\frac{g' + l'}{d + |c|}. \quad (4.42)$$

At $k = k^m$, the connection between different tongues is located at infinitely large delays, so that it isn't visible in the (k, δ) -plane, which only shows the bifurcation lines for $\tau = T = 5$. However, if k further decreases, the merged tongue borders approach the vertical bifurcation lines of the uncoupled system, which are located at τ_r^* (Fig. 4.14(c)). Hence, if $\tau_r^* < T$, the connection point of two tongues crosses T for some value of k . At this value of k , the bifurcation lines in the (k, δ) -plane connect. In this example, only τ_0^* is smaller than T . Therefore, we only see the merging of bifurcation lines with $r = 0$ in the (k, δ) -plane. The distinction between merging and non-merging bifurcation lines can be used to identify the stable areas. Stable areas can only be found inside merging bifurcation lines and only outside bifurcation lines, consisting of a single tongue border (r, s) .

The distinction between tongues with $\tau_r^* < T$ and $\tau_r^* > T$ also tells us if we have to consider the L- or the R-branch. As we saw in section 4.4, we always have to consider the R-branch for $T > \tau_r^*$. But for the merged bifurcation lines with $\tau_r^* < T$, only the lower border of a tongue (r, s) is described by the R-branch, whereas the upper part is described by the L-branch. Note, that in merged bifurcation lines in the (k, δ) -plane, the upper part of the bifurcation lines is actually the lower border of a tongue $(r, s + 1)$, whereas the lower part is the upper border of the tongue (r, s) . Hence, for merged bifurcation lines in the (k, δ) -plane, the upper part is described by the R-branch and the lower part is described by the L-branch.

Finally, note that for large k , bifurcation lines approach horizontal lines. Hence, the offset of these lines determine the stability of the system for large k . These offsets are calculated in section 4.5.1.

Topological eigenvalues with $0 < |c| < d$

For $0 < |c| < d$, Eq. (4.31) yields

$$k_{1,2} = \frac{1}{\tau} \frac{dh \pm \sqrt{a}}{d^2 - |c|^2}, \quad (4.43)$$

with

$$a = d^2 h^2 - (d^2 - |c|^2)(f^2 + h^2). \quad (4.44)$$

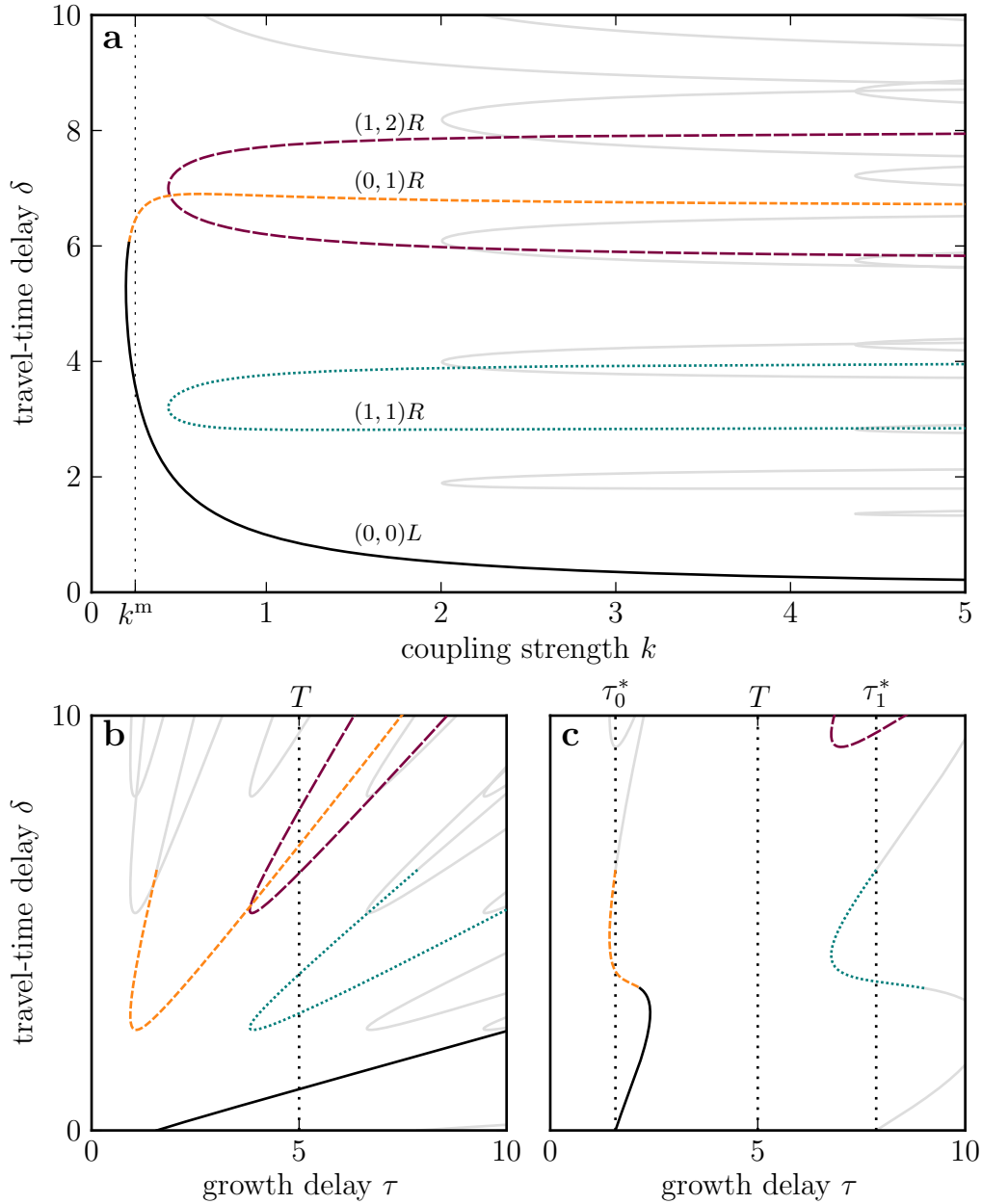


Figure 4.14: Bifurcation lines for $|c| = d$ in the (k, δ) -plane (a) and in the (τ, δ) -plane for $k = 1$ (b) and $k = 0.1$ (c). The delay τ used in (a) is denoted by T . For some bifurcation lines, the index pair (r, s) is given, and R and L denote the according branch. For $k < k^m = 1/4$, bifurcation lines with the same index r and different s merge. The merging of bifurcation lines with index r can only be observed in (a) if $\tau_r^* < T$. Other parameters are: $g' = -1, l' = 0, d = 2, \psi_c = 0, T = 5$.

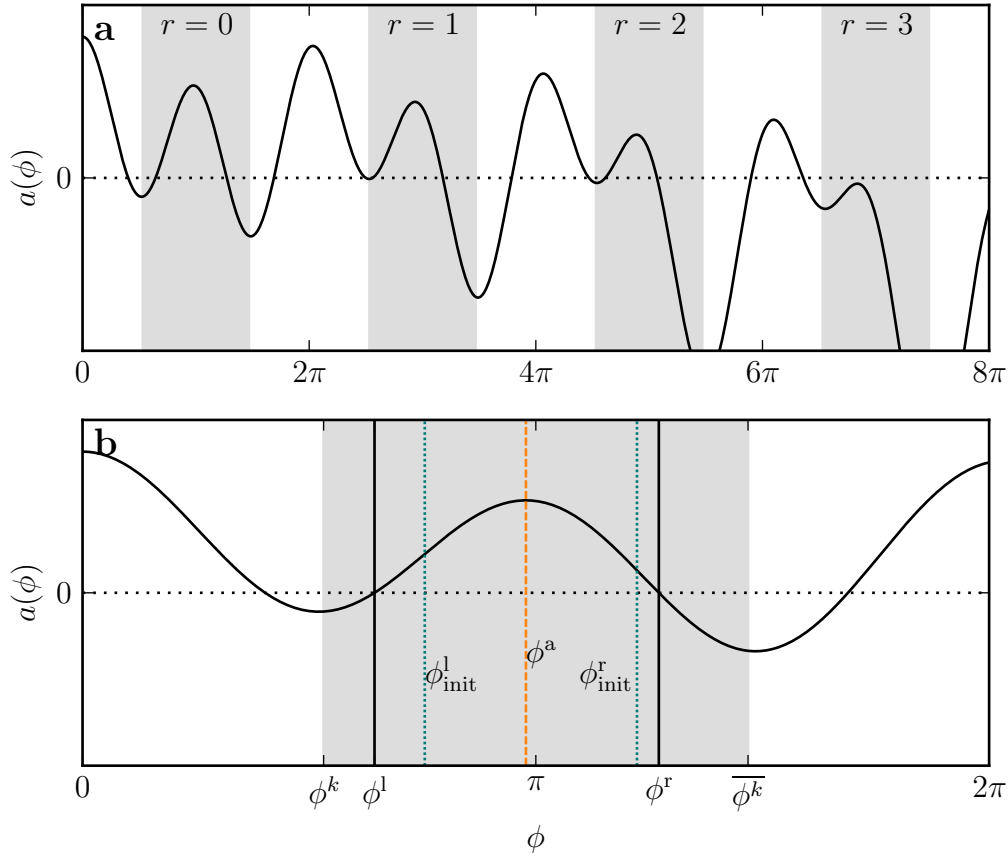


Figure 4.15: Calculation of the domain of $k(\phi)$. Positive real-valued solutions of k (Eq. (4.43)) only exist if $a > 0$ and if $h > 0$ (inside light gray areas). Thus, no solutions exist for large ϕ and r , respectively (a). (b) Zoom into interval $r = 0$. In order to estimate the domain borders ϕ^l and ϕ^r , we determine the maximum ϕ_a of a inside $I^k = [\phi^k, \bar{\phi}^k]$ and numerically estimate the roots of a with the initial guesses ϕ_{init}^l and ϕ_{init}^r , which are the center positions between ϕ_a and the interval borders of I^k .

In order to obtain real-valued solutions for k , a needs to be positive. In this case, we see from Eq. (4.44) that $\sqrt{a} < dh$ because $(d^2 - c^2)$ is positive. For $\sqrt{a} < dh$, both branches of k provide positive solutions if and only if $h > 0$. Thus, as for the case $|c| = d$, we need to restrict ϕ to the intervals I_r^k (gray areas in Fig. 4.15). But the condition $a > 0$ requires further restrictions on ϕ . The according intervals can be calculated numerically. In contrast to the case $|c| = d$, the interval size depends on r , and there is a maximum value of r for which solutions can be found.

Restricting ϕ to the intervals $I_r^k = [\phi_r^k, \bar{\phi}_r^k]$ is not sufficient to guarantee that $a > 0$. For each interval I_r^k , we need to estimate ϕ^l and ϕ^r , so that $a > 0$ for all $\phi \in [\phi^l, \phi^r]$. These intervals are denoted as I_r . The left and the right borders of the intervals, ϕ^l and ϕ^r , are calculated numerically (Fig. 4.15(b)). For this purpose, we numerically

estimate ϕ^a for which a becomes maximal inside the interval I_r^k . If the maximum is smaller than 0, no solutions exist inside the interval I_r^k . Otherwise, we numerically estimate the closest roots of a , ϕ^l and ϕ^r , by using the initial values ϕ_{init}^l and ϕ_{init}^r , respectively, with

$$\phi_{\text{init}}^l = (\phi^k + \phi^a)/2, \quad (4.45)$$

$$\phi_{\text{init}}^r = (\overline{\phi^k} + \phi^a)/2. \quad (4.46)$$

These values give the center between the maximum positions ϕ^a and the left and right border of the interval I^k .

We see from figure 4.15(a) that solutions inside intervals I_r^k only exist for small r , because $a(\phi) < 0$ for sufficiently large ϕ . We check for the existence of valid solutions by calculating the maximum of $a(\phi)$ inside each interval I_r^k . In general, we find that if a maximum is smaller than 0 for a certain interval r then also the maximum of intervals r' with $r' > r$ are smaller than 0. Hence, in order to find all valid solutions, we begin with $r = 0$ and increase r until no valid solutions can be found inside I_r^k .

Figure 4.16(a) shows the bifurcation lines in the (k, δ) -plane with $\tau = 5$. Again, we denote the delay τ used for the (k, δ) -figure by T . In comparison to the case $|c| = d$, we note that bifurcation lines do not approach horizontal lines for large k . Instead, the two ends merge, so that no bifurcation lines can be found for large k .

From section 4.1, we know that tongues disappear for $c^* > |c|$, this condition can be transformed into $k > k^e$ with

$$k^e = -\frac{g+l}{d-|c|}. \quad (4.47)$$

Thus, no bifurcation lines exist for $k > k^e$, so that no bifurcation line crosses the vertical line at k^e in figure 4.16(a). Hence, eigenvalues with $|c| < d$ cannot destabilize the system for coupling strength $k > k^e$.

Note that the bifurcation lines do not even reach to k^e , but only to a smaller value k_r^{max} , which depends on the tongue index r . This is because tongues do not simply vanish when k approaches k^e , but they move to infinitely large delays (cmp. Fig. 4.16(b,c)). At k_r^{max} , the tips of the tongues (r, s) cross T (Fig. 4.16(c)), so that the bifurcation line only reaches to k_r^{max} in figure 4.16(a).

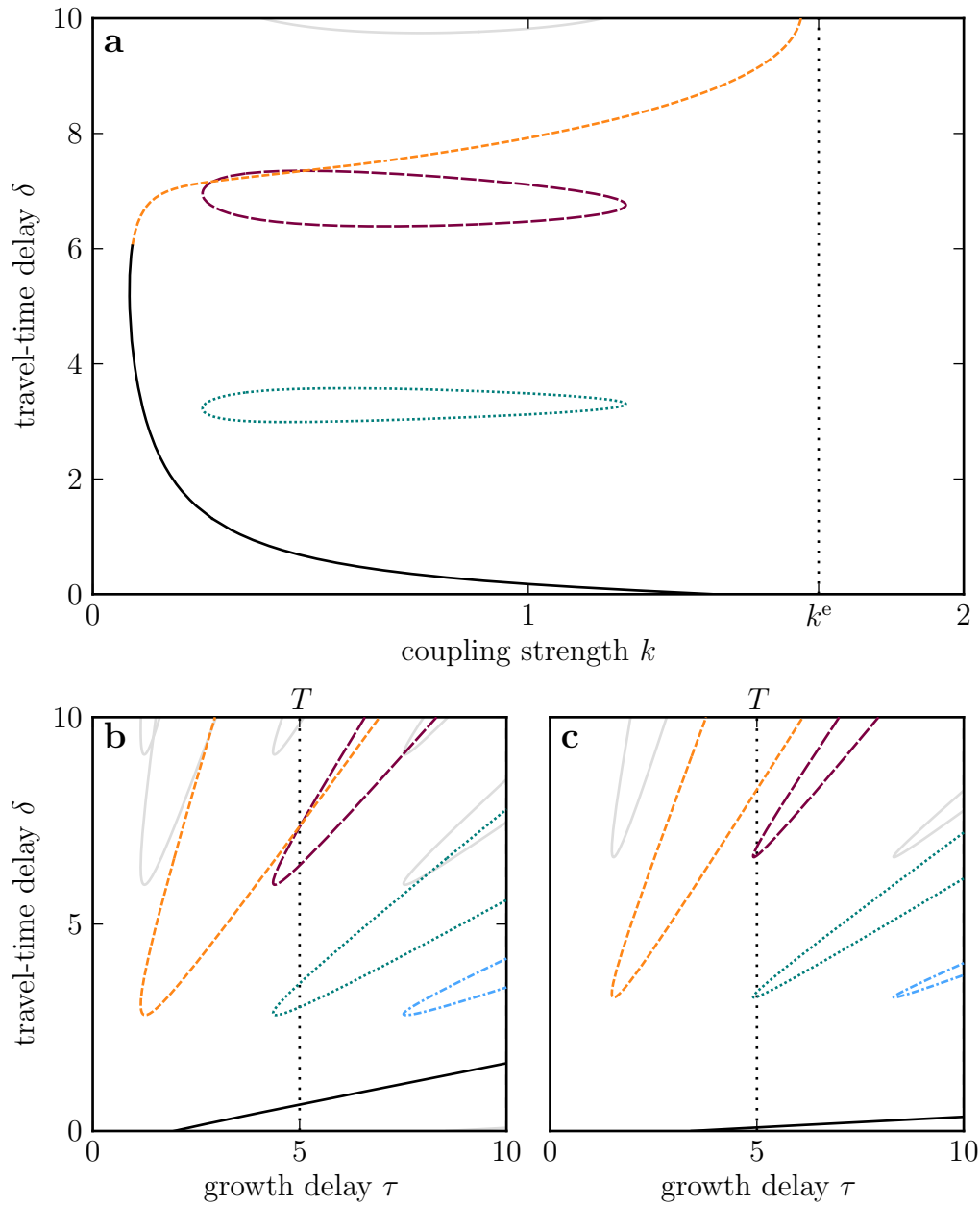


Figure 4.16: Bifurcation lines for $0 < |c| < d$ in the (k, δ) -plane (a) and in the (τ, δ) -plane for $k = 0.5$ (b) and $k = 1.2$ (c). The delay τ used in (a) is denoted by T . (b,c) Tongues in the (τ, δ) -plane vanish by moving to infinitely large delays if k approaches $k^e = 12/3$. However, bifurcation lines in (a) reach only to the value of k for which the tip of the according tongue in the (τ, δ) -plane crosses the vertical line at T (c). Other parameters are: $g' = -1, l' = 0, d = 5, c = 4.4, \psi_c = 0, T = 5$.

4.5.1 The limit of large coupling strength

We just found that topological eigenvalues with $|c| < d$ do not destabilize the system for coupling strength $k > k^e$. Hence, for sufficiently large k , we only need to consider topological eigenvalues with $|c| = d$.

For $|c| = d$, the two ends of a bifurcation line (r, s) in the (k, δ) -plane approach horizontal lines (Fig. 4.17(a)). The positions $\delta_{r,s}^t$ and $\delta_{r,s}^b$ of the top and bottom lines are given by the limits of the Eqs. (4.34,4.35),

$$\delta^{L,R} = \frac{\psi^{L,R} + \psi_c + 2\pi s}{\phi} \tau, \quad (4.48)$$

$$\psi^{L,R} = \pm \cos^{-1} \left(\frac{d}{|c|} + \frac{l' - g' \cos(\phi)}{|c|k} \right). \quad (4.49)$$

as ϕ approaches the left and the right domain borders, ϕ_r^k and $\overline{\phi_r^k}$. If ϕ approaches ϕ_r^k or $\overline{\phi_r^k}$, k diverges to infinity. Thus, $\psi^{L,R}$ approaches 0 and Eq. (4.48) provides

$$\delta_{r,s}^t = \frac{2\pi s + \psi^c}{\phi_r^k} \tau, \quad \delta_{r,s}^b = \frac{2\pi s + \psi^c}{\overline{\phi_r^k}} \tau. \quad (4.50)$$

The bifurcation points $\delta_{r,s}^{t,b}$ for large coupling strength k are independent of the network parameters d and $|c|$. Therefore, we might expect that these values are valid even for non degree-homogeneous networks. Further, τ enters Eq. (4.50) only as a multiplicative factor. Thus, bifurcation lines for systems with different τ might look similar if we rescale δ by τ . But for larger values of τ , additional tongues with larger r need to be considered, so that the rescaled stability patterns contains more bifurcation lines.

4.5.2 Amplitude death in networks

In order to study the phenomena of amplitude death, we only consider growth delays $\tau > \tau^*$ (Eq. (3.15)), so that the single node system is unstable. Hence, the uncoupled node may show oscillatory or chaotic behavior. By properly choosing the coupling strength k and the coupling delay δ , we might induce amplitude death, which stabilizes the whole network. But a network is stable only if none of the topological eigenvalues destabilizes the system. Therefore, the parameters for which amplitude death occurs need to be stable with respect to all topological eigenvalues.

General restrictions on amplitude death

The topological eigenvalue $c = d$ is present in all degree-homogeneous networks. Hence, amplitude death in an degree-homogeneous network can only occur in parameter regions, where the eigenvalue $c = d$ does not cause the system to be unstable. Therefore, the bifurcation lines of this eigenvalue provide a general restriction for the occurrence of amplitude death in degree-homogeneous networks.

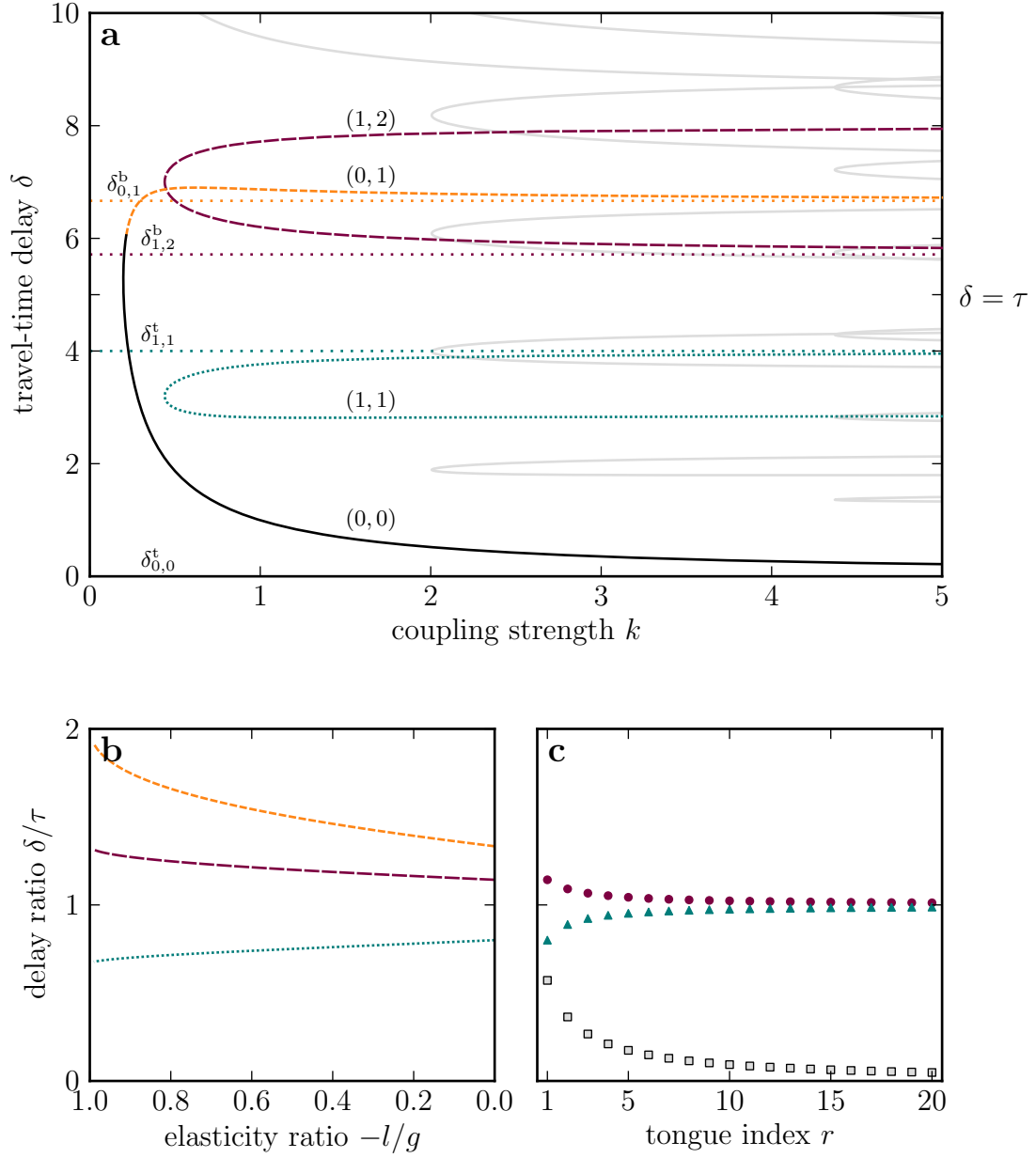


Figure 4.17: Bifurcations for large coupling strength k . (a) Bifurcation lines in the (k, δ) -plane for $|c| = d$. The ends of the bifurcation lines approach straight horizontal lines at $\delta_{r,s}^{b,t}$ (Eq. (4.34)). (b) Ratios $\delta_{r,s}^{b,t}/\tau$ for the three horizontal lines in (a) (line style as for the according tongues in (a)). (c) Limits $\delta_{r,r+1}^b$, $\delta_{r,r}^t$ and $\delta_{r,1}^b$ (circles, triangles, squares) for different tongue indexes r . Other parameters are: $g' = -1, l' = 0, c = d = 2, \psi_c = 0, \tau = 5$

For $c = d$, a stable area can exist inside the bifurcation line composed of the tongues $(0, 0)$ and $(0, 1)$ (Fig. 4.17(a)). The lower and upper part of the bifurcation line approach the lines at $\delta_{0,0}^t = 0$ and $\delta_{0,1}^b = 2\pi/\overline{\phi^k}\tau > \tau$ (Eq. (4.50)). The ratios of the $\delta_{r,s}^{b,t}$ and τ only depend on the ratios of the elasticities $-l/g$. In order to find tongues of instability, the ratio $-l/g$ needs to be between 0 and 1. In this range $\delta_{0,1}^b/\tau$ is between $4/3$ and 2 , whereas $\delta_{0,0}^t$ is always 0 (Fig. 4.17(b)). Even for small values of k , the bifurcation line of the tongue $(0, 1)$ is close to the limit value $\delta_{0,1}^b/\tau$. Thus, amplitude death does not occur for δ much larger than τ (cmp. Sec. 4.4).

Inside the potentially stable area between the tongues $(0, 0)$ and $(0, 1)$, other tongues can destabilize the system. With increasing k more tongues appear in the (k, δ) -plane. Many of these tongues overlap, so that no stable areas can exist between them. However, there are two stable channels that persist even for large k : The channel around $\delta = \tau$ and the channel close to $\delta = 0$, which lies above the bottom bifurcation line $(0, 0)$.

The stable channel at $\delta = \tau$ is bordered by the bottom border of the tongue $(r, r+1)$ and the top border of the tongue (r, r) . With increasing r the limits $\delta_{r,r+1}^b$ and $\delta_{r,r}^t$ approach 1 from below and above, respectively (Fig. 4.17(c)). Hence, the stable channel around $\delta = \tau$ becomes more narrow with increasing k but the line $\delta = \tau$ remains stable. When increasing l so that the ratio $-l/g$ increases from 0 to 1, tongues become smaller, so that the stable channel gets larger (Fig. 4.17(b)). However the qualitative behavior remains the same. Thus, in degree-homogeneous networks with $-l/g$ between 0 and 1, a stable channel at $\delta = \tau$ can exist but this channel becomes arbitrarily narrow for sufficiently large k .

The channel at $\delta = 0$ is bordered by the bottom bifurcation lines, which is the top border of the tongue $(0, 0)$, and by the bottom border of the tongues $(r, 1)$. The limit $\delta_{0,0}^t$ is 0, whereas the limits $\delta_{r,1}^t$ are positive but approach 0 for r approaching infinity (Fig. 4.17(c)). Thus, as the channel around $\delta = \tau$, the channel at $\delta = 0$ becomes arbitrarily narrow for sufficiently large k .

In contrast to the channel at $\delta = \tau$, the lower border of the channel at $\delta = 0$ approaches the limit for large k from above and not from below. Therefore, it might be possible that the channel between the tongue $(0, 0)$ and the tongues $(r, 1)$ is closed even though the limit values for large k show a gap. For instance, in figure 4.18(b), a bifurcation line of $c = -d$ crosses the bottom bifurcation line. However, in section 4.5.3, we will see that this does not happen for sufficiently large k .

Amplitude death in specific networks

After the discussion of general restrictions of amplitude death we now discuss amplitude death in specific networks by studying a fully-connected and a bipartite network.

A fully-connected graph has the topological eigenvalues $c = d$ and $c = -1$. We found that the eigenvalue $c = -1$ destabilizes the system only for $k < k^e$ (Eq. (4.47)).

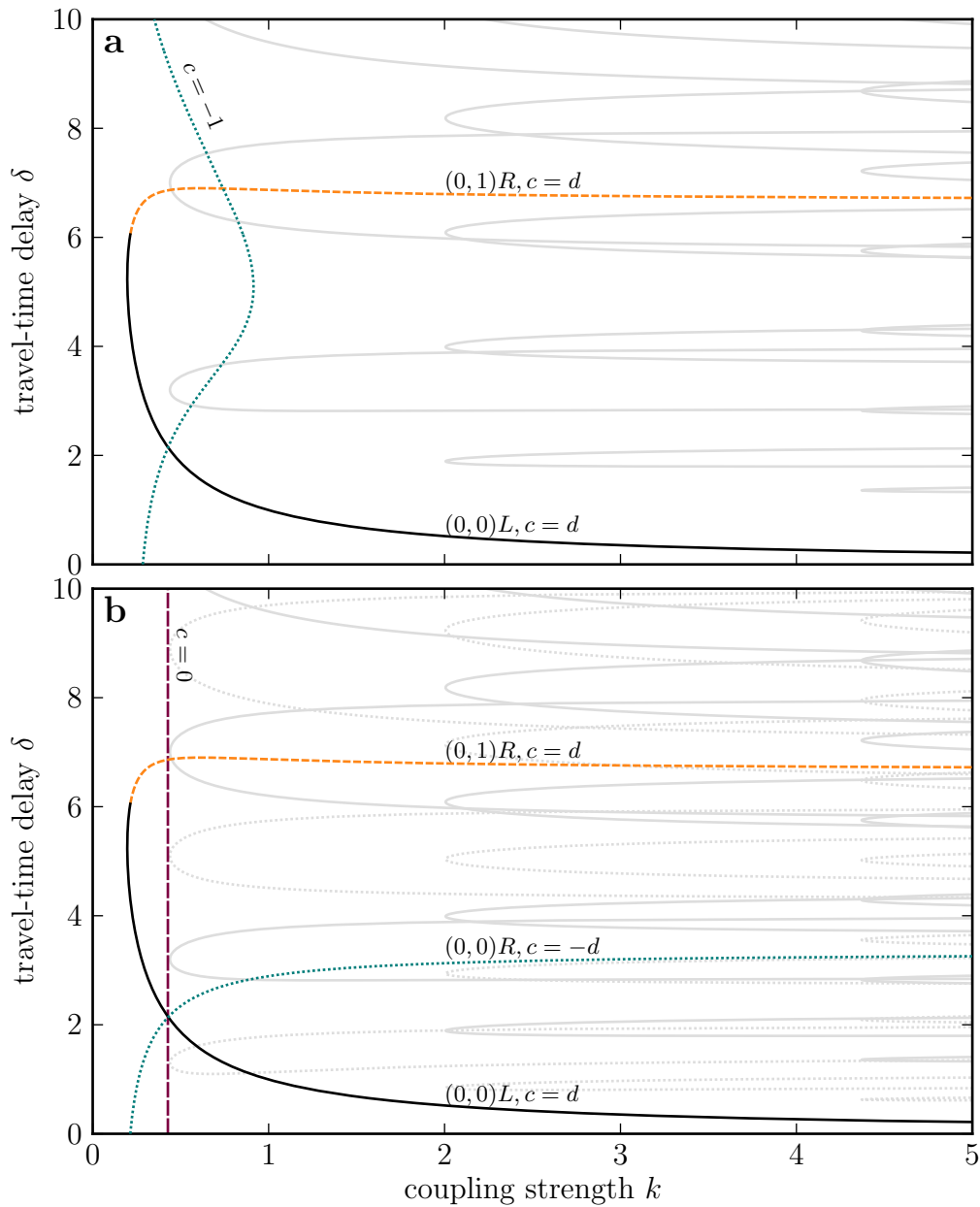


Figure 4.18: Stability and bifurcation lines for a fully-connected net with $N = 3$ nodes (a) and for the bipartite square network with $N = 4$ nodes from Fig. 4.8 (b). Stable systems exist only between the lines $(0,0)L$ and $(0,1)R$ of $c = d = 2$ (solid black and dashed orange line). (a) The fully-connected net is unstable left of the line of $c = -1$ (dotted green line). (b) The bipartite net is only stable for δ below the line $(0,0)R$ of $c = -d$ (dotted green line). The line of $c = 0$ does not influence the stability (long dashed violet line). Gray lines come from the eigenvalues $c = d$ (solid lines) and $c = -d$ (dotted lines). Other parameters are: $g' = -1, l' = 0, \tau = 5$.

Hence, we can ignore this eigenvalue for sufficiently large k . For such k , only the eigenvalue $c = d$ determines the stability of the system. However, the case $c = d$ has already been discussed above.

In the bipartite network, the eigenvalue $c = d$ and $c = -d$ both satisfy $|c| = d$. Hence, these eigenvalues can destabilize the network for arbitrary large k . Stable systems can only be found between the bifurcation line $(0, 0)$ of the topological eigenvalue $c = d$ and the bifurcation line $(0, 0)$ for $c = -d$ (Fig. 4.18(b)). Further, the system is unstable inside the other bifurcation lines that lie inside this area. Thus the eigenvalue $c = -d$ dramatically reduces the parameter space, where amplitude death can be observed. For instance, the channel around $\delta = \tau$ is unstable now. But even though the stable channel close to 0 is narrower than for the fully-connected network, it still exist, allowing amplitude death for small coupling delays δ .

We saw that in the bipartite network, stable areas can only occur between the bifurcation line $(0, 0)$ for $c = d$, which approaches 0 and the bifurcation line $(0, 0)$ for $c = -d$ which approaches $\delta_{0,0}^b = \psi^c / \psi^k$, with $\psi^c = \pi$. This limit is larger 0 for all ψ^c expect for $c = d$. Hence, we might find stable areas between 0 and $\delta_{0,0}^b$ for any eigenvalue $|c| = d$. Therefore, we can expect that amplitude death is possible in all networks, including directed ones, if k is chosen large enough and δ is chosen small enough.

The common bifurcation point

Finally, note that for the bipartite network, bifurcation lines of the eigenvalues $c = 0, c = d$ and $c = -d$ intersect at the same point in the (k, δ) -plane. At this common point, the bifurcation line $c = 0$ coincides with the stability border. However, our conjecture that the stability is governed by the smallest negative and the largest positive eigenvalue (sec. 4.2.2) is still valid: For values of δ below this point, the network losses it's stability because of the eigenvalue $c = d$ before k crosses the bifurcation line of $c = 0$, above the point the eigenvalue $c = -d$ destabilize the system first.

Comparing figures 4.18(a) and (b), we see that the common point is also crossed by the bifurcation line of $c = -1$. In fact, a numerical continuation of the bifurcation point for varying c shows that this point is crossed by bifurcation lines of any eigenvalue c between $-d$ and d .

Summary

Since all degree-homogeneous networks share the eigenvalue $c = d$ the bifurcation lines of these eigenvalues provide a general restriction on the occurrence of amplitude death. These stable areas can be found between the right border of the tongue $(0, 1)$ and the left border of the tongue $(0, 0)$. With increasing k , more and more tongues arise that cover large parts of this area. However, two stable channels can persist for arbitrary large k . One at $\delta = \tau$ and the other close to $\delta = 0$, which lies above the bottom bifurcation line. The first one can be completely covered due to

other eigenvalues that satisfy $|c| = d$, whereas other eigenvalues cannot destabilize the system for sufficiently large k . The eigenvalues $|c| = d$ are related to special topological properties as for instance in bipartite network. The channel at $\delta = 0$ seems to be stable for sufficiently large k in all networks. In the following section, we study this channel in more detail.

4.5.3 Amplitude death for small coupling delays

In the previous section, we saw that amplitude death is possible for large coupling strength k and small delays δ above the bifurcation line of the tongue $(0, 0)$ of the topological eigenvalue $c = d$. However, amplitude death for identical oscillators requires a coupling delay. It is therefore interesting to study how the bifurcation line approaches $\delta = 0$ as k is increased.

In order to find a representation $\delta(k)$ of the bifurcation line for large k , we start from the parametric representation from the Eqs. (4.34,4.41). The asymptotic behavior of the bottom tongue $(0, 0)$ is described by the L-branch as ϕ approaches $\phi^k = \cos^{-1}(l'/g')$. Thus, the parametric representation of the bifurcation line is given by

$$k = \frac{1}{\tau} \frac{f^2 + h^2}{2dh}, \quad (4.51)$$

$$\delta = \frac{\tau}{\phi} \cos^{-1} \left(1 - 2 \frac{h^2}{f^2 + h^2} \right), \quad (4.52)$$

where we used Eq. (4.51) to obtain Eq. (4.52).

If ϕ approaches $\phi^k = \cos^{-1}(l'/g')$, $h = (g' \cos(\phi) - l')\tau$ approaches 0. In this case, we can approximate δ by using $\cos^{-1}(1 - x) \approx \sqrt{2|x|}$. Together with Eq. (4.51), this yields

$$\delta = \frac{|f(\phi^k)|}{\phi^k} \frac{1}{dk}. \quad (4.53)$$

From Eq. (3.15), we know that the stability border τ^* of the single node system is given by $\tau^* = \phi^k / \sqrt{g' - l'}$. Together with $\phi^k = \cos^{-1}(l'/g')$, we obtain

$$f(\phi^k) = \phi^k + g'\tau \sin(\phi^k) = \sqrt{g'^2 - l'^2}(\tau^* - \tau), \quad (4.54)$$

Considering that bifurcation lines only exist for $\tau > \tau^*$, Eq. (4.53) becomes

$$\delta = \left(\frac{\tau}{\tau^*} - 1 \right) \frac{1}{dk}. \quad (4.55)$$

Comparing the exact solution with the approximation from Eq. (4.55) in a linear (Fig. 4.19(a)) and a logarithmic (Fig. 4.19(b)) representation, we see that the approximation gives good results even for small coupling strength down to 1. Larger deviations can only be observed close to the turning point of the bifurcation line.

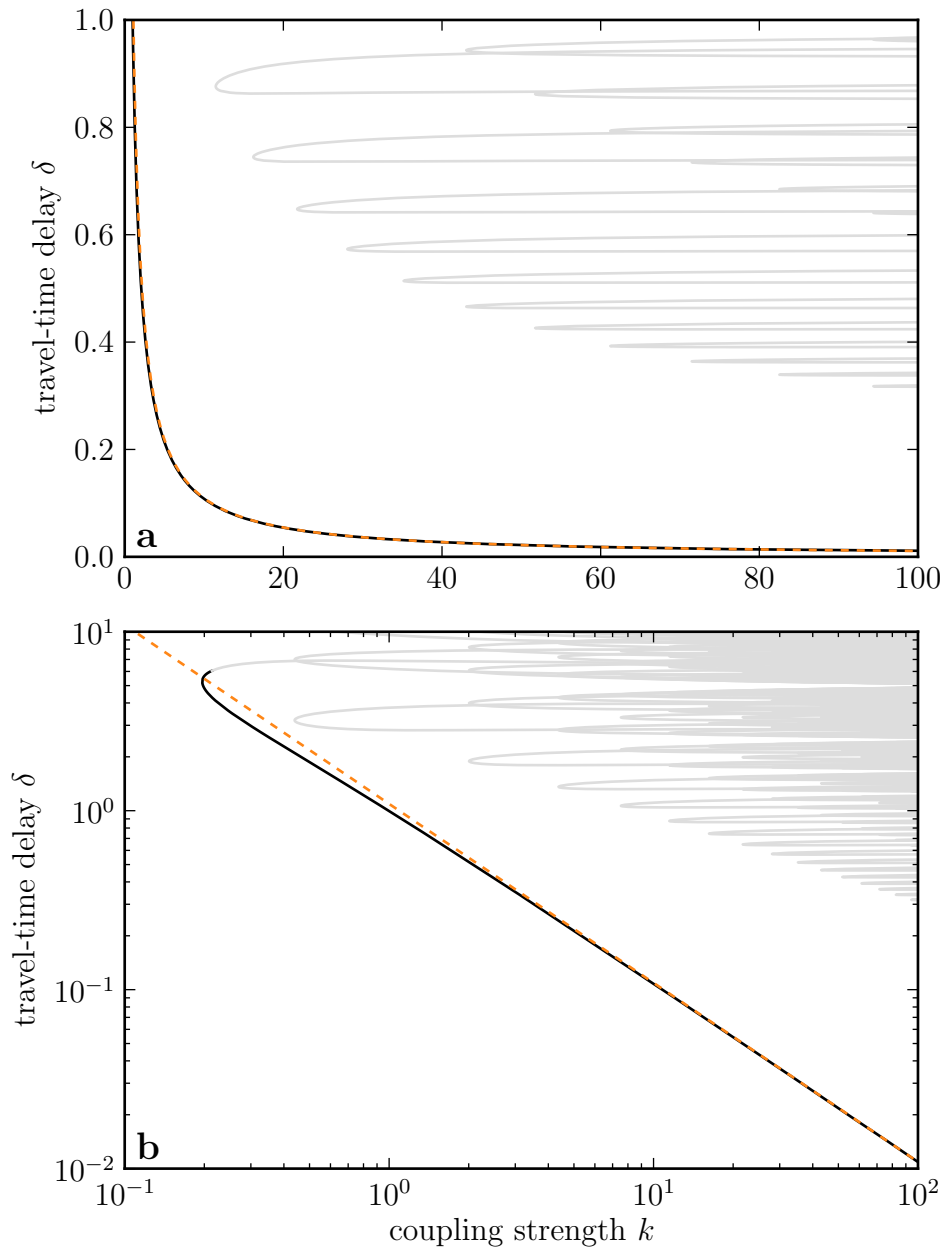


Figure 4.19: Comparison between the bottom bifurcation line (solid black line), and the approximation from Eq. (4.55) (dashed orange line). Other bifurcation lines are drawn with solid gray lines. The approximation shows good agreement with the bottom bifurcation line in both, the linear (a) and the logarithmic (b) representation. There, exists a stable area between the bottom bifurcation line and the lowest tongues (solid gray lines). The logarithmic representation shows that the relative δ -width of this area increases with the coupling strength k . Other parameters are: $g' = -1, l' = 0, d = 2, \tau = 5$.

In the logarithmic representation, we observe that the relative distance between the bottom bifurcation line and the other bifurcation lines increase with increasing coupling strength. This range gives the area where amplitude death appears. Thus, amplitude death is not prevented by the newly appearing tongues of instability as the coupling strength increases.

In the previous sections, we found that eigenvalues with $|c| < d$ do not influence the system for sufficiently large coupling strength. Hence, amplitude death for large coupling strength and small coupling delays is not affected by these eigenvalues. In contrast, eigenvalues with $|c| = d$, can reduce the parameter space in which amplitude death occurs even for large coupling strength. However, as for the eigenvalue $c = d$, the relative distance between the bottom bifurcation line and the additional bifurcation lines of other eigenvalues satisfying $|c| = d$ increases with increasing k . Therefore, we find amplitude death in all degree-homogeneous network for large enough k and small enough δ above the bottom bifurcation line.

It has been shown that amplitude death in identical oscillators requires that the coupling is time-delayed. The commonly used model to study amplitude death is the Stuart-Landau oscillator. There, amplitude death only appears for finite coupling strength and coupling delays [30, 91, 92]. In contrast, we find here that amplitude death is also possible for infinitely large coupling strength and infinitely small coupling delays, because the onset delay for amplitude death approaches 0 like $1/(dk)$, where dk can be regarded as the total coupling strength acting on each node.

4.6 Summary

In this chapter, we studied the stability of degree-homogeneous networks by deriving analytical expressions for the bifurcation lines in the delay and in the coupling space. In the delay space, the bifurcation lines border tongues of instability that can be characterized by the tip position and the slopes of the two ends of the line. Each (topological) eigenvalue of the adjacency matrix can give rise to a set of bifurcation lines. The lines in each set can be enumerated by the indexes r and s , so that the line (r, s) can be obtained by shifting the line $(0, 0)$ by $2\pi r/\omega$ along the τ -axis and by $2\pi s/\omega$ along the δ -axis (Sec. 4.1).

In undirected networks, the sets of tongues can be subdivided into sets that arise because of positive eigenvalues and sets that arise because of negative eigenvalues (Sec. 4.2.2). Sets of negative eigenvalues are denoted as diagonal sets (DS), because they include tongues with tips on the diagonal. Accordingly, other sets are denoted as off-diagonal sets (OS). We observed that only the OS that arises because of the largest positive eigenvalue, $c = d$, and only the DS that arises because of the smallest negative eigenvalue govern the stability of the network (also see Sec. 4.5.2).

From section 3.4, we know that all networks, including degree-heterogeneous networks, need to give rise to bifurcation lines that cross the points $\tau = \tau_r^*$, $\delta = 0$, where the τ_r^* are the bifurcation delays of the single node system. In degree-

homogeneous networks these bottom bifurcation lines arise because of the eigenvalue $c = d$, which is present in all degree-homogeneous networks. However, corresponding bifurcation lines also need to exist in degree-heterogeneous networks. Similarly, bifurcation lines that correspond to $c = -d$ should exist in all bipartite networks.

By comparing the stability of a network with the stability of a single node system, we have seen that the coupling is rather stabilizing and thus gives rise to amplitude death (Sec. 4.4). This phenomena has been studied in section 4.5, where we found that amplitude death should occur for large coupling strength and small coupling delays. In the next chapter, we study if this is true for general degree-heterogeneous networks.

The next chapter deals with degree-heterogeneous networks. These networks are analyzed numerically, so that we do not see a direct relation between the topological eigenvalues and the bifurcation lines. However, we may observe bifurcation lines that correspond to bifurcation lines of special eigenvalues in the degree-homogeneous network, such as the eigenvalues $c = d$ and $c = -d$. We study similarities and differences between corresponding bifurcation lines, as well as differences to basic stability patterns found in degree-homogeneous networks. For instance, the existence of DS and OS, and the finding that the stability is governed by only one DS and one OS. Of course, we also study the influence of the degree distribution.

5 Degree-heterogeneous networks

In the previous chapter, we studied the system described by the Jacobian from Eq. (3.7) for degree-homogeneous networks (DHONs). We found a direct relation between the topological eigenvalues and the bifurcation lines. Therewith, we were able to relate topological properties to certain stability patterns. In this chapter, we numerically analyze degree-heterogeneous networks (DHENs). Even though a simple relation between the eigenvalues and the bifurcation line is not available, we can use the numerical methods to study if the relations between the topological properties and the stability patterns found for DHONs are also valid for DHENs. Further, we investigate the influence of the degree distribution on the stability.

Whereas DHONs can be analyzed analytically by decomposing the eigenvalue equation of the Jacobian $\mathbf{J}(\lambda)$, such a decomposition is not possible for DHENs. Still the stability of the system can in principle be obtained by estimating the eigenvalues, i.e. the roots of the characteristic polynomial of the Jacobian. Though, for delay equations, the Jacobian itself depends on the eigenvalue λ , turning the characteristic polynomial into a transcendental equations with infinitely many roots. Hence, by using standard root finding algorithms we can never be sure that we found the leading eigenvalue with the largest real-part. Therefore, we cannot be sure if a given system is stable.

In the past decades, new methods have been developed to analyze the stability of delay differential equations [129–132]. These include methods to efficiently calculate the leading eigenvalue [130, 132] and methods to determine the number of eigenvalues with positive real-part (EVPs) [131]. Here, we follow the latter approach and use it to investigate stability properties of random DHENs.

5.1 The numerical method

In order to calculate the number of EVPs for general delay differential equations, we follow Luzyanina and Roose [131] and apply Cauchy’s Argument principle. For analytic functions such as the characteristic polynomial $P(\lambda)$, the number of roots inside a contour C is given by the winding number of $P(\lambda)$ on the contour C ,

$$N_C = \frac{1}{2\pi i} \int_C \frac{P'(\lambda)}{P(\lambda)} d\lambda \quad (5.1)$$

Choosing C inside the positive half-plane so that all EVPs have to lie within C , the winding number N_C is equal to the number of EVPs, and a change of N_C , due to

a parameter variation, indicates a bifurcation. Hence, the steady state is stable if $N_C = 0$ and unstable otherwise.

Choosing an appropriate contour C

When choosing a contour C , we have to ensure that no EVPs can be found outside C and that C does not include areas with negative real-part. For this purpose, we choose a rectangle spanning $[0, \kappa^{\max}]$ along the real-axis and $[-\omega^{\max}, \omega^{\max}]$ along the imaginary axis.

Proper values for κ^{\max} and ω^{\max} can be estimated by applying the Gershgorin Circle Theorem as demonstrated in section 3.6. There, we found that all eigenvalues have to lie inside circles around $D_i = -l' - kd_i$ with radii $R_i(\kappa) = |g'| \exp(-\kappa\tau) + kd_i \exp(-\kappa\delta)$, where i is indexing the nodes of the system. Considering a node i , we see from figure 5.1 that the real-part of an EVP needs to be smaller than κ_i^{\max} that solves

$$R_i(\kappa_i^{\max}) + D_i = \kappa_i^{\max}, \quad (5.2)$$

and the imaginary-part needs to be smaller than

$$\omega_i^{\max} = \sqrt{R_i(0)^2 - |D_i|^2}. \quad (5.3)$$

Therefore, we can choose $\kappa^{\max} = \max_i(\kappa_i^{\max})$ and $\omega^{\max} = \max_i(\omega_i^{\max})$.

Note that this method can easily be extended to networks of non-identical delay oscillators, where each node has an own set of parameters g' , l' and τ , because κ_i^{\max} and ω_i^{\max} are calculated for each node independently. Further, the system can be extended to systems with multiple delays in the node and in the coupling. Assuming that the Jacobian is of the form

$$J_{ij} = \sum_k a_{ijk} e^{-\lambda\tau_{ijk}} + \sum_l b_{ijl}, \quad (5.4)$$

then

$$D_i = \sum_l b_{iil}, \quad (5.5)$$

$$R_i(\kappa) = \sum_j \sum_k |a_{ijk}| e^{-\kappa\tau_{ijk}} + \sum_{j \neq i} \sum_k |b_{ijk}|. \quad (5.6)$$

$$(5.7)$$

Calculating the winding number N_C

Instead of calculating the winding number with Eq. (5.1), Luzyanina and Roose [131] used the geometric interpretation of the Argument Principle, which states that

$$N_C = \frac{1}{2\pi} \Delta_C \arg P(\lambda), \quad (5.8)$$

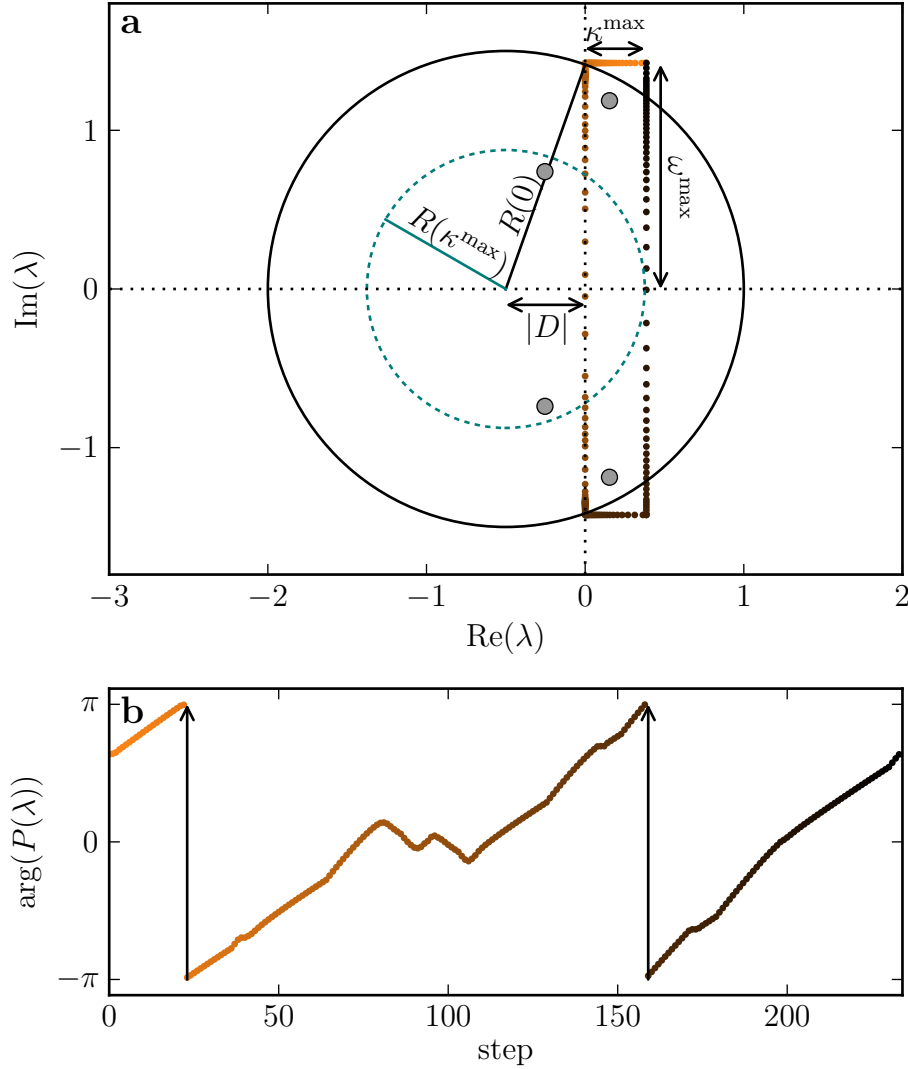


Figure 5.1: Method to estimate the number of eigenvalues with positive real-part κ (EVPs). (a) Calculation of κ^{\max} and ω^{\max} , which define the contour C (dots on the rectangle). EVPs can only exist inside circles in the complex plane that are centered around D and have a radius $R(\kappa)$. Because $R(\kappa)$ is decreasing with κ , the absolute value of the imaginary part of an EVP needs to be smaller than $\omega^{\max} = \sqrt{R(0)^2 - |D|^2}$ (solid black circle), and the real-part needs to be smaller than κ^{\max} , which satisfies $R(\kappa^{\max}) - |D| = \kappa^{\max}$ (dotted green circle). Gray circle mark the eigenvalues. (b) The number of EVPs, N_C , is given by the total increase of $\arg(P(\lambda))/2\pi$ as λ follows the contour C . If both jumps from π to $-\pi$ are eliminated by shifting the subsequent values up, we note that the total increase of $\arg(P(\lambda))$ is 4π and hence $N_C = 2$. Thus, we obtain N_C by counting all jumps from π to $-\pi$ and subtracting the number of jumps from $-\pi$ to π . The line is composed of dots which correspond to dots of the same color in (a).

where $\arg P(\lambda) = \text{Im}(\log(P(\lambda)))$ is the argument of $P(\lambda)$ and $\Delta_C \arg P(\lambda)$ is the total increase of the argument as λ moves counter-clockwise along C , so that

$$\Delta_C \arg P(\lambda) = \sum_i P(\lambda_{i+1}) - P(\lambda_i), \quad (5.9)$$

where the λ_i are subsequent points on the contour C with infinitely small distance. However, the value of $\Delta_C \arg P(\lambda)$ is given by $2\pi N_C$, and hence, needs to be a multiple of 2π . Therefore, the precision of the calculation only needs to be good enough to find the right integer value for N_C .

We obtain N_C , similar to Luzyanina and Roose, by choosing the domain of $\arg P(\lambda)$ as $(-\pi, \pi]$ and counting the crossings of the domain border as λ follows the contour C . For this purpose, we initialize a counter n with 0 and follow $\arg P(\lambda)$ counter-clockwise along the contour C . Whenever $\arg P(\lambda)$ jumps from $-\pi$ to π , we increase n by 1, and we decrease it by 1 whenever $\arg P(\lambda)$ jumps from π to $-\pi$. After one full turn on the loop C , $n = N_C$ (Fig. 5.1(b)).

When calculating N_C with the above algorithm, we need to ensure that we do not miss any jumps of $\arg P(\lambda)$ from $-\pi$ to π and vice versa. For this purpose, we apply an adaptive step-size algorithm. We follow $\arg P(\lambda)$ along C by stepping from a point λ_i to a subsequent point $\lambda_{i+1} = \lambda_i + h\mathbf{v}$, where \mathbf{v} is a unit vector pointing along the contour C at position λ_i . The step-size h is accepted if the following three conditions are satisfied

- $\Delta = D(\arg P(\lambda_i + h\mathbf{v}) - \arg P(\lambda_i)) < \epsilon$
- $D(\arg P(\lambda_i + \frac{h}{2}\mathbf{v}) - \arg P(\lambda_i)) < \Delta$,
- $D(\arg P(\lambda_i + \frac{h}{2}\mathbf{v}) - \arg P(\lambda_i + \mathbf{v})) < \Delta$,

with $D(x) = \min(|x|, ||x| - 2\pi|)$ and $x \in (-2\pi, 2\pi)$. The first condition simply says that the distance between $\arg P(\lambda)$ for two subsequent steps need to be smaller than ϵ , which we choose to be 0.1 in the following. The latter two conditions guarantee that the value of $\arg P(\lambda)$ for the center between the two subsequent steps lies between the values of $\arg P(\lambda)$ for the two subsequent steps (Fig. 5.2). If one of the three conditions is violated, the step size is reduced by a factor of 2: $h \rightarrow h/2$. After each successful step, we set h to $h \max(2, \epsilon/\Delta)$.

This adaptive step-size algorithm allows us to calculate the number of EVPs of a delay network. In the following two sections, we test the reliability of the algorithm by comparing it's results to the analytical results we obtained for degree-homogeneous networks. Further, we use this numerical method to test the conjecture from section 3.5.

5.1.1 Comparison with analytical results

In order to test the numerical method, we compare it's results for a fully-connected network with $N = 3$ nodes with the analytical solutions. For this purpose, we

compare the analytical bifurcation lines in the (τ, δ) -plane and in the (k, δ) -plane with the stable and the unstable areas we obtain with the numerical method (Fig. 5.3).

The stable and unstable areas in the two different parameter planes are obtained by sampling the parameter space. For this purpose, we randomly draw the parameters of interest from a uniform distribution, while all other parameters are fixed. Then, we use the numerical method to calculate the number of EVP. If the number of EVPs is 0, the system is stable and we draw a green point. If the number of EVPs is greater than 0, the system is unstable and we draw a red point. Thus, by sampling the parameter space, the stable and unstable areas are filled with green and red points, respectively. The figures 5.3(a,c) show only the stable systems, whereas the figures 5.3(b,d) show only the unstable systems. Thus, the unstable area in the first two figures should be empty, as well as the stable area in the latter two figures. Indeed, even close to the bifurcation lines, the numerical method provides correct results.

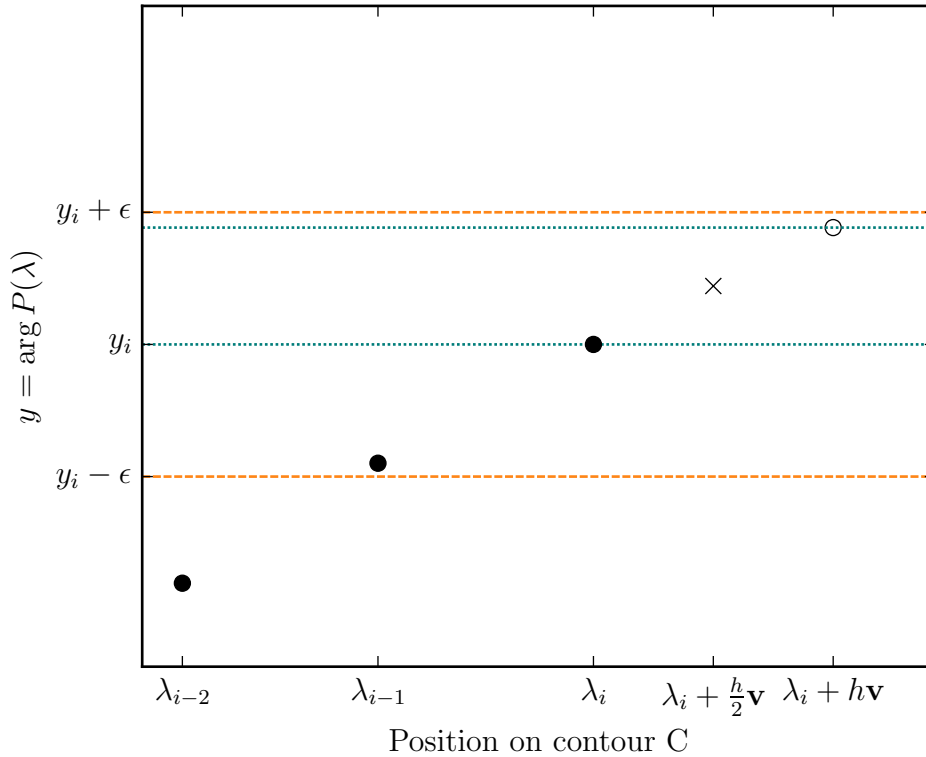


Figure 5.2: Schematic representation of the adaptive step-size algorithm. A new point λ_{i+1} (open circle) is calculated from the previous point λ_i with $\lambda_{i+1} = \lambda_i + h\mathbf{v}$, where \mathbf{v} is a unit vector along the contour C and h is the step-size. The step is accepted if $y_{i+1} = \arg P(\lambda_{i+1})$ lies inside an ϵ -environment around y_i (dashed orange lines) and if $\arg P(\lambda_i + \frac{h}{2}\mathbf{v})$ (cross) lies between y_i and y_{i+1} (dotted green lines). If the step is not accepted, h is reduced by a factor of 2. In the following, we use $\epsilon = 0.1$.

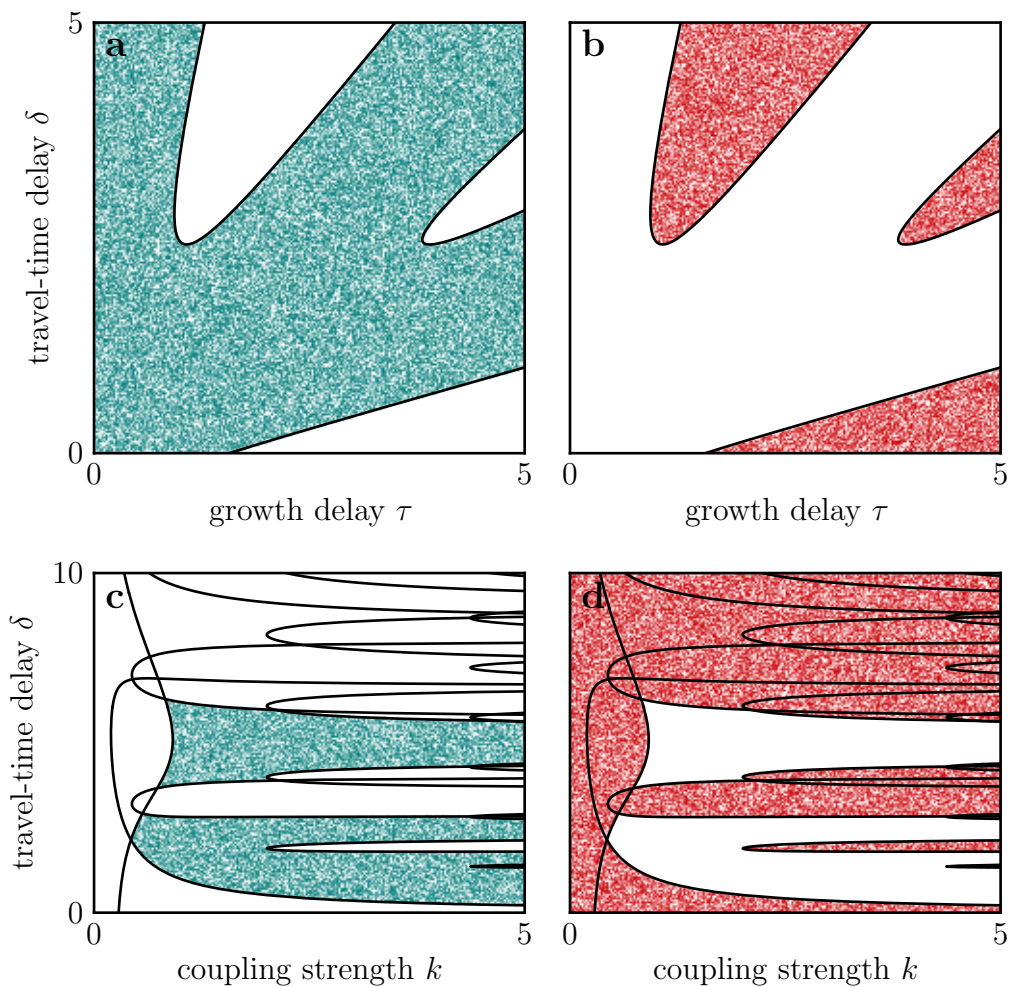


Figure 5.3: Comparison of the results of the numerical method and the analytical bifurcation lines for the fully-connected network with $N = 3$ nodes in the (τ, δ) -plane (a,b) and in the (k, δ) -plane (c,d). For the numerical method, we draw the axis-parameters randomly from a uniform distribution and calculate the number of EVPs. (a,c) If the number of EVPs is 0, the system is stable and we draw a green dot. (b,d) If the number of EVPs is greater than 0, the system is unstable and we draw a red dot. For each figure 100000 pairs of parameters have been drawn. Other parameters are: $g' = -1, l' = 0, k = 1, \tau = 5$.

5.1.2 Test of the sufficient stability condition

In section 3.6, it was shown that all networks with $g' < l'$ are stable. Further, we formulated the conjecture that all networks are unstable for $g' > l'$ (Sec. 3.5). If this conjecture is true, the stability of networks with $g' > 0$ is independent of the topology, the coupling strength and the delays. In this section, we test this assumption with the introduced numerical method, because it allows us to calculate the stability for a large number of different topologies and parameters. The procedure we use is also

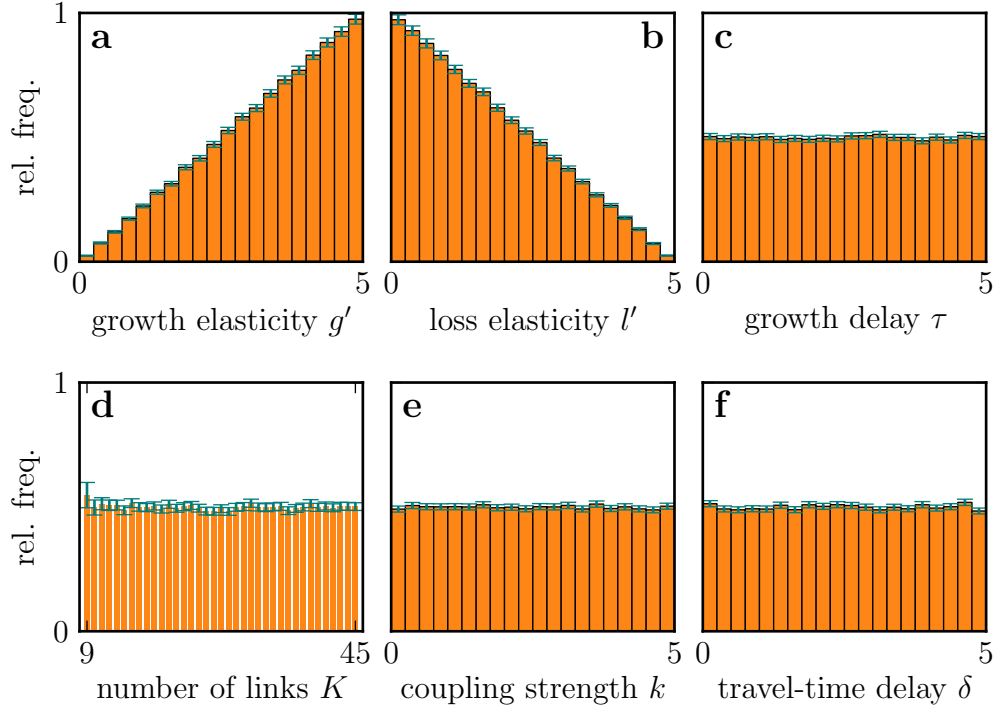


Figure 5.4: Relative frequency of unstable Erdős-Rényi networks with $N = 10$ nodes dependent on the parameters g' (a), l' (b), τ (c), K (d), k (e) and δ (f). The rel. frequency is given by the ratio of the number of unstable nets and the total number of nets in each bin. The green error bars show the standard deviation of the bin heights. For the generation of the 10^5 networks, all parameter except for the number of links K are drawn from uniform distributions between 0 and 5. The parameter K is drawn from a uniform distribution between 9 and 45. But if a non-connected network is generated a new value for K is drawn. This is more likely for small K , so that these networks are generated less often. Therefore, the standard deviation is slightly higher for small K than for large K . As expected a correlation between stability and parameter values can only be found for g' and l' .

well suited to obtain first insights into an unknown system.

We test the above assumption, by generating a large number of random networks with random parameters with $g' > 0$. If the assumption is correct, then the stability should not be affected by any parameters except for g' and l' . Thus, histograms of only unstable networks, should only show a correlation between stability and the parameter values for these two parameters. Further, a scatter plot of stable and unstable networks in the (g', l') -plane should reveal the stability condition $g' < l'$.

We generate 10^5 Erdős-Rényi networks with $N = 10$ nodes and K links. In order to obtain connected networks, K needs to be larger than $N - 1 = 9$. A fully-connected network has $N(N - 1)/2 = 45$ links. Therefore, we randomly draw K from 9 to 45. However, small values of K are likely to result in disconnected networks. In this case, a new K is drawn.

The histograms in figure 5.4 show the relative frequency F of unstable nets for each bin. If the number of unstable nets in a bin is given by U and the total number of networks in the bin is given by H then $F = U/H$. The standard deviation of F is calculated with

$$\sigma_F = \sqrt{\left(\frac{\sigma_U}{H}\right)^2 + \left(\frac{U}{H^2}\right)^2 \sigma_H^2}, \quad (5.10)$$

where $\sigma_U = \sqrt{U}$ and $\sigma_H = \sqrt{H}$ are the standard deviations of U and H .

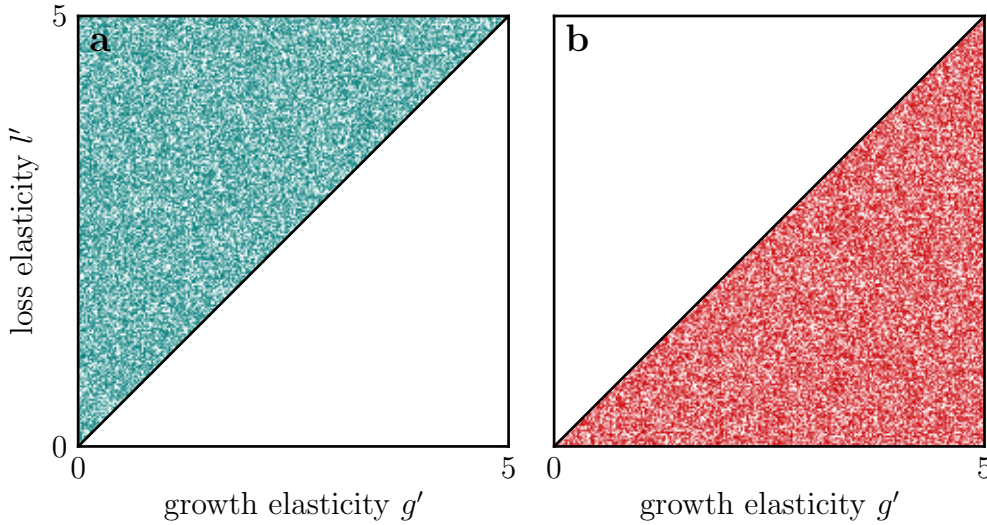


Figure 5.5: Scatter plot of stable (a) and unstable (b) networks from Fig. 5.4 in the (g', l') -plane. No stable systems are found for $g' > l'$ (right of the diagonal in (a)) and no unstable systems are found for $g' < l'$ (left of the diagonal in Fig. (b)). Hence, the stability criterion $g' < l'$ seems to be true for all random networks.

As expected, the stability seems to depend only on g' and l' (Fig. 5.4(a,b)), whereas the variation of bin heights in the other histograms is of the order of the standard deviation. However, in order to test the validity of the stability condition $g' < l'$, it is more informative to consider the scatter plot of stable and unstable nets in the (g', l') -plane (Fig. 5.5). There, we see that all systems with $g' > l'$ are unstable and that all systems with $g' < l'$ are stable. Thus, for $g' > 0$, the stability is determined only by g' and l' .

Histograms such as in figure 5.4 and scatter plot such as in figure 5.5 can help to obtain first insights into unknown systems and to estimate the most important parameters, which then can be studied in more detail. This is particularly useful for system with many parameters. Alternatively, important parameters can be identified by calculating the correlation between the parameters and the stability, as it has been done in other systems investigated with the generalized modeling approach [15, 19].

5.1.3 Conclusions

The numerical sampling method offers a simple and efficient way to analyze delay systems. Note, that the method is not restricted on finding only stable and unstable areas, but is able to determine the number of EVPs at any point in parameter space. Thus, it is possible to visualize the bifurcation lines for any pair of parameters.

Even if bifurcation lines can be obtained analytically for some parameters, this can become prohibitively complex for other pairs of parameters. Further, for the analytical derivation of bifurcation lines, the different solution branches must not be mixed. Such mistakes can be detected by using the numerical method. Additionally, from the bifurcation lines, it is not obvious which areas are stable. In contrast, the numerical method directly provides the stability of each point. Further, this method can be used in support of other numerical methods. For instance, the continuation of bifurcation lines through parameter space requires initial values, which can be obtained by sampling the parameter space.

The numerical sampling method is particularly suited to analyze large delay networks, because the computation is based predominantly on matrix operations, for which optimized algorithms are available. Further, each sample point is calculated independently, so that the computation can be run on multiple computers in parallel. The analysis of large networks allows to study the influence of large-scale network properties such as a scale-free degree-distribution.

In section 5.1.2, we have seen that histograms of stable or unstable networks can provide first information about the parameter dependence of the stability. A more precise analysis of the parameter dependence can be obtained by scatter plots such as in figure 5.3. A quick overview of the system can be obtained by sampling the parameter space with a comparable small number of points. Then, regions of interest can be studied in more detail.

Note that this algorithm allows us to calculate the number of EVPs and hence the stability of a system only by calculating the characteristic polynomial for different values of λ . Thus, this method can easily be applied to more complicated models with several delays and non-identical parameters for each node.

5.2 Stability of ensembles of random networks

After we have verified that the stability of DHENs with $g' > 0$ is topology independent, we now investigate the topology dependence for $g' < 0$. For this purpose, we study scatter plots of small Erdős-Rényi networks with $N = 10$ nodes and a fixed number of links K . Like in section 5.1.1, we randomly draw the delays τ and δ from a uniform distribution between 0 and 5. But instead of choosing only a single network, we generate a new random network for each sample point. Hence, each scatter plot shows the stability of an ensemble of random networks.

As for the undirected DHONs, the stability in the delay space is governed by a diagonal and an off-diagonal set of $2\pi/\omega$ -periodic tongues (Fig. 5.6). For the bipartite

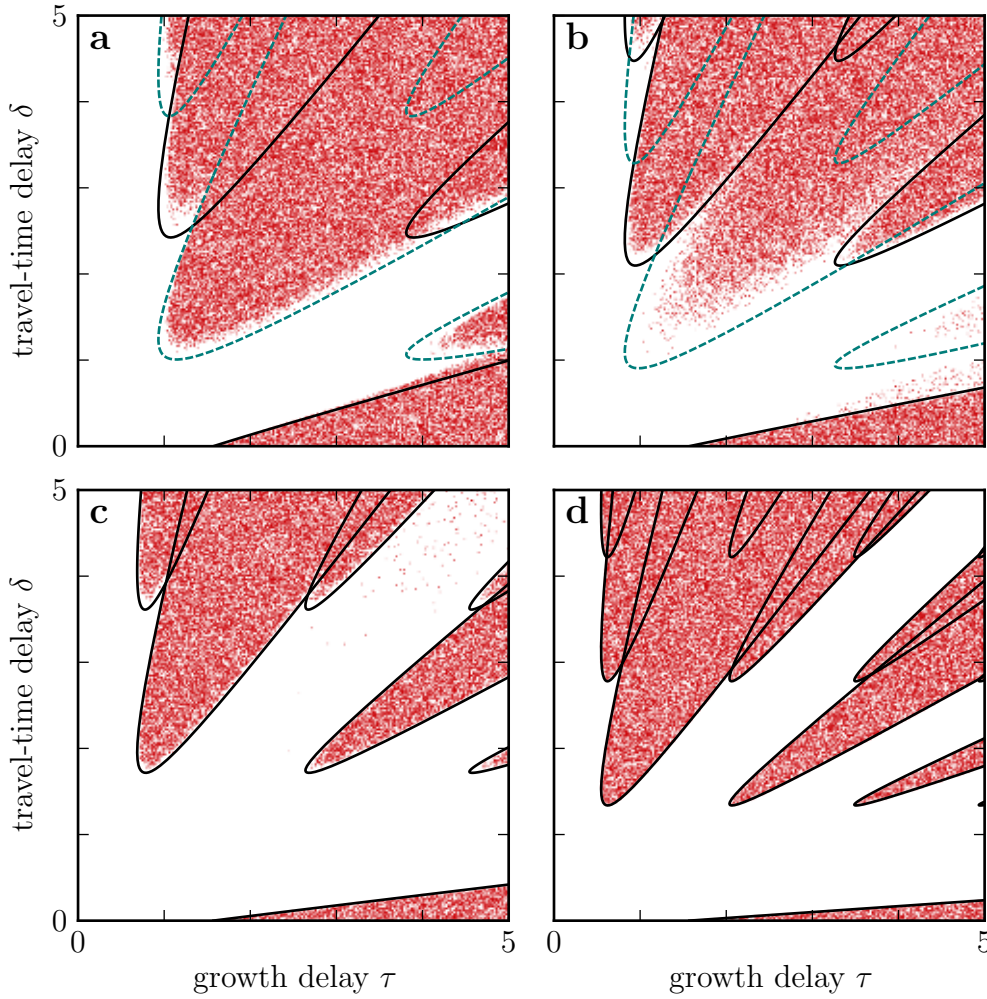


Figure 5.6: Scatter plots of unstable Erdős-Rényi networks with $N = 10$ nodes and $K = 9$ (a), $K = 15$ (b), $K = 25$ (c), and $K = 45$ links. The numerical results are compared to the analytical bifurcation lines of a DHON with $c = d = 2K/N$ (solid black lines). In (a,b) also the bifurcation lines of the eigenvalue $c = -d$ are shown (dashed green lines). For each plot 10^5 networks are generated. As for the DHONs, the stability pattern of DHENs is governed by an diagonal set and an off-diagonal set of tongues. For the bipartite trees, OS and DS are shifted by π/ω . With increasing K , the DS vanishes. Other parameters are: $g' = -1, l' = 0, k = 1$.

trees, both sets give rise to the π/ω -periodicity along the δ -axis (Fig. 5.6(a)). When increasing the number of links, the diagonal tongues vanish by moving to infinitely large delays, so that the stability pattern resembles the one of a fully-connected network that only gives rise to an off-diagonal set of tongues (Fig. 5.6(a-d)).

In comparison to the scatter plots for a single network (Fig. 5.6(d)), we note that the borders between stable and unstable areas are fuzzy if networks are drawn from

an ensemble. Even though each individual network has a sharp stability border, which is given by the corresponding bifurcation lines, the stability border of the ensemble is fuzzy because the bifurcation lines of different networks in the ensemble are shifted relatively to each other. Thus, in these fuzzy areas, the stability depends on the topology of the networks in the ensemble. In this case, the density of points provides a rough estimate of the fraction of unstable networks.

First, we study the stability pattern of trees in more detail (Fig. 5.6(a)). For the diagonal tongue, we see that the density profile of unstable networks does not change much when following the border of the tongue from the tip to the right. Thus, studying the tip of a tongue may reveal information that are valid for the whole right part of the tongue. In particular, this might include the order in which networks lose stability when delay values enter the tongue.

The density profile also reveals that the bifurcation lines of the different trees coincide at the left part of the tongues but seem to be shifted towards each other at the right part of the tongue. This becomes more obvious in section 5.3, where we compare the bifurcation lines of particularly stable and unstable trees. Here, this observation is only made for the diagonal, because the border of the off-diagonal tongue is covered by the diagonal tongue. However, we can expect the same pattern for the off-diagonal, because of the π/ω -periodicity of the tongues. In fact, we make the same observation for all bifurcation lines of DHENs that correspond to bifurcation lines of the eigenvalues $c = d$ and $c = -d$ of the DHONs. However, in the figures (Fig. 5.6(c,d)) the shift between the $c = d$ bifurcation lines is too small to be visible. A better example can be found in section 5.2.2.

If the bifurcation lines of DHENs only differ from the corresponding bifurcation lines of the DHONs by a shift of the right part of the line, then the slopes of corresponding lines are identical for large delays. In section 4.1.4, we related the slopes to the emergence and merging of tongues. Whereas we already know that the corresponding bifurcation lines of DHONs and DHENs have to emerge for the same parameters, the identical slopes of corresponding bifurcation lines suggest that the bifurcation lines also merge for the same parameters.

Now, we want to study changes in the stability pattern as the number of links are increased from $K = 9$ to $K = 45$ (Fig. 5.6). As the diagonal tongues vanish towards infinitely large delays the stability transition along the diagonal becomes more fuzzy. Thus, the influence of the topology increases. In contrast, the off-diagonal tongues move to smaller delays and the stability transition becomes sharper until it is given by the stability border of the fully-connected network. The stability transition at the bottom bifurcation line is rather sharp for most values of K . However, for comparably small values of K around $K = 15$, we observe a fuzzy stability transition for delays $\tau \gtrsim 3$. In the following, we want to study the different stability transitions for small and large values of K in more detail. Further, we want to take a closer look on the stability borders of the diagonal and off-diagonal tongues. For this purpose we investigate the fraction of unstable networks along the four sections through the delay-plane shown in figure 5.7.

5.2.1 Stability transitions along sections through delay-plane

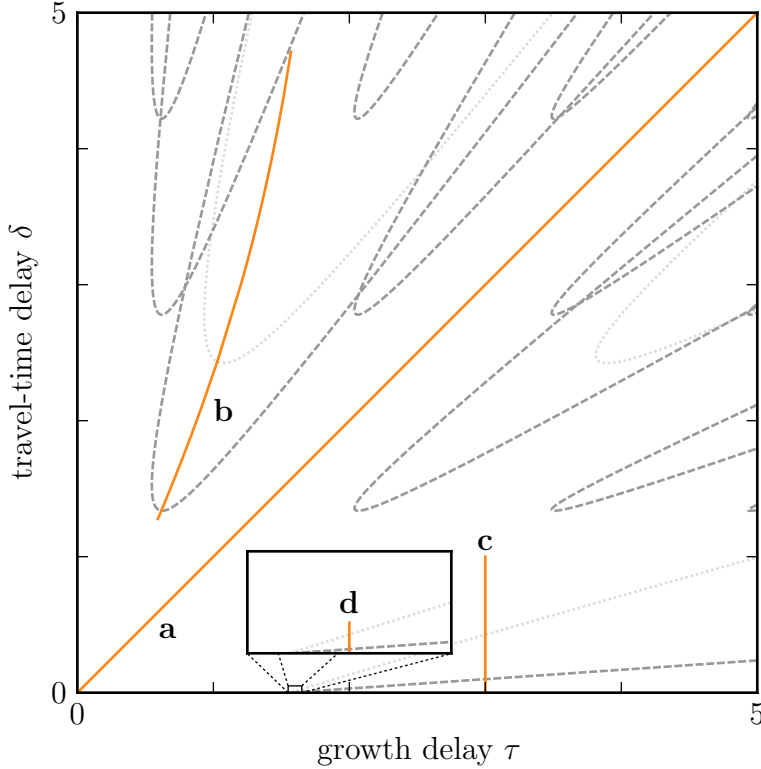


Figure 5.7: Sections through the delay space (solid orange lines) used to study the stability transition at the diagonal tongue, the off-diagonal tongue, and the bottom stability border. In Fig. 5.6(b), we see that the bottom stability border is fuzzy for large τ and sharp for small. Therefore, we consider two sections across this border, one at $\tau = 3$ (c) and one at $\tau = 1.6$ (d). Section (a) crosses the tips of diagonal tongues in an DHON, and section (b) crosses the tips of the off-diagonal tongues of the eigenvalue $c = d$. The dashed and dotted lines show the bifurcation lines of the eigenvalues $c = d = 9$ (dashed lines) and $c = d = 2$ (dotted lines). Other parameters are: $g' = -1, l' = 0, k = 1$.

In order to study the stability transition at the diagonal tongue, the off-diagonal tongue, and at the bottom bifurcation line, we calculate the fraction of unstable networks along the lines (a-d) shown in figure 5.7. The lines (a) and (b) describe tip positions of tongues in DHONs. The diagonal line (a) includes the tip position of the tongues (i, i) with negative topological eigenvalues c and the line (b) gives the tip position of the tongue $(0, 1)$ for the eigenvalue $c = d$, where $d \in [0, 10]$.

Beside the diagonal and the off-diagonal tongue, we also want to study the bottom stability border in more detail. However, for ensembles with small numbers of links, the bottom stability border has different properties for small and large delays τ (Fig. 5.6(a,b)). For $\tau < 2$, all networks seem to share the same stability border,

which is given by the bifurcation line of the DHONs with $d = 2K/N$. But for $\tau \gtrsim 3$, some networks remain unstable considerably above the bifurcation line, which gives rise to a fuzzy stability border. In order to study, these different properties of the bottom stability border, we calculate the fraction of unstable networks along the lines (c) and (d), which are vertical lines at $\tau = 3$ and $\tau = 1.6$, respectively.

The fraction of unstable networks along the vertical lines (c,d) are computed by drawing δ from a uniform distribution between 0 and 0.015 for $\tau = 1.6$ and between 0 and 0.5 for $\tau = 3$. For the diagonal line (a), the delays $\tau = \delta$ are drawn from a uniform distribution between 0 and 5 and for the line (b), the degree d is drawn from a uniform distribution between 0 and 10. With the degree d , τ and δ are calculated using the Eqs. (4.19,4.20). For each histogram, 10^5 networks are generated and each histogram consist of 100 equally sized bins. The bin height is color coded and gives the ratio of the number of unstable and the total number of networks in each bin. This allows us to visualize the K -dependence of the distribution in 2d-color plots (Fig. 5.8).

The diagonal tongue

When adding links to tree networks, the diagonal tongue moves towards larger delays and finally disappears (Fig. 5.6(a-d)). As the diagonal tongue diverges towards infinity, the size of the fuzzy area on the diagonal, in which stable and unstable networks coexist, diverges as well (green-shaded areas in Fig. 5.8(a)). However, when further increasing K the fraction of unstable networks on the diagonal decreases to zero so that all networks are stable on the diagonal.

In principle, we can explain the disappearing of the diagonal tongue as K increases with the analytical results for the DHONs. From the Eqs. (4.19,4.20), we see that the diagonal tongue vanishes by moving towards infinitely large delays as the most negative topological eigenvalue c^{\min} increases beyond $-c^* = -d - (g' + l')/k$.

In order to compare the analytical results for the DHONs to the numerical results for the DHENs, we estimate the ensemble average $\langle c^{\min} \rangle$ for each K -ensemble by calculating the average of c^{\min} of 1000 Erdős-Réni networks with $N = 10$ nodes and K links. By using $d = 2K/N$, we calculate the δ -value of the tongue tip from Eq. (4.20) and compare it with the stability border shown in figure 5.8(b). For small K , the δ -value from Eq. (4.20) is smaller than the according border of the histogram but as K increases it diverges earlier towards infinity. Thus, the analytical solutions for the DHONs describe the DHENs only qualitatively.

The off-diagonal tongue

Whereas the stability border of the diagonal tongue becomes more fuzzy and approaches infinity as K increases, the stability border of the off-diagonal tongue becomes sharper and approaches the bifurcation lines of the DHONs with $c = d$ (Fig. 5.8(b)), which we compute with the Eqs. (4.19,4.20). Obviously, for $K = 45$, the stability border has to match the bifurcation line of the fully-connected network

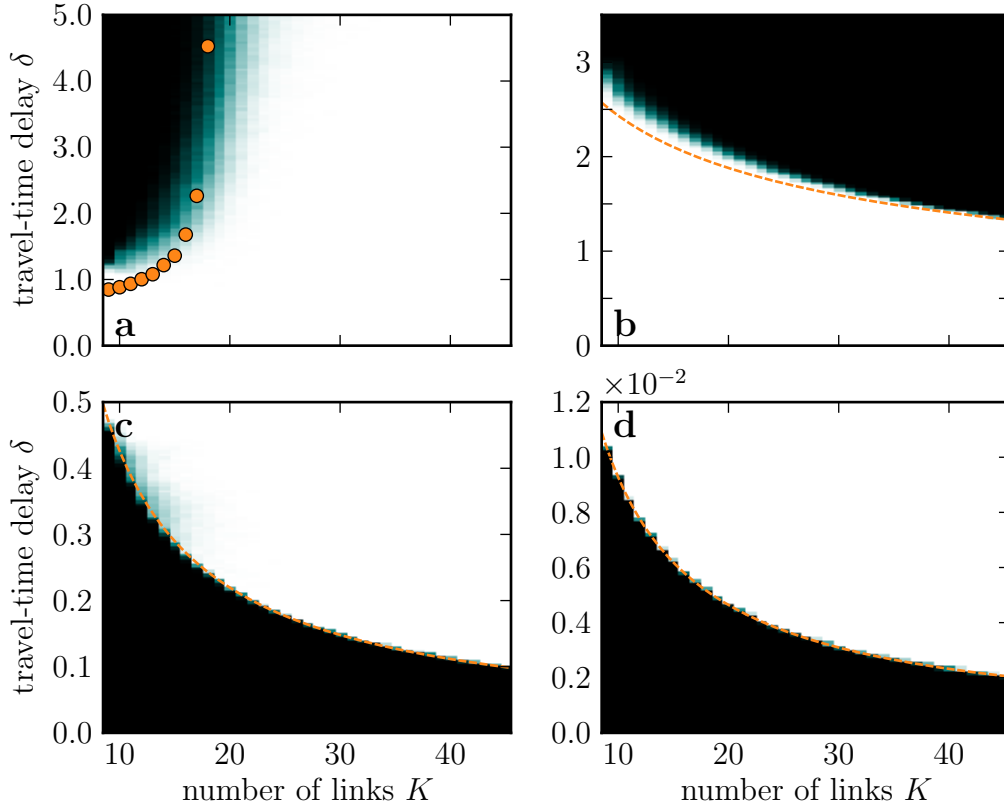


Figure 5.8: Histograms of unstable networks along the four lines (a-d) shown in Fig. 5.7 for different values of K . For each histogram, 10^5 networks are generated. The ratio of unstable to the total number of nets is color coded. Black is used if all nets are unstable, white if all nets are stable. Intermediate values are shown in shades of green. The orange circles and lines show the analytical solutions for DHONs, with $d = 2K/N$. The topological eigenvalues c , which are required to calculate the circles in (a), are estimated by averaging the smallest eigenvalue of 1000 adjacency matrices of Erdős-Rényi networks with $N = 10$ nodes and K links. In general, there is a good agreement between the numerical results and the analytic bifurcation lines for the DHONs. Parameters are chosen as in Fig. 5.6.

with $d = 9$, because this is the only realization of a network with $N = 10$ nodes and $K = 45$ links (Fig. 5.6(d)). For the same reason, we observe the sharp stability transition for $K = 44$. We might expect that the fuzzy area becomes maximal for an intermediate number of K , because the number of different networks in the ensemble becomes maximal for these values. However, it appears that the δ -range in which the stability is topology dependent is maximal for rather small values of K (green-shaded area in Fig. 5.8(b)).

Comparing the stability border of ensembles of DHENs with the bifurcation lines for the DHONs with $d = 2K/N$, we observe that the stability borders of the DHENs is shifted to larger delays as compared to the bifurcation lines of the DHONs

(Fig. 5.8(b)). Hence, networks with a heterogeneous degree distribution seem to be more stable than DHONs. However, this is not a strict rule. Thus, we will see in section 5.3 that DHENs exist that become unstable before the DHONs when delays are changed along section (b). But such networks are comparably rare, so that we might say that DHENs tend to be more stable than DHONs.

The bottom stability border

The most obvious exception to the rule that DHENs are more stable than DHONs can be observed at the bottom bifurcation line for $\tau > 2$ and small values of K (Fig. 5.6(a,b)). For these parameters, a relatively small fraction of networks remains unstable for δ -values considerably above the bifurcation line of the DHONs, whereas the stability border of the other networks seem to coincide with the bifurcation line (Fig. 5.8(c)). For small values of τ close to τ^* , the stability borders of all DHENs seem to coincide with the border of the DHONs (Fig. 5.8(d)), which decreases with increasing K .

Conclusions

The comparison between the numerically obtained stability borders of ensembles of random DHENs with the analytical results for DHONs shows at least a qualitative agreement. The largest deviations are found at the diagonal tongue and at the bottom bifurcation line for large delays τ and small values of K (Fig. 5.8(c)). However, for large values of K or small values of τ , the analytical bifurcation line seem to perfectly describe the stability border of the DHENs (Fig. 5.8(c,d)). The stability border at the off-diagonal tongue is described well by the analytical solution. However, considering the off-diagonal tongues, DHENs seem to be generally more stable than DHONs and this deviation is larger for small values of K . Since, for sufficiently large K , the diagonal tongues vanish and the bottom stability border coincides with the border of the DHONs, the stability of a network is dominated by the off-diagonal tongues. Hence, we may say that DHENs tend to be more stable than DHONs.

Note that from figure 5.8(b) it is not possible to see if some DHENs exist that are less stable than DHONs. In section 5.3, we study DHENs that are particularly stable and particularly unstable. There, we will see that, in fact, degree-inhomogeneous networks exist that are less stable than the DHONs. However, such networks have to be rare to be invisible in figure 5.8(b).

We just stated that DHENs tend to be more stable than DHONs. Thus, we might expect that networks with broader degree distributions tend to be more stable than networks with a narrow degree distribution. This conjecture is tested in the next section by comparing the stability of ensembles of Erdős-Rényi networks with the stability of ensembles of Barabási-Albert networks.

5.2.2 Influence of the degree distribution

From the scatter plots of the ensembles of small Erdős-Rényi networks (ERNs) with $N = 10$ nodes, we see that the off-diagonal tongues can be approximated by the analytic bifurcation lines for $c = d$, where d is set to the average degree of the network (Fig. 5.6). This approximation is better for large numbers of links, and is of course exact for a fully-connected network. Further, all diagonal tongues disappear for sufficiently large numbers of links, so that the stability of the ensemble of random networks can be estimated by the bifurcation lines for $c = d$. However, the approximation shows a systematic error, as DHENs appear to be in general more stable than DHONS. Therefore, we may expect that DHENs with a broader degree-distribution tend to be even more stable than DHENs with a rather narrow distribution such as for the small ERNs studied in the previous section. In this section, we study the influence of the degree distribution by comparing the stability of ensembles of larger ERNs with the stability of ensembles of Barabási-Albert networks (BANs), which have a broad scale-free degree distribution. Further, we test if the stability of both types of networks can be approximated by the stability of a fully-connected network with the same average degree.

In order to study the influence of the degree distribution, we compare ensembles of BANs with ensembles of ERNs with $N = 50$ nodes, and with $K = 96$ and $K = 400$ links. Using the Barabási-Albert model, we obtain such BANs by setting the number of links per added node to $m = 2$ and $m = 10$. Further, we compare the four scatter plots to the analytic bifurcation lines of a fully-connected network with $d = 2K/N$.

For $m = 2$, respectively $K = 96$, we note that the diagonal tongue is present for the ERNs and for the BANs. As we have seen above, especially for small average degrees, the border of the off-diagonal tongue is shifted to larger delays for ERNs as compared to the bifurcation lines (Fig. 5.9(a)). This deviation is nearly two to three times as large for the BANs (Fig. 5.9(b)). Further, the diagonal tongue also seems to be shifted towards larger delays. Hence, not only networks with distributed degrees seem to be more stable than networks with homogeneous degree, but networks with a broad degree distribution seem to be more stable than networks with a narrow distribution.

With an increasing number of links, both, the stability borders of the ERNs and of the BANs approach the corresponding bifurcation lines for $c = d$. Still, the BANs are slightly more stable than the ERNs, but both stability areas can be well approximated by the stability area of a fully-connected network with the same average degree.

The observation that BANs are more stable than the ERNs is also true for the bottom bifurcation line. The quite general statement that DHENs are more stable than DHONS is violated by the ERNs that are unstable above the bottom bifurcation line (Fig. 5.9(a)). However, such networks are not present in the ensemble of BANs. Hence, even though only a heterogeneous degree distribution gives rise to these unstable networks above the bottom bifurcation line, a broad degree distribution such as in the BANs seems to be stabilizing, there. This, shows that there are

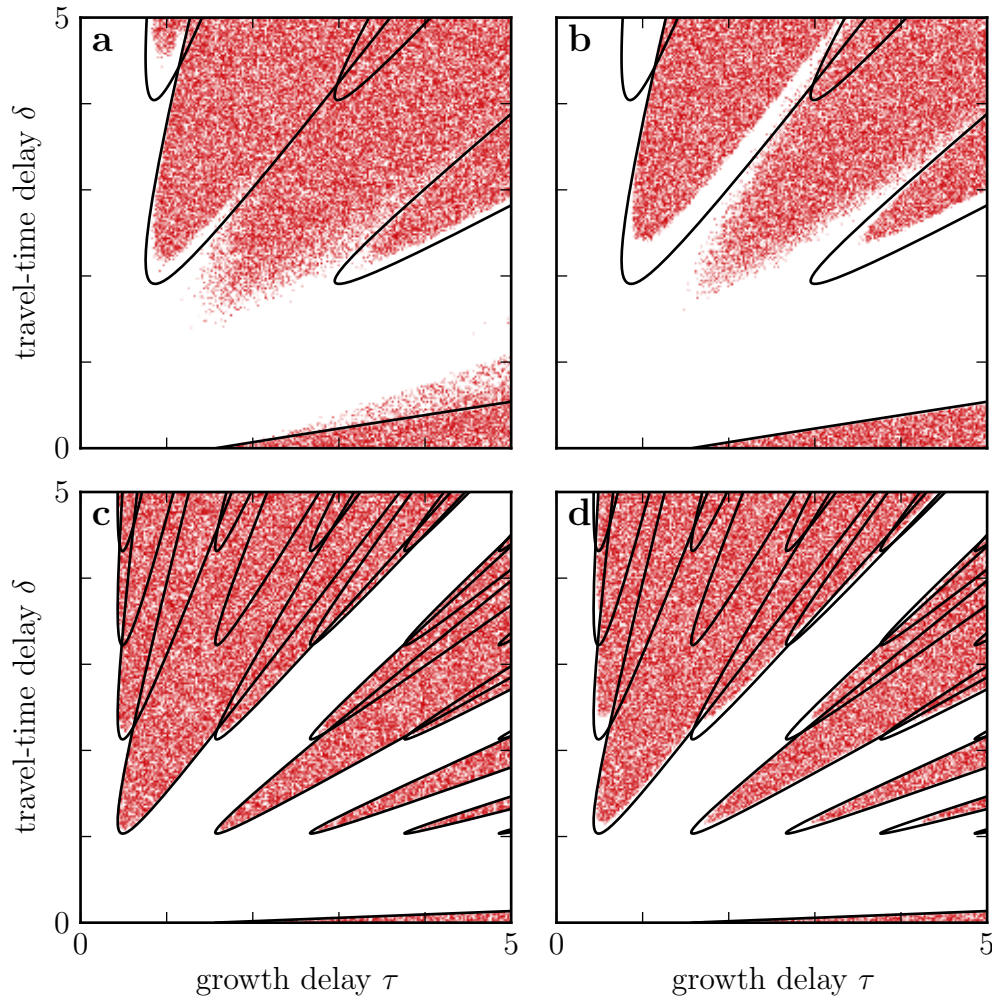


Figure 5.9: Comparison between Erdős-Rényi (ERNs) (a,c) and Barábasi-Albert (BANs) (b,d) networks with $N = 50$ nodes, and $K = 96$ (a,b) and $K = 400$ links (c,d). Only the unstable networks of the 10^5 random networks drawn for each scatter plot are shown. Ensembles of BANs tend to be more stable than ensembles of ERNs. However, for sufficiently large K , the stability of both network types can be approximated by the stability of a fully-connected network with the same average degree. Other parameters are: $g' = -1, l' = 0, k = 1$.

non-trivial relations between the topology and the stability. This is further studied in the next section, where we compare network topologies that are particularly stable and unstable.

5.3 Particularly stable and unstable topologies

In the previous sections, we have seen that the stability borders of the ensembles of random networks are fuzzy, which shows that the stability depends on topological differences between networks in an ensemble. For instance, at the off-diagonal tongue, networks with heterogeneous degrees tend to be more stable than the DHONs, whereas some DHENs remain unstable considerably above the bottom bifurcation line of the DHONs in figure 5.6(a,b). This suggests that networks that are particularly stable at one stability border might be particularly unstable at another border.

Here, we are interested in the network topologies that are particularly stable or unstable along the four sections (a-d) shown in figure 5.7. Therewith, we can study the stability transitions at the diagonal, the off-diagonal and the bottom bifurcation line at $\tau = 1.6$ and $\tau = 3$. Particularly stable (unstable) networks at the diagonal and off-diagonal tongues are those that become unstable for comparable large (small) delays as delays are chosen on the sections (a) and (b). For the two transitions at the bottom bifurcation line, the networks that become stable for comparable small (large) values of δ are considered to be particularly stable (unstable).

In order to find a particularly stable network along one of the the four lines, we randomly draw a network from an ensemble and determine the stability border along the line by the binary search method: Starting with an interval on the line that is sufficiently large so that the network is stable at one end and unstable at the other, we subdivided the interval and chose the sub-interval for which the stability of the two ends differs. We repeat this until the final interval width is less than 10^{-6} . Then, we set the delays to the values given by the interval border at which the network is unstable and repeat drawing networks from the ensemble until we find another stable one. In this way, for each considered stability border and for each K -value, we identified the most stable and unstable networks out of at least 10^6 randomly drawn Erdős-Réni networks with $N = 10$ nodes.

Whereas the generation of 10^6 random networks of size $N = 10$ should be sufficient to find the most stable and most unstable networks in ensembles with small or large numbers of links, we cannot assume that we find the most stable and most unstable networks for ensembles with an intermediate number of links. Nonetheless, the networks found can be used to identify stabilizing and destabilizing topological properties.

Trees

Figure 5.10 shows the scatter plot of an ensemble of connected Erdős-Réni networks with $N = 10$ and $K = 9$ links. We denote the networks shown on the left-hand side as star, chain and fork. The star topology is most stable for all four considered stability transitions. The most unstable topology for the diagonal, the off-diagonal and the bottom bifurcation line at $\tau = 1.6$, is the linear chain. Unsurprisingly, the most stable and unstable networks are identical for the diagonal and the off-diagonal

border, because of the periodicity in bipartite networks. More surprisingly, the same is true for the bottom bifurcation line at $\tau = 1.6$. At the bottom bifurcation line at $\tau = 3$, the most unstable network is the rather irregular fork topology. The reason for the destabilizing effect of such irregular networks is studied in more detail in section 5.3.1.

Note that the star topology that is most stable at all considered borders is the tree with the broadest degree distribution, whereas the linear chain that is most unstable in most cases has the most homogeneous degree distribution. This supports our finding that DHENs tend to be more stable than DHONs.

We already observed in figure 5.6(a) that bifurcation lines of different DHENs coincide at the left part of the tongues and seem to be shifted with respect to each other at the tip and the right part of the tongue. Here, we see this more clearly by comparing the bifurcation lines of the star and the chain topology.

Note that the shift of the bifurcation lines of degree-heterogeneous networks with respect to degree-homogeneous networks results in a shift of the tip, so that the tip

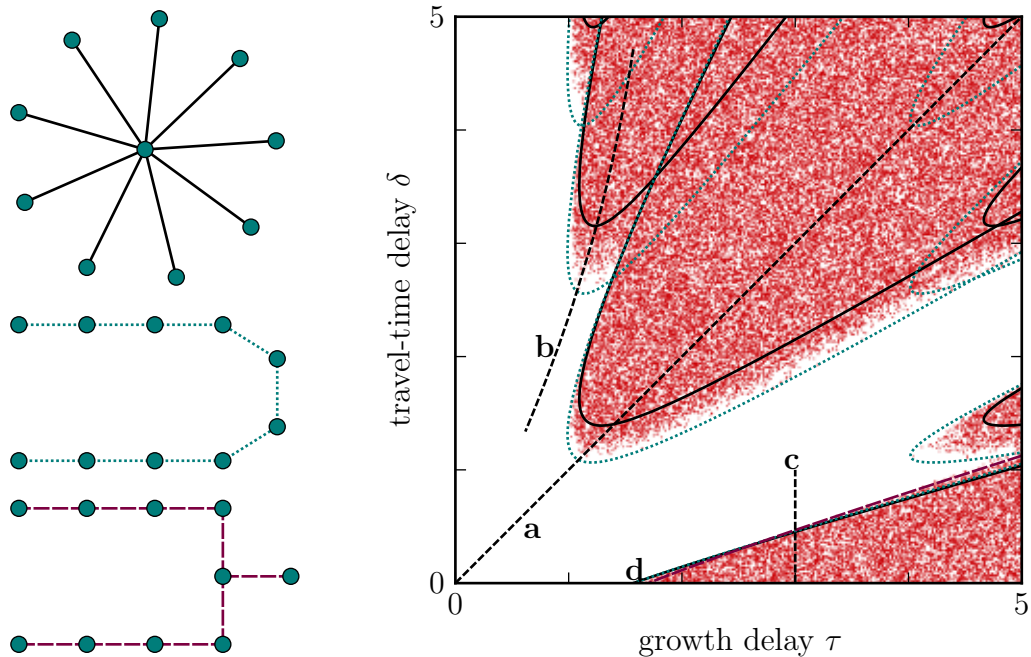


Figure 5.10: Scatter plot of ensembles of connected Erdős-Rení networks with $N = 10$ nodes and $K = 9$ links. The three networks on the left are denoted as star, chain and fork. The star is the most stable networks along all considered lines (a-d) (Line (d) is a hardly visible vertical line at $\tau = 1.6$). The chain is the most unstable network along the lines (a,b,d), and the fork is the most unstable network along the line (c). Bifurcation lines of the star, the chain, and the fork are drawn with solid black, dotted green and long dashed violet lines. Other parameters are: $g' = -1, l' = 0, k = 1$.

of diagonal tongues is in generally not exactly on the diagonal. However, the distance is small enough, so that the tongues can still be related to either the OS or the DS.

Other networks

We just saw that for the diagonal and the off-diagonal tongue, the most stable network is the star and the most unstable network is the chain. We can explain this identity by the π/ω -periodicity of bipartite networks. However, networks with more than $N - 1$ links are not bipartite in general. Hence, we cannot expect that the most stable and most unstable networks are identical for the diagonal and the off-diagonal tongues. In this section, we compare the most stable and unstable networks with $K = 10$ to $K = 15$ links for the four considered stability borders and identify some characteristic properties of these networks.

The diagonal tongue vanishes by moving to infinitely large delays as the number of links is increased. Thus, with an increasing number of links, the stability border of the most stable network diverges to infinity. For even larger numbers of links, more and more networks can be found that are stable for arbitrary large delays. Thus, three networks with $K = 13$ links have been found that remain stable for delays larger than 1000. For smaller numbers of links, the most stable networks become unstable for finite delays. All these networks are composed of triangles that seem to be evenly distributed. In contrast, the most unstable networks found on the diagonal do not contain any triangles but only even loops. Thus, these networks are all bipartite (Fig. 5.11).

At the off-diagonal tongue, the most stable networks are composed of a highly connected center, and all remaining nodes connect to the center so that the links are evenly distributed to the central nodes. Thus, the central nodes have a rather homogeneous degree distribution, whereas the whole network has a broad distribution, because the central nodes have a high degree whereas the other links have a degree of 1. This also holds for the star topology. The most unstable networks at the off-diagonal, except for the one with $K = 10$, are also composed of a highly connected component but the remaining nodes make tree structures (Fig. 5.12).

At the bottom stability border at $\tau = 3$, the most stable networks are comparably irregular. However, even those networks all seem to have a highly connected head with an attached network. But the attached networks may also contain loops. The most unstable networks show a more regular pattern. They are composed of an highly connected head, with either one or two attached chains, where both chains are connected to the same node of the highly connected sub-graph. When deleting the highly connected sub-graph, the remaining chains have an odd length of either tree or five (Fig. 5.13).

At $\tau = 1.6$, the most stable networks found are similar to the most unstable networks found at the off-diagonal. Except for the network with $K = 10$, we obtain the most stable networks from the most unstable at the off-diagonal by replacing the attached tree by a linear chain. In the most unstable networks, the degree seems

to be as homogeneous as possible, so that for $K = 10$ and $K = 15$ all nodes have a degree of 2 and 3, respectively. This property is rather unique in the presented list of networks. However, the network with $K = 15$ is also the most unstable network at the diagonal and the ring topology is the most unstable network for all considered stability borders except for the bottom bifurcation line at $\tau = 3$ (Fig. 5.14).

In general, we can conclude that networks are particularly stable or unstable only with respect to certain areas in delay space. This is most apparent for the network with $K = 15$ that is the most stable one at the bottom bifurcation line at $\tau = 1.6$ but the most unstable at $\tau = 3$. For most considered stability borders, we find characteristic properties of the most stable and most unstable networks. However, this is not possible for the whole bottom bifurcation line, because there the most stable and unstable networks change with the delay τ . The reason for this irregularity is studied in the next section.

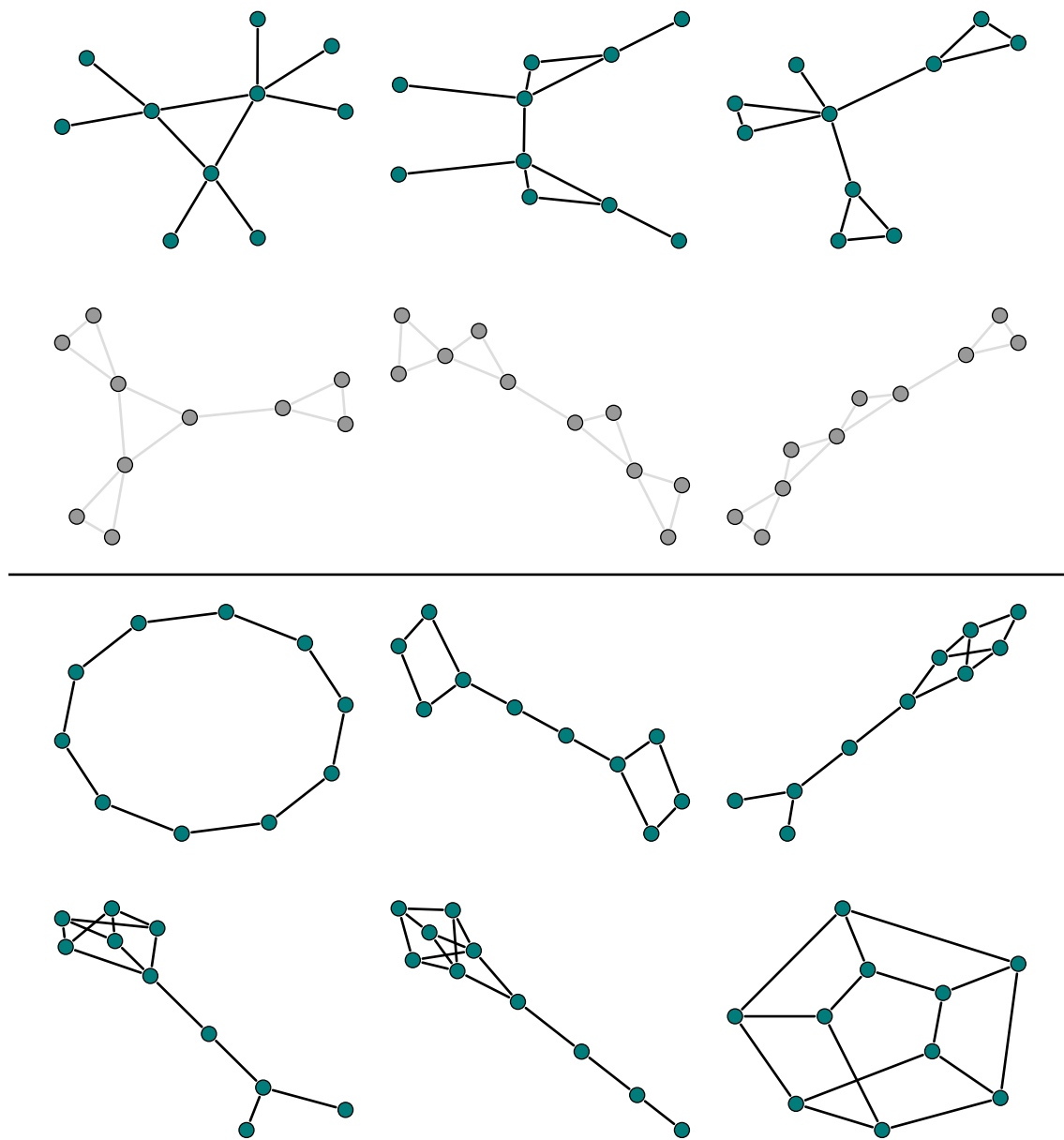


Figure 5.11: Most stable (upper six) and most unstable (lower six) networks with $N = 10$ nodes for the diagonal tongue. For $K = 13$, three networks (gray networks in second row) are found that are stable for arbitrary large delays. The first row show the most stable networks with $K = 10$ to $K = 12$ links. The lower two rows show the most unstable networks with $K = 10$ to $K = 15$ links (from upper left to lower right).

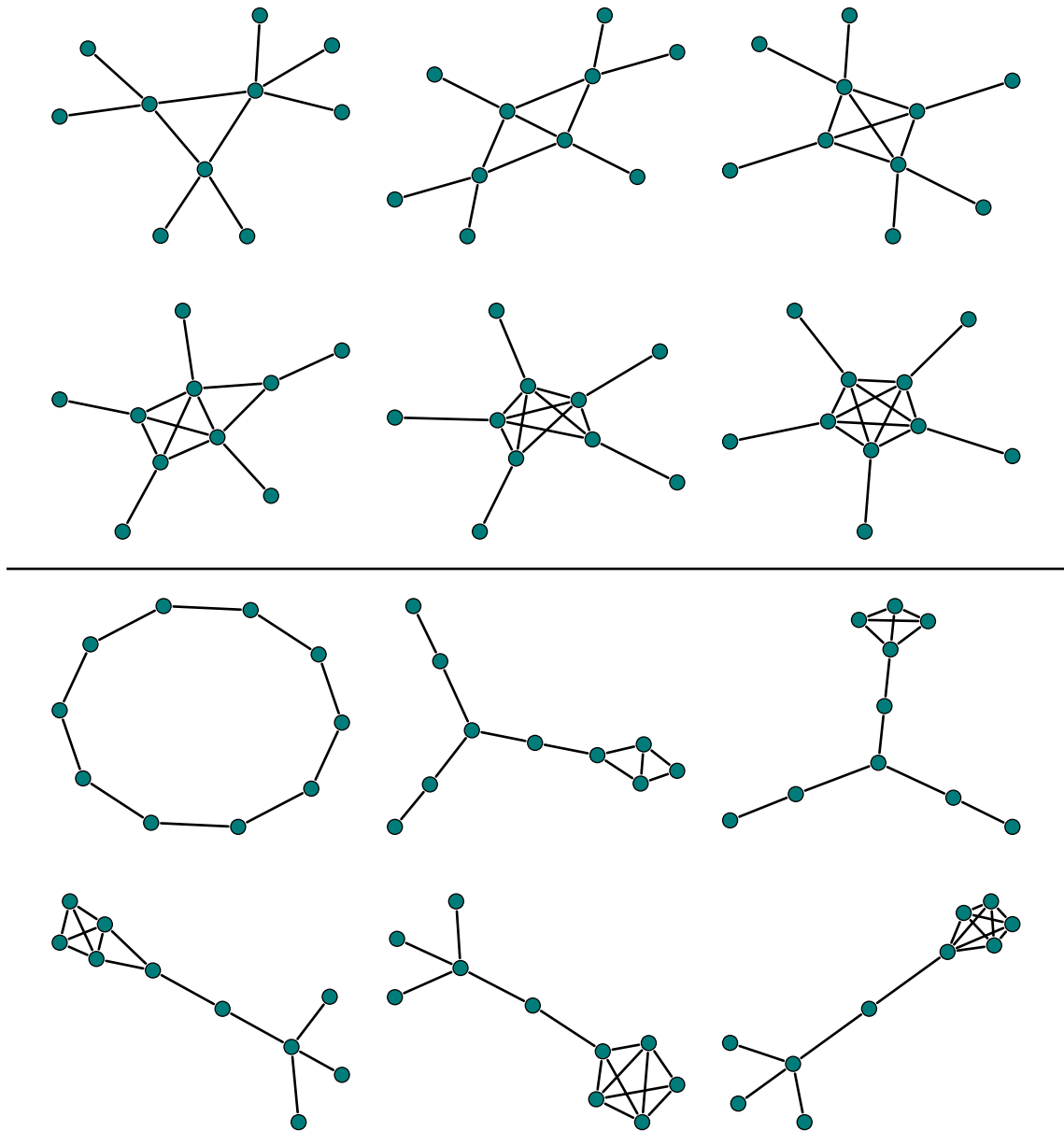


Figure 5.12: Most stable (upper six) and most unstable (lower six) networks with $N = 10$ nodes and $K = 10$ to $K = 15$ links (from upper left to lower right) for the off-diagonal tongue.

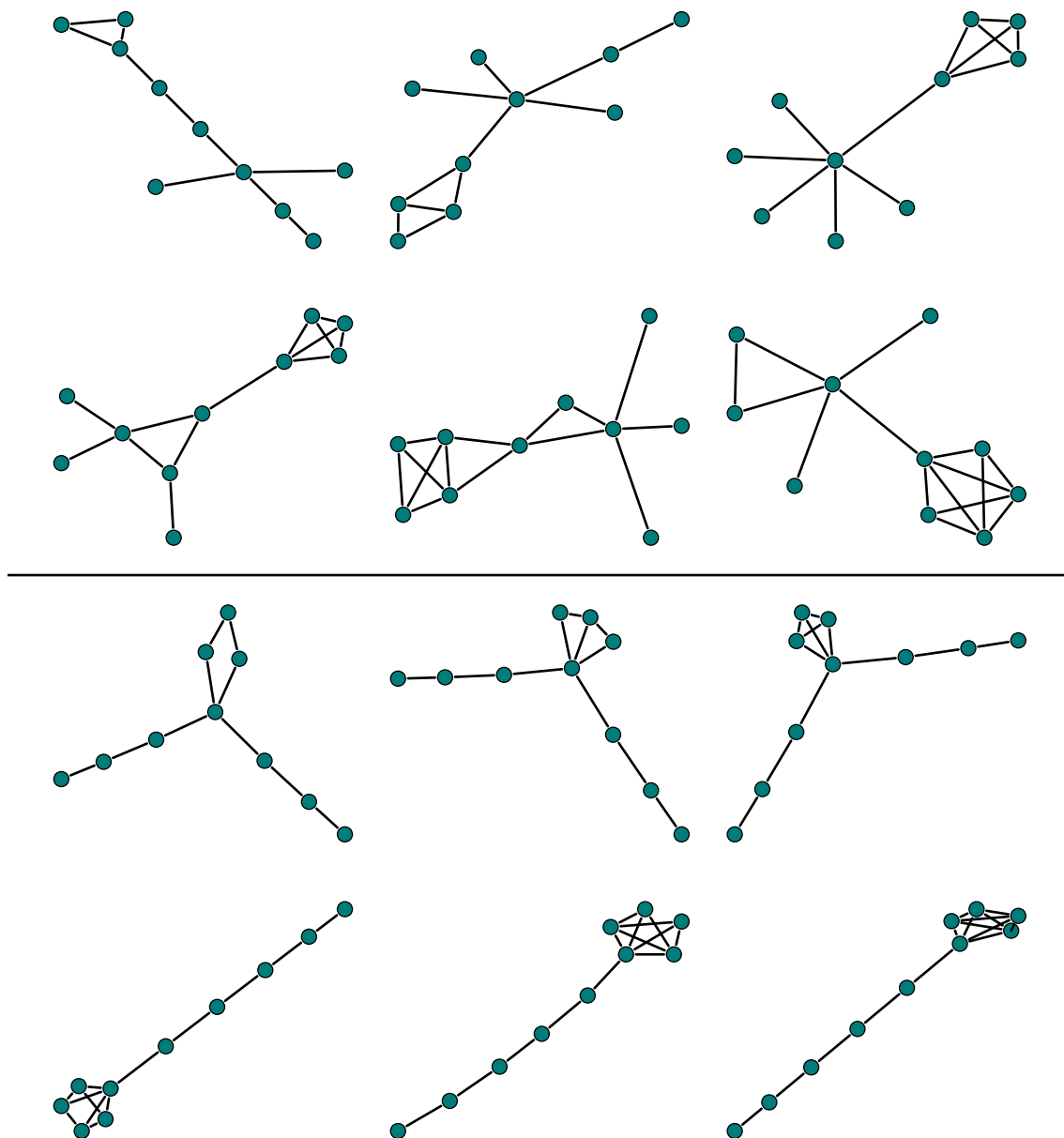


Figure 5.13: Most stable (upper six) and most unstable (lower six) networks with $N = 10$ nodes and $K = 10$ to $K = 15$ links (from upper left to lower right) for the bottom bifurcation line at $\tau = 3$.

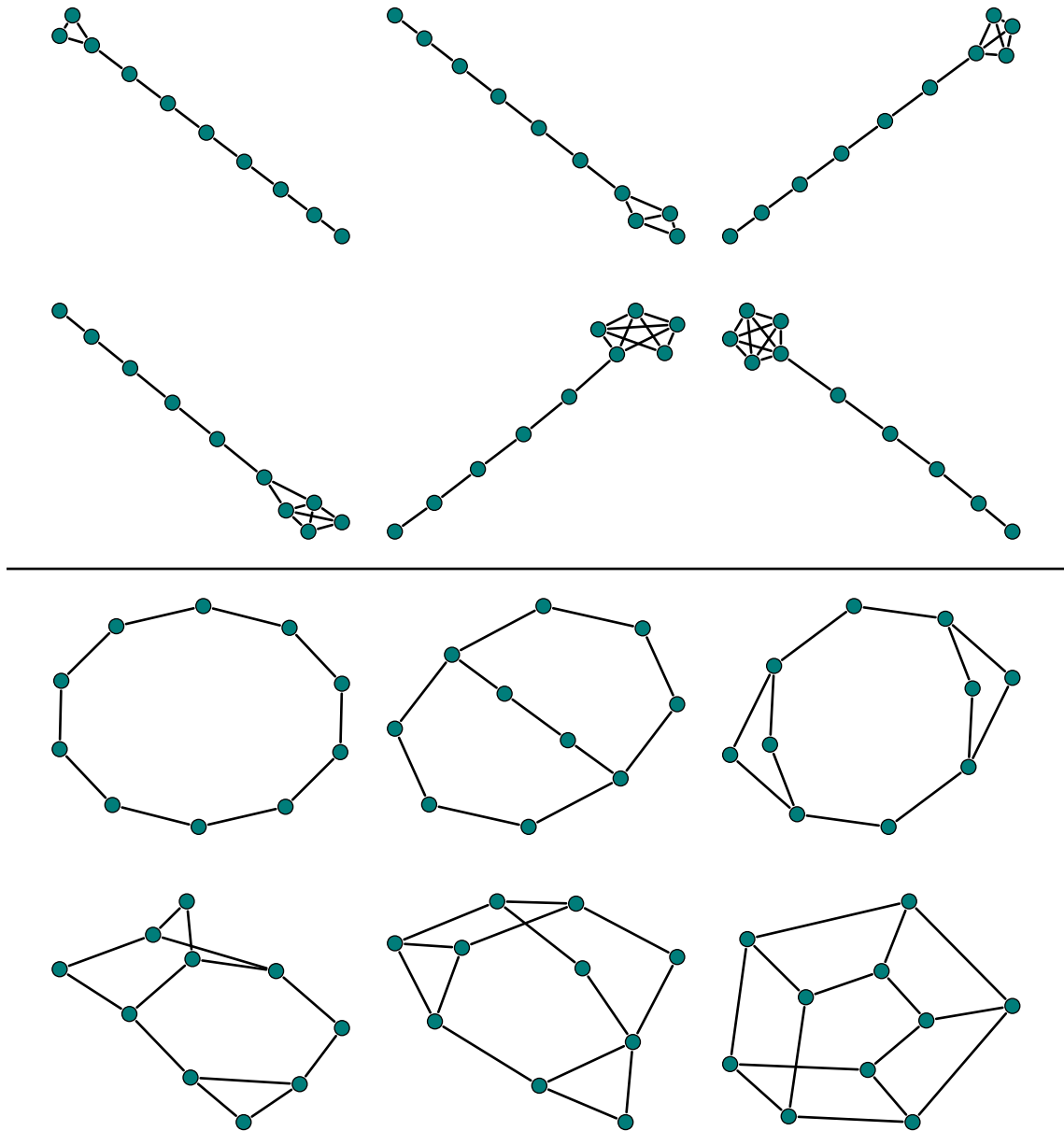


Figure 5.14: Most stable (upper six) and most unstable (lower six) networks with $N = 10$ nodes and $K = 10$ to $K = 15$ links (from upper left to lower right) for the bottom bifurcation line at $\tau = 1.6$.

5.3.1 Unstable networks above the bottom bifurcation line

We have seen that for small values of K and large values of τ , some DHENs remain unstable well above the bottom bifurcation line of the DHONs, whereas the stability border of most other networks coincide with the bifurcation line (Fig. 5.6(b) and Fig. 5.8(c)). Here, we want to study the reason for this instability by studying the bifurcation lines of a network that is particularly unstable at the bottom stability border for $\tau = 3$.

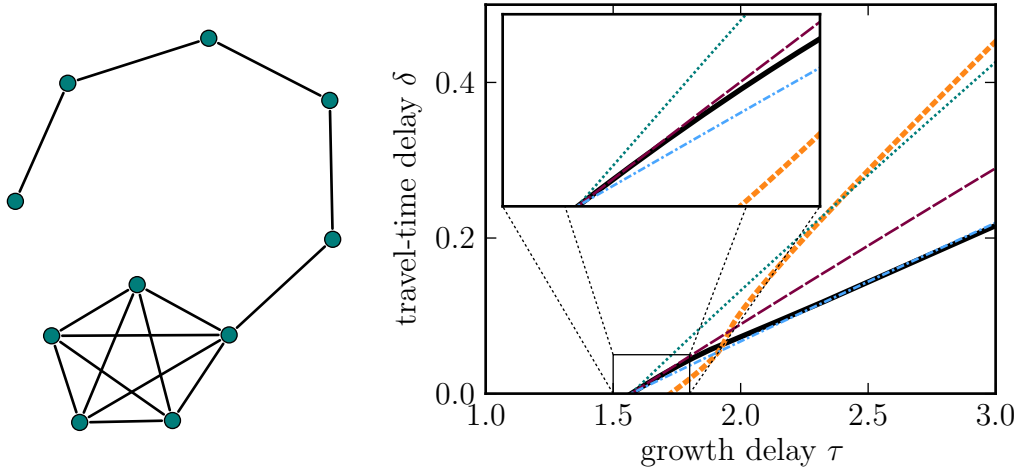


Figure 5.15: Comparison of the bottom bifurcation lines for the network on the left-hand side and for the DHONs with $d = 2$, $d = 3$ and $d = 4$ (dotted green, long dashed violet and dash-dotted blue lines). We denote the bifurcation line of the network that crosses the point $(\tau^*, 0)$ as primary bifurcation line (thick solid black line), whereas the other line (thick dashed orange line) is denoted as secondary line. In contrast to DHONs, two bifurcation lines affect the stability. For large τ , these might be related to sub-graphs of the network. However, for τ close to τ^* , one line approaches the line of DHONs with $d = 2K/N$. Other parameters are: $g' = -1, l' = 0, k = 1$.

For the network in figure 5.15, the bottom stability border is governed by two bifurcation lines. In contrast, we found for DHONs that the bottom stability border is given only by the bifurcation line of the eigenvalue $c = d$. A corresponding bifurcation line, which also crosses the point $(\tau^*, 0)$, must exist in all DHENs. Indeed, one of the two bifurcation lines crosses this point. We denote this line as the primary bifurcation line, whereas we denote the other as secondary line.

We assume that the two different bifurcation lines might be related to sub-graphs of the network. Therefore, we compare the two bifurcation lines to the bottom bifurcation lines of DHONs with degrees $d = 3$, $d = 2$ and $d = 4$, because the network has $N = 10$ nodes and $K = 15$ links and consists of a fully-connected network of 5 nodes and an attached linear chain of 5 nodes. Hence, the average degree is 3, the degree of the fully connected sub-graph is 4 and the linear chain has a degree close to

2. We observe that the secondary bifurcation line is close to the ($d = 2$)-line, which suggests that the chain sub-graph is crucial there. The primary bifurcation line is close to the ($d = 4$)-line, which suggest that this line is mostly influenced by the fully-connected sub-graph. But most interestingly, the primary branch approaches the bifurcation line for $d = 3$ for τ approaching τ^* .

In summary, the bottom stability border of some DHENs is governed by two bifurcation lines, whereas it is governed by only a single line in DHONs. However, for small values of τ the stability borders of DHENs and DHONs seem to coincide. This is studied in more detail in the next sections.

5.3.2 Topology-independence of the bottom stability border

In the previous section, we found that the bottom stability border of a DHEN with average degree $d = 2K/N$ approaches the bottom bifurcation line of DHONs with the same degree d if τ approaches τ^* . From the figures (5.6(a,b),5.8(d)), we see that this seems to be true for all DHENs. Thus, except for the average degree, the stability borders seem to be almost independent of the topology.

In order to study the topology dependence of the stability border close to τ^* , we use the data obtained while searching for the most stable and the most unstable networks at the bottom stability border at $\tau = 1.6$. For each network, we estimated the δ -value for which the network changes its stability. In figure 5.16, we mark the area between the δ -value of the most stable and the most unstable network by a black bar. Though, a minimum height ensures that bars remain visible. By comparing these bars for networks with different numbers of links, we can compare the influence of the number of links with the influence of other topological properties. We observe that the bars for different numbers of links do not overlap. Hence, the number of links K is the major factor that determines the stability border.

Even though the number of links is the major influence that determines the position of the stability border at $\tau = 1.6$, the finite widths of the bars show that other topological properties influence the stability, too. It is plausible to assume that these properties become more relevant for larger networks. However, in section 5.3.1, we saw that the primary bifurcation line of a DHEN with K links approaches the bifurcation line of DHONs with $d = 2K/N$ if τ approaches τ^* . Hence, we can assume that for τ approaching τ^* , the average degree becomes more crucial for the stability at the bottom bifurcation line, so that all other topological properties can be neglected even in large networks.

In the following, we test the assumption that topological properties, except for the average degree, become irrelevant for the bottom stability border as τ approaches τ^* . Recall that the stability close to τ^* is determined by the primary bottom bifurcation line that crosses the point $(\tau^*, 0)$ for all DHENs. Close to τ^* , the stability border can be approximated by a straight line whose slope S is identical to the slope of the bifurcation line at τ^* . For DHONs, we found that the bottom bifurcation line

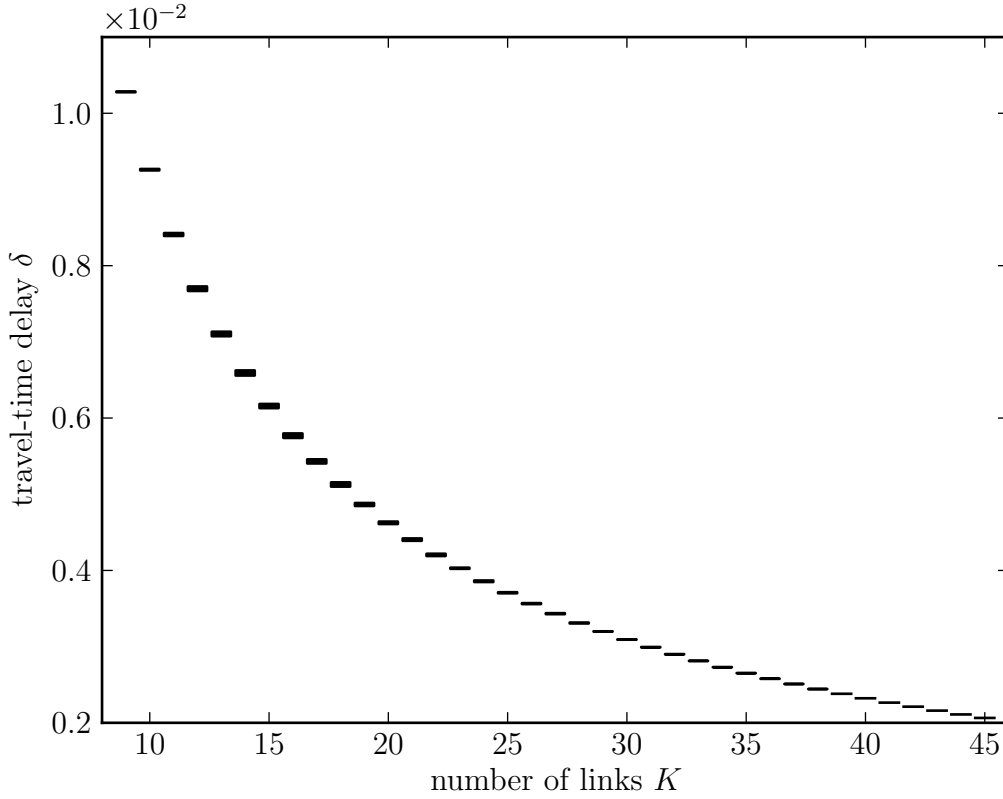


Figure 5.16: Position of the bottom stability border at $\tau = 1.6$ for ensembles of Erdős-Rényi networks with different numbers of links K . The bars mark the δ -region from the most stable to the most unstable network out of at least 10^6 randomly sampled networks. Though, a minimum height ensures that bars remain visible. Bars for different numbers of links do not overlap, which shows that the stability border is determined mainly by the number of links.

approaches

$$\delta = \left(\frac{\tau}{\tau^*} - 1 \right) \frac{1}{dk} \quad (5.11)$$

for small values of δ (Sec. 4.5.3). Thus, the slope at τ^* is given by

$$S_d = \frac{1}{dk\tau^*}. \quad (5.12)$$

If the above assumption is true, then the slopes S for all DHENs with an average degree d approach S_d when τ approaches τ^* .

In order to test if the slopes S of DHENs with an average degree d approach S_d , we perform a numerical continuation of the primary bottom bifurcation line of the most stable and the most unstable networks with $K = 14$, $K = 15$ and $K = 16$ links we found at $\tau = 1.6$. Instead of calculating the slope S at any point (τ, δ) on the

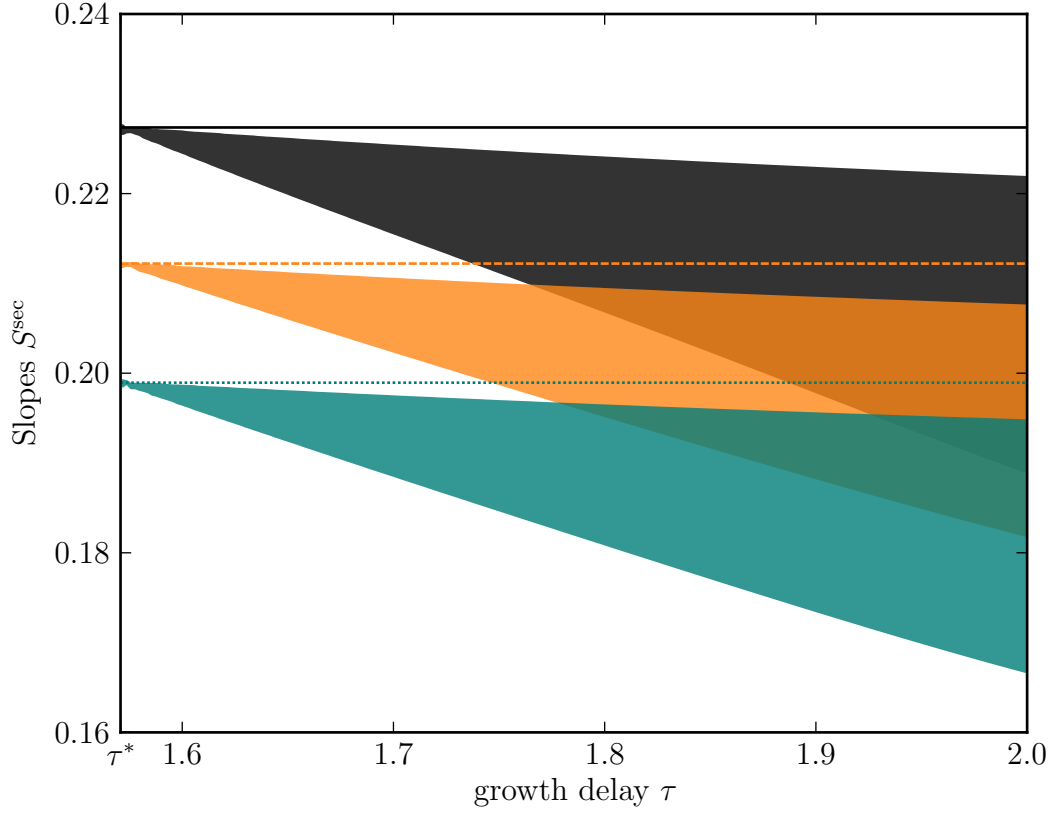


Figure 5.17: Slopes $S^{\text{sec}}(\tau)$ of the secant crossing $(\tau^*, 0)$ and (τ, δ) on the bottom bifurcation line of the most stable (lower border of shaded area) and the most unstable (upper border of shaded area) network with $K = 14$ (top black area), $K = 15$ (middle orange area) and $K = 16$ (bottom green area) links. The slopes for DHENs with an average degree of $d = 2K/N$ approach the corresponding slope S_d (Eq. 5.12) as τ approaches τ^* .

bifurcation line, we calculate the slope $S^{\text{sec}}(\tau)$ of the secant crossing $(\tau^*, 0)$ and (τ, δ) (Fig. 5.17). However, both slopes are identical at $\tau = \tau^*$. The areas between the lines for the most stable and the most unstable network with the same number of links are shaded, because the slopes of the bifurcation lines of other networks with the same number of links lie somewhere inside the area. For each K , the slopes of the most stable and the most unstable network both approach the corresponding value of S_d as τ approaches τ^* . Thus, the average degree is the only topological property that remains relevant if τ approaches τ^* .

Note that we assumed that the most stable and the most unstable networks we found at $\tau = 1.6$ remain the most stable and the most unstable network as τ approaches τ^* . This assumption seems to be justified by the smooth shape of the bifurcation lines and the fact that all bifurcation lines have to cross $(\tau^*, 0)$. Further, if even the bifurcation lines that are most distinct at $\tau = 1.6$ converge as τ approaches

τ^* , we may expect that the other bifurcation lines converge as well.

Recall that the bifurcation lines of any network can be mapped to other bifurcation lines by shifting each point by multiples of $2\pi/\omega$ along τ or δ . Thus, the left part of each bifurcation line of the eigenvalue $c = d$ or corresponding bifurcation lines in the DHENs, can be obtained by a mapping of the bottom bifurcation line. If we assume that the different networks with the same K not only share the same bottom bifurcation line in the (τ, δ) -plane but also share the same values for the imaginary-part ω of the purely imaginary eigenvalue λ , then the left part of each of these tongues is similarly sharp as the bottom line. In fact, the stability borders are only fuzzy at the right part of the tongues, whereas the left part of the tongue borders is sharp (Fig. 5.6(a,b)).

The observation that the bottom stability border close to τ^* is solely given by the average degree, which is a global property of the network, is rather surprising. Thus, each link is equally important independent of its location. Further, the dependence on a global property requires an interaction between distant parts of the network. Therefore, we may assume that there is some kind of interaction length that diverges at $\tau = \tau^*$.

5.4 Amplitude death for small coupling delays

In the previous section, we saw that all DHENs with $d = 2K/N$ approach the same bottom bifurcation line if τ approaches τ^* . This line is given by Eq. (5.11), which has been derived for DHONs under the condition that δ approaches 0 (Sec. 4.5.3). This condition not only includes the case that τ approaches τ^* but also the limit of large coupling strength for arbitrary delays τ . Here, we want to study if Eq. (5.11) is valid in the limit of large coupling strength k and if an amplitude death regions exist above this stability border for all DHENs.

To answer the question if Eq. (5.11) describes the bottom bifurcation line of DHENs for large coupling strength k is not trivial. We found that the bottom bifurcation lines of DHENs do not coincide with the bifurcation lines of the DHONs with $d = 2K/N$ for large values of τ and δ , but both lines do coincide for τ close to τ^* , where δ is close to 0. So, on the one hand δ approaches 0 if k increases; Hence, we might expect that both bifurcation lines coincide. On the other hand τ might be significantly larger than τ^* , so that we shall not expect that both lines coincide.

Even if both bifurcation lines coincide, we cannot be sure that all DHENs give rise to amplitude death above this bifurcation line. For DHENs, additional tongues of instability might arise that destabilize the system above the bottom bifurcation line.

In order to test that the bottom stability border of DHENs is given by Eq. (5.11) with $d = 2K/N$, we observe the scatter plots in figure 5.18. Figure (a) shows all stable networks and figure (b) all unstable networks out of 10^5 randomly drawn Erdős-Rényi networks. The two delays have been drawn from a uniform distribution in the logarithmic space. For large k all networks are unstable below the line described by

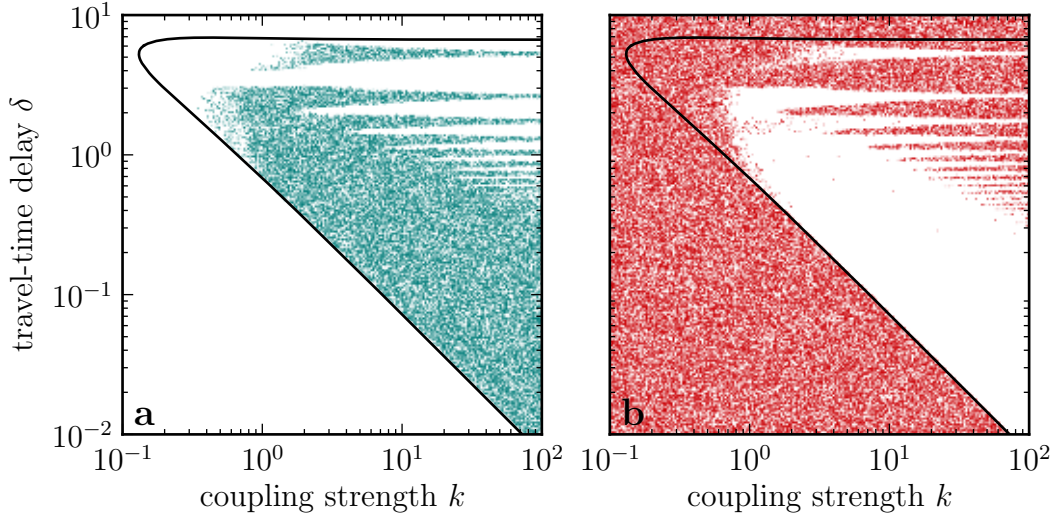


Figure 5.18: Scatter plots of 10^5 Erdős-Rényi networks with $N = 10$ nodes and $K = 15$ links. Figure (a) shows only the stable networks and figure (b) only the unstable networks. Delays are drawn from a uniform distribution in the logarithmic scale. For large coupling strength, the bottom stability border for all DHENs coincides with the border of DHONs. For sufficiently large coupling strength and sufficiently small coupling delays above the bottom stability border, amplitude death occurs in all DHENs. Other parameters are: $g' = -1, l' = 0, k = 1$.

Eq. (5.11) (Fig. 5.18(a)), whereas all network are stable above the line (Fig. 5.18(b)). Hence, Eq. (5.11) seems to be valid for all DHENs and all networks display the phenomena of amplitude death above the bottom bifurcation line.

5.5 Summary

In this chapter, we studied the stability of degree-heterogeneous networks (DHENs) using a numerical method, which allows us to calculate the number of eigenvalues with positive real-part (Sec. 5.1). By comparing the stability patterns of ensembles of random networks with K links to the bifurcation lines of degree-homogeneous networks with $d = 2K/N$, we found that the stability pattern of DHENs resembles the pattern of the DHONs (Sec. 5.2). The pattern is governed by a diagonal set of tongues (DS) and an off-diagonal set of tongues (OS). For trees, both sets give rise to a π/ω -periodicity along the δ -axis such as in bipartite DHONs. Thus, it appears that all bipartite networks give rise to a π/ω -periodic stability pattern. With an increasing number of links K , the DS vanishes towards infinitely large delays, which can in principle be understood by the analytical results as well: The ensemble average of the smallest negative eigenvalue c^{\min} increases with increasing K and thus violates the condition for the existence of tongues, $|c| > c^*$, for sufficiently large K .

The deviation between the analytical bifurcation lines of DHONs and the stability border of the ensemble of DHENs is rather large for the diagonal tongue as compared to other stability borders. However, for sufficiently large K , the DS vanishes, and the stability borders can be approximated by the stability borders of a fully-connected network with $N = d + 1$ nodes. The approximation has a systematic error, as DHENs tend to be more stable than DHONs. Further, a comparison of ensembles of Erdős-Rényi networks with ensembles of Barabási-Albert networks suggests that DHENs with a broad degree distribution tend to be more stable than DHENs with a narrow distribution (Sec. 5.2.2).

When stating that DHENs tend to be more stable than DHONs, we admit that this is not always true. First, stating that a given topology is more or less stable than another is not possible in general, because the order in which networks lose stability depends on the actual stability border under considerations. However, for sufficiently large numbers of links, when the stability is only governed by the OS, DHENs seem to be more stable than DHONs. Nonetheless, the most unstable networks at the off-diagonal tongue are degree-heterogeneous. However, such particularly unstable DHENs are rare in the ensembles of random networks.

Unlike, the DHONs, the stability of DHENs is not fully determined by just two sets of tongues, but other bifurcation lines can affect the stability of the system. Thus, for some DHENs with a rather small number of links, we observed a second bottom bifurcation line that destabilized the system for τ significantly larger than τ^* (Sec. 5.3.1). Therefore, the order in which different networks lose stability changes along the bifurcation line. However, for τ close to τ^* , the stability of all DHENs is governed by the bottom bifurcation lines that corresponds to the bottom bifurcation line of the DHONs.

The bottom bifurcation lines of DHENs corresponding to the line of DHONs, not only cross the point $(\tau^*, 0)$ in the delay space, but they cross this point with the same slope as the line of the DHONs. The slope depends on the average degree d . Thus, for τ larger but close to τ^* , the stability at the bottom bifurcation line is governed by the average degree, which is a global property of the network, but the stability is independent of all other topological properties (Sec. 5.3.2).

The bottom stability borders of all DHENs are not only identical for small τ but also for sufficiently large coupling strength k . Thus, such as for DHONs (Sec. 4.5.3), the bottom bifurcation line approaches $\delta = 0$ as k approaches infinity. Further, we observed that all DHENs exhibit amplitude death above this bifurcation line (Sec. 5.4).

6 Discussion and Outlook

In this thesis, I demonstrated the application of generalized modeling to delay networks and used this approach to study a model of delay-coupled delay oscillators, where the coupling is mediated by conserved flows between nodes. The auto-catalytic growth of the node loads is delayed by the growth delay τ and the time needed for loads to flow from one node to another is given by the travel-time delay δ . Within the generalized modeling approach, the model is analyzed by a local stability analysis based on the Jacobian matrix of the system. For degree-homogeneous networks (DHONs), the Jacobian can be decomposed by means of the eigenvalues of the adjacency matrix. Therewith, it is possible to calculate the bifurcation lines analytically. In order to investigate degree-heterogeneous networks (DHENs), I applied a numerical sampling method that uses Cauchy's Argument Principle to calculate the number of eigenvalues with positive real-parts.

After we have identified parameter regions where the stability is governed by the single node system and hence independent of the network topology, we restricted ourselves to the analysis of the remaining parameter space. There, the system gives rise to Hopf-bifurcations indicating the transition from a stable to an unstable steady state, usually resulting in oscillatory dynamics.

In the (τ, δ) -delay space, the bifurcation lines display a $2\pi/\omega$ -periodicity, where ω is the imaginary part of the eigenvalue that crosses the imaginary axis. Thus, it is reasonable to group them into periodic sets and denote the lines in each set by integers r and s , enumerating the lines along the τ - and the δ -direction. Depending on the parameters, the two ends of each line either approach straight lines running to infinitely large delays, or lines with the same index r merge, so that the otherwise separate bifurcation lines form connected lines reaching from $\delta = 0$ to infinity. In the first case, each bifurcation line borders a tongue of instability and stable channels can exist between them. In the latter case, tongues are merged, so that no stable channels exist.

Stability and topology

For DHONs, there is a direct relation between the (topological) eigenvalues of the adjacency matrix and the bifurcation lines. Each eigenvalue gives rise to one set of tongues. A complex phase ψ^c of an eigenvalue $c = |c| \exp(i\psi^c)$ does not change the bifurcation line, except that it shifts the lines by ψ^c/ω along the δ -direction. The absolute value of the eigenvalue determines the size of the tongue. Larger absolute values result in larger tongues, which usually fully cover tongues of eigenvalues with

the same complex phase but with a smaller absolute value.

For bidirectional DHONs, the stability is governed by the tongues arising from the largest positive eigenvalue $c = d$ and the smallest negative eigenvalue. The smallest negative eigenvalue is maximal for a fully-connected network, for which it is -1 , and is minimal for bipartite networks, for which it is $-d$. Hence, the fully-connected network and all bipartite networks provide the most stable and most unstable topologies for a given degree d . A similar conclusion has been drawn from the analysis of delay-coupled oscillators without an internal node delay [50]. The finding that bipartite networks are least stable has also been made in a model of delay-coupled maps, for which it was shown that bipartite networks cannot stabilize maps that are unstable without coupling [75]. However, in our model, and in the model of the delay-coupled oscillators, bipartite networks are still able to stabilize unstable nodes and hence give rise to amplitude death. But the parameter space in which this effect occurs is minimal for bipartite networks.

The direct dependency of the bifurcation lines on the topological eigenvalues allows to relate bifurcation lines to certain properties of the network that are well-known to be related to the eigenvalues [133]. For instance, the spectral density of Erdős-Rényi networks differs significantly from the spectral density of Barabási-Albert networks[134]. Further, certain singular eigenvalues in network spectra have been related to local sub-graphs such as stars and fully-connected cliques [135, 136]. Additionally, certain eigenvalues of symmetric motifs are conserved in embedding networks if the connections to the embedding network retains the symmetry of the motif[137].

It should be noted that the works relating network topologies to the eigenvalue spectra usually consider degree-heterogeneous networks. But for these networks, there is in general no direct relation between the spectra and the bifurcation lines. However, even for these networks the analytical solutions for the DHONs might provide a good approximation. Further, for embedded symmetric motifs, the analytical solutions is probably precise if the motif itself is degree-homogeneous. In this case d should be set to the common degree of the motif nodes. Thus, even a visual inspection of the network topology can provide information about the stability of the network.

Even though there is no direct relating between the eigenvalues and the bifurcation line in DHENs, it is still possible to relate topological properties to certain stability patterns. Thus, the relation between bipartite networks and the π/ω -periodicity of the bifurcation lines, which we first saw in the analytical solutions for the DHONs, can be found in DHENs as well. Further, similar to the DHONs the stability of bidirectional DHENs is mostly governed by only two sets of tongues. One exception is the second bifurcation line in some DHENs that destabilizes the network above the bottom bifurcation line that is known from the DHONs.

A major result of this thesis is that the stability of ensembles of large random networks with sufficiently many links resembles the stability of a fully-connected network with similar degree. This is rather surprising because of the great diversity of topologies which are realized in the ensemble. However, networks with special

properties such as bipartite networks or networks with cliques are very rare and hence unlikely to be drawn, so that such networks hardly influence the stability of the ensemble.

Amplitude death and heterogeneity

A rather general rule has been found that states that DHENs tend to be more stable than DHONs and that DHENs with a broad degree distribution tend to be more stable than DHENs with a narrow distribution. Thus, it appears that heterogeneity in the network structure has a stabilizing effect and hence supports the occurrence of amplitude death.

Regarding amplitude death as synchronization to a common steady state, the finding that heterogeneous network structures support amplitude death is consistent with results obtained from delay-coupled maps. In these systems it was found that random networks are more likely to synchronize than regular nets [74]. Further, heterogeneous delays are more likely to give rise to amplitude death than homogeneous delays [76, 79]. Also considering that amplitude death even arises in systems without delays if the oscillators are non-identical [70–72], we may state that heterogeneity in general supports the occurrence of amplitude death.

Stability dependence on global properties

Maybe the most surprising result in this thesis is that the only topological property that affects the bottom stability border for small delays δ is the average degree. This is particularly surprising because the average degree is a global property for which each link is equally important. Therefore, topological information need to be transmitted through the whole network, which suggest a diverging interaction length.

For small values of δ , the bottom stability borders for all DHENs with the same average degree fall on the same line, which is described by an analytical formula derived for the DHONs. The critical delay δ is proportional to $1/(dk)$, where dk can be viewed as an effective coupling strength. A sampling of random networks showed that in all sampled networks, amplitude death occurs in a small area above the bifurcation line. In contrast to the delay-coupled Stuart-Landau oscillators [30], we find amplitude death for arbitrary small coupling delays if the coupling strength becomes sufficiently large.

Outlook

Many results that have been found numerically might as well be proved in a mathematical rigorous way. This includes the topology- and delay-independent stability condition for $g' > l'$ and the finding that the bottom bifurcation lines of DHENs approach the line of DHONs for small δ .

The numerical method I used to investigate the degree-heterogeneous networks can be applied to general delay networks with arbitrary many delays in the node dynamics or in the coupling. In this thesis, I only analyzed networks with identical nodes and links. But the method also allows to study networks with non-identical delay oscillators, and non-identical coupling. Thus, we might also study the phenomena of amplitude death in non-identical oscillators. It is known that amplitude death either requires non-identical oscillators or delayed coupling. Hence, for delay-coupled non-identical delay oscillators, we might expect that the parameter space of amplitude death can be extended towards smaller coupling delays.

Networks with non-identical nodes are likely to result in non-trivial steady states and hence a non-trivial normalization of the node loads. In this case, the formulation of the model in terms of the normalized loads hinders the description of conserved flows between nodes. Therefore, a generalized analysis of such systems is more complicated. However, instead of a generalized analysis, we may use the numerical method to investigate specific models. In most cases, the steady state does not depend on the delays. However, delays are likely to influence the stability of steady states. Hence, the steady state and the required coefficients of the Jacobian matrix can be calculated from the system without delays, whereas the influence of the delays can be studied using the numerical sampling method.

The efficiency of the numerical method, also allows us to study large numbers of networks. Therewith, particularly stable and unstable networks can be identified as demonstrated in section 5.3. Instead of just drawing the networks from a random ensemble, the method can be improved by using evolutionary algorithms to modify the networks. Such algorithms can be used to identify networks that realize a feedback control to stabilize an otherwise unstable system. Such networks might find applications in engineering, for instance in coupled laser systems [122].

The generality of the model, probably allows to apply the results to real-world system, such as gene-regulatory network. Even though our models aims at describing systems with conserved flows between nodes, we saw that the results can also be applied to systems in which only the average of all inputs influences the node dynamics. Even in systems that are not well described with our model, some fundamental results, such as the the basic stability pattern in the delay space, might still be valid.

Bibliography

- [1] Romualdo Pastor-Satorras and Alessandro Vespignani. Epidemic spreading in scale-free networks. *Physical Review Letters*, 86(14):3200–3203, 2001. doi:10.1103/PhysRevLett.86.3200.
- [2] Matt J. Keeling and Ken T. D. Eames. Networks and epidemic models. *Journal of The Royal Society Interface*, 2(4):295–307, 2005. doi:10.1098/rsif.2005.0051.
- [3] José M. Montoya, Stuart L. Pimm, and Ricard V. Solé. Ecological networks and their fragility. *Nature*, 442(7100):259–264, 2006. doi:10.1038/nature04927.
- [4] Robert M. May. Food-web assembly and collapse: Mathematical models and implications for conservation. *Philosophical Transactions of the Royal Society B*, 364(1524):1643–1646, 2009. doi:10.1098/rstb.2008.0280.
- [5] Stefano Boccaletti, Vito Latora, and Yamir Moreno, editors. *Handbook on Biological Networks*. World Scientific, 2010.
- [6] Timothy S. Gardner, Charles R. Cantor, and James J. Collins. Construction of a genetic toggle switch in *Escherichia coli*. *Nature*, 403(6767):339–342, 2000. doi:10.1038/35002131.
- [7] Ron Weiss, Subhayu Basu, Sara Hooshangi, Abigail Kalmbach, David Karig, Rishabh Mehreja, and Ilka Netravali. Genetic circuit building blocks for cellular computation, communications, and signal processing. *Natural Computing*, 2(1):47–84, 2003. doi:10.1023/A:1023307812034.
- [8] Ralf Steuer, Thilo Gross, Joachim Selbig, and Bernd Blasius. Structural kinetic modeling of metabolic networks. *Proceedings of the National Academy of Sciences of the United States of America*, 103(32):11868–11873, 2006. doi:10.1073/pnas.0600013103.
- [9] Thilo Gross and Ulrike Feudel. Generalized models as a universal approach to the analysis of nonlinear dynamical systems. *Physical Review E*, 73(1):016205, 2006. doi:10.1103/PhysRevE.73.016205.
- [10] Thilo Gross, Wolfgang Ebenhöf, and Ulrike Feudel. Enrichment and foodchain stability: The impact of different forms of predator-prey interaction. *Journal of Theoretical Biology*, 227(3):349–358, 2004. doi:10.1016/j.jtbi.2003.09.020.

- [11] Thilo Gross, Wolfgang Ebenhöf, and Ulrike Feudel. Long food chains are in general chaotic. *Oikos*, 109(1):135–144, 2005. doi:10.1111/j.0030-1299.2005.13573.x.
- [12] Martin Baurmann, Thilo Gross, and Ulrike Feudel. Instabilities in spatially extended predator-prey systems: Spatio-temporal patterns in the neighborhood of Turing-Hopf bifurcations. *Journal of Theoretical Biology*, 245(2):220–229, 2007. doi:10.1016/j.jtbi.2006.09.036.
- [13] Georg A. K. van Voorn, Dirk Stiefs, Thilo Gross, Bob W. Kooi, Ulrike Feudel, and S. A. L. M. Kooijman. Stabilization due to predator interference: Comparison of different analysis approaches. *Mathematical Biosciences and Engineering*, 5(3):567–583, 2008. doi:10.3934/mbe.2008.5.567.
- [14] Dirk Stiefs, Ezio Venturino, and Ulrike Feudel. Evidence of chaos in eco-epidemic models. *Mathematical Biosciences and Engineering*, 6(4):855–871, 2009. doi:10.3934/mbe.2009.6.855.
- [15] Thilo Gross, Lars Rudolf, Simon A. Levin, and Ulf Dieckmann. Generalized models reveal stabilizing factors in food webs. *Science*, 325(5941):747–750, 2009. doi:10.1126/science.1173536.
- [16] Thilo Gross and Ulrike Feudel. Local dynamical equivalence of certain food webs. *Ocean Dynamics*, 59(2):417–427, 2009. doi:10.1007/s10236-008-0165-2.
- [17] Dirk Stiefs, George A. K. van Voorn, Bob W. Kooi, Ulrike Feudel, and Thilo Gross. Food quality in producer-grazer models: A generalized analysis. *The American Naturalist*, 176(3):367–380, 2010. doi:10.1086/655429.
- [18] Justin Yeakel, Dirk Stiefs, Mark Novak, and Thilo Gross. Generalized modeling of ecological population dynamics. *Theoretical Ecology*, 4(2):1–16, 2011. doi:10.1007/s12080-011-0112-6.
- [19] Martin Zumsande and Thilo Gross. Bifurcations and chaos in the MAPK signaling cascade. *Journal of Theoretical Biology*, 265(3):481–491, 2010. doi:10.1016/j.jtbi.2010.04.025.
- [20] Martin Zumsande, Dirk Stiefs, Stefan Siegmund, and Thilo Gross. General analysis of mathematical models for bone remodeling. *Bone*, 48(4):910–917, 2011. doi:10.1016/j.bone.2010.12.010.
- [21] Ralf Steuer, Adriano Nunes Nesi, Alisdair R. Fernie, Thilo Gross, Bernd Blasius, and Joachim Selbig. From structure to dynamics of metabolic pathways: application to the plant mitochondrial tca cycle. *Bioinformatics*, 23(11):1378–1385, 2007. doi:10.1093/bioinformatics/btm065.

- [22] Ed Reznik and Daniel Segrè. On the stability of metabolic cycles. *Journal of Theoretical Biology*, 266(4):536–549, 2010. doi:10.1016/j.jtbi.2010.07.023.
- [23] Eva Gehrmann and Barbara Drossel. Boolean versus continuous dynamics on simple two-gene modules. *Physical Review E*, 82(4):046120, 2010. doi:10.1103/PhysRevE.82.046120.
- [24] Hiromi Hirata, Yasumasa Bessho, Hiroshi Kokubu, Yoshito Masamizu, Shuichi Yamada, Julian Lewis, and Ryoichiro Kageyama. Instability of Hes7 protein is crucial for the somite segmentation clock. *Nature Genetics*, 36(7):750–754, 2004. doi:10.1038/ng1372.
- [25] Vito Volterra. *Leçons sur la théorie Mathématique de la lutte pour la vie*. Éditions Jaques Gabay, Paris, 1990.
- [26] Jim M. Cushing and Mohamed Saleem. A predator prey model with age structure. *Journal of Mathematical Biology*, 14(2):231–250, 1982. doi:10.1007/BF01832847.
- [27] Len Nunney. The effect of long time delays in predator-prey systems. *Theoretical Population Biology*, 27(2):202–221, 1985. doi:10.1016/0040-5809(85)90010-3.
- [28] Julian Eggert and J. Leo van Hemmen. Modeling neuronal assemblies: Theory and implementation. *Neural Computation*, 13(9):1923–1974, 2001. doi:10.1162/089976601750399254.
- [29] Hidde De Jong. Modeling and simulation of genetic regulatory systems: A literature review. *Journal of Computational Biology*, 9(1):67–103, 2002. doi:10.1089/10665270252833208.
- [30] Dodla V. Ramana Reddy, Abhijit Sen, and George L. Johnston. Time delay induced death in coupled limit cycle oscillators. *Physical Review Letters*, 80(23):5109–5112, 1998. doi:10.1103/PhysRevLett.80.5109.
- [31] Johannes M. Höfener, Gautam C. Sethia, and Thilo Gross. Stability of networks of delay-coupled delay oscillators. *EPL*, 95(4):40002, 2011. doi:10.1209/0295-5075/95/40002.
- [32] Yuri A. Kuznetsov. *Elements of applied bifurcation theory*. Springer, New York, 1995.
- [33] Mark E. J. Newman. The structure and function of complex networks. *SIAM Review*, 45(2):167–256, 2003. doi:10.1137/S003614450342480.
- [34] Béla Bollobás. *Modern Graph Theory*. Springer, New York, 1998.

- [35] Morris H. Hirsch and Stephen Smale. *Differential equations, dynamical systems, and linear algebra*. Academic Press, London, 1974.
- [36] Norman MacDonald. *Biological delay systems*. Cambridge University Press, 1989.
- [37] John Guckenheimer and Philip Holmes. *Nonlinear Oscillations, Dynamical Systems, and Bifurcations of Vector Fields*. Springer, New York, 1983.
- [38] J. Doyne Farmer. Chaotic attractors of an infinite-dimensional dynamical system. *Physica D*, 4(3):366–393, 1982. doi:10.1016/0167-2789(82)90042-2.
- [39] Michael C. Mackey and Leon Glass. Oscillation and chaos in physiological control systems. *Science*, 197(4300):287–289, 1977. doi:10.1126/science.267326.
- [40] Kensuke Ikeda and Kenji Matsumoto. High-dimensional chaotic behavior in systems with time-delayed feedback. *Physica D*, 29(1-2):223–235, 1987. doi:10.1016/0167-2789(87)90058-3.
- [41] Jérôme Losson, Michael C. Mackey, and André Longtin. Solution multistability in first-order nonlinear differential delay equations. *Chaos*, 3(2):167–176, 1993. doi:10.1063/1.165982.
- [42] Giovanni Giacomelli and Antonio Politi. Relationship between delayed and spatially extended dynamical systems. *Physical Review Letters*, 76(15):2686–2689, 1996. doi:10.1103/PhysRevLett.76.2686.
- [43] Michael Schanz and Axel Pelster. Analytical and numerical investigations of the phase-locked loop with time delay. *Physical Review E*, 67(5):056205, 2003. doi:10.1103/PhysRevE.67.056205.
- [44] Matthias Wolfrum and Serhiy Yanchuk. Eckhaus instability in systems with large delay. *Physical Review Letters*, 96(22):220201, 2006. doi:10.1103/PhysRevLett.96.220201.
- [45] Boualem Mensour and André Longtin. Power spectra and dynamical invariants for delay-differential and difference equations. *Physica D*, 113(1):1–25, 1998. doi:10.1016/S0167-2789(97)00185-1.
- [46] Fatihcan M. Atay, editor. *Complex Time-Delay Systems Theory and Applications*. Springer, Berlin, 2010. doi:10.1007/978-3-642-02329-3.
- [47] Robert M. Corless, Gaston H. Gonnet, Dave E. G. Hare, David J. Jeffrey, and Donald E. Knuth. On the Lambert W function. *Advances in Computational Mathematics*, 5(1):329–359, 1996. doi:10.1007/BF02124750.

- [48] Farshid M. Asl and A. Galip Ulsoy. Analytical solution of a system of homogeneous delay differential equations via the Lambert function. In *Proceedings of the 2000 American Control Conference*, volume 4, pages 2496–2500, 2000. doi:10.1109/ACC.2000.878632.
- [49] Jürgen Jost and Maliackal Poulo Joy. Spectral properties and synchronization in coupled map lattices. *Physical Review E*, 65(1):016201, 2001. doi:10.1103/PhysRevE.65.016201.
- [50] Fatihcan M. Atay. Oscillator death in coupled functional differential equations near Hopf bifurcation. *Journal of Differential Equations*, 221(1):190–209, 2006. doi:10.1016/j.jde.2005.01.007.
- [51] Paul Erdős and Alfréd Rényi. On random graphs, i. *Publicationes Mathematicae (Debrecen)*, 6:290–297, 1959.
- [52] Réka Albert and Albert-László Barabási. Statistical mechanics of complex networks. *Reviews of Modern Physics*, 74(1):47–97, 2002. doi:10.1103/RevModPhys.74.47.
- [53] Albert-László Barabási and Réka Albert. Emergence of scaling in random networks. *Science*, 286(5439):509–512, 1999. doi:10.1126/science.286.5439.509.
- [54] Arkady Pikovsky, Michael Rosenblum, and Jürgen Kurths. *Synchronization: A Universal Concept in Nonlinear Sciences*. Cambridge University Press, 2005. doi:10.2277/0511074417.
- [55] Alex Arenas, Albert Díaz-Guilera, Jürgen Kurths, Yamir Moreno, and Changsong Zhou. Synchronization in complex networks. *Physics Reports*, 469(3):93–153, 2008. doi:10.1016/j.physrep.2008.09.002.
- [56] Pascal Fries. A mechanism for cognitive dynamics: neuronal communication through neuronal coherence. *Trends in Cognitive Sciences*, 9(10):474–480, 2005. doi:10.1016/j.tics.2005.08.011.
- [57] Kazuki Horikawa, Kana Ishimatsu, Eiichi Yoshimoto, Shigeru Kondo, and Hiroyuki Takeda. Noise-resistant and synchronized oscillation of the segmentation clock. *Nature*, 441(7094):719–723, 2006. doi:10.1038/nature04861.
- [58] Shun Yamaguchi, Hiromi Isejima, Takuya Matsuo, Ryusuke Okura, Kazuhiro Yagita, Masaki Kobayashi, and Hitoshi Okamura. Synchronization of cellular clocks in the suprachiasmatic nucleus. *Science*, 302(5649):1408–1412, 2003. doi:10.1126/science.1089287.

- [59] David J. D. Earn, Simon A. Levin, and Pejman Rohani. Coherence and conservation. *Science*, 290(5495):1360–1364, 2000. doi:10.1126/science.290.5495.1360.
- [60] Fatihcan M. Atay. Total and partial amplitude death in networks of diffusively coupled oscillators. *Physica D*, 183(1-2):1–18, 2003. doi:10.1016/S0167-2789(03)00154-4.
- [61] Kedma Bar-Eli. On the stability of coupled chemical oscillators. *Physica D*, 14(2):242–252, 1985. doi:10.1016/0167-2789(85)90182-4.
- [62] Dodla V. Ramana Reddy, Abhijit Sen, and George L. Johnston. Experimental evidence of time-delay-induced death in coupled limit-cycle oscillators. *Physical Review Letters*, 85(16):3381–3384, 2000. doi:10.1103/PhysRevLett.85.3381.
- [63] Ramon Herrero, M. Figueras, J. Rius, F. Pi, and G. Orriols. Experimental observation of the amplitude death effect in two coupled nonlinear oscillators. *Physical Review Letters*, 84(23):5312–5315, 2000. doi:10.1103/PhysRevLett.84.5312.
- [64] Awadhesh Prasad, Ying-Cheng Lai, Athanasios Gavrielides, and Vassilios Kovanis. Amplitude modulation in a pair of time-delay coupled external-cavity semiconductor lasers. *Physics Letters A*, 318(1-2):71–77, 2003. doi:10.1016/j.physleta.2003.08.072.
- [65] Atsuko Takamatsu, Teruo Fujii, and Isao Endo. Time delay effect in a living coupled oscillator system with the plasmodium of *Physarum polycephalum*. *Physical Review Letters*, 85(9):2026–2029, 2000. doi:10.1103/PhysRevLett.85.2026.
- [66] Keiji Konishi, Katsuhisa Senda, and Hideki Kokame. Amplitude death in time-delay nonlinear oscillators coupled by diffusive connections. *Physical Review E*, 78(5):056216, 2008. doi:10.1103/PhysRevE.78.056216.
- [67] Steven H. Strogatz. Nonlinear dynamics: Death by delay. *Nature*, 394(6691):316–317, 1998. doi:10.1038/28488.
- [68] Yoko Yamaguchi and Hiroshi Shimizu. Theory of self-synchronization in the presence of native frequency distribution and external noises. *Physica D*, 11(1-2):212–226, 1984. doi:10.1016/0167-2789(84)90444-5.
- [69] Mastoshi Shiino and Marek Frankowicz. Synchronization of infinitely many coupled limit-cycle type oscillators. *Physics Letters A*, 136(3):103–108, 1989. doi:10.1016/0375-9601(89)90187-4.

- [70] Donald G. Aronson, G. Bard Ermentrout, and Nancy Kopell. Amplitude response of coupled oscillators. *Physica D*, 41(3):403–449, 1990. doi:10.1016/0167-2789(90)90007-C.
- [71] G. Bard Ermentrout. Oscillator death in populations of “all to all” coupled nonlinear oscillators. *Physica D*, 41(2):219–231, 1990. doi:10.1016/0167-2789(90)90124-8.
- [72] Renato E. Mirollo and Steven H. Strogatz. Amplitude death in an array of limit-cycle oscillators. *Journal of Statistical Physics*, 60(1):245–262, 1990. doi:10.1007/BF01013676.
- [73] Robert M. May. Simple mathematical models with very complicated dynamics. *Nature*, 261(5560):459–467, 1976. doi:10.1038/261459a0.
- [74] Fatihcan M. Atay, Jürgen Jost, and Andreas Wende. Delays, connection topology, and synchronization of coupled chaotic maps. *Physical Review Letters*, 92(14):144101, 2004. doi:10.1103/PhysRevLett.92.144101.
- [75] Fatihcan M. Atay and Ozkan Karabacak. Stability of coupled map networks with delays. *SIAM Journal on Applied Dynamical Systems*, 5:508–527, 2006. doi:10.1137/060652531.
- [76] Cristina Masoller and Arturo C. Martí. Random delays and the synchronization of chaotic maps. *Physical Review Letters*, 94(13):134102, 2005. doi:10.1103/PhysRevLett.94.134102.
- [77] Arturo C. Martí, Marcelo Ponce, and Cristina Masoller. Steady-state stabilization due to random delays in maps with self-feedback loops and in globally delayed-coupled maps. *Physical Review E*, 72(6):066217, 2005. doi:10.1103/PhysRevE.72.066217.
- [78] Xiaofeng Gong, Shuguang Guan, Xingang Wang, and Choy-Heng Lai. Stability of the steady state of delay-coupled chaotic maps on complex networks. *Physical Review E*, 77(5):056212, 2008. doi:10.1103/PhysRevE.77.056212.
- [79] Marcelo Ponce, Cristina Masoller, and Arturo C. Martí. Synchronizability of chaotic logistic maps in delayed complex networks. *The European Physical Journal B*, 67(1):83–93, 2009. doi:10.1140/epjb/e2008-00467-3.
- [80] Heinz Georg Schuster and Peter Wagner. Mutual entrainment of 2 limit-cycle oscillators with time delayed coupling. *Progress of Theoretical Physics*, 81(5):939–945, 1989.
- [81] Seunghwan Kim, Seon Hee Park, and C. S. Ryu. Multistability in coupled oscillator systems with time delay. *Physical Review Letters*, 79(15):2911–2914, 1997.

- [82] M. K. Stephen Yeung and Steven H. Strogatz. Time delay in the Kuramoto model of coupled oscillators. *Physical Review Letters*, 82(3):648–651, 1999. doi:10.1103/PhysRevLett.82.648.
- [83] Wai Shing Lee, Edward Ott, and Thomas M. Antonsen. Large coupled oscillator systems with heterogeneous interaction delays. *Physical Review Letters*, 103(4):044101, 2009. doi:10.1103/PhysRevLett.103.044101.
- [84] Otti D’Huys, Raul Vicente, Thomas Erneux, Jan Danckaert, and Ingo Fischer. Synchronization properties of network motifs: Influence of coupling delay and symmetry. *Chaos*, 18(3):037116, 2008. doi:10.1063/1.2953582.
- [85] Matthew G. Earl and Steven H. Strogatz. Synchronization in oscillator networks with delayed coupling: A stability criterion. *Physical Review E*, 67(3):036204, 2003. doi:10.1103/PhysRevE.67.036204.
- [86] Ernst Niebur, Heinz Georg Schuster, and Daniel M. Kammen. Collective frequencies and metastability in networks of limit-cycle oscillators with time-delay. *Physical Review Letters*, 67(20):2753–2756, 1991.
- [87] Gautam C. Sethia, Abhijit Sen, and Fatihcan M. Atay. Clustered chimera states in delay-coupled oscillator systems. *Physical Review Letters*, 100(14):144102, 2008. doi:10.1103/PhysRevLett.100.144102.
- [88] Damián H. Zanette. Propagating structures in globally coupled systems with time delays. *Physical Review E*, 62(3):3167–3172, 2000. doi:10.1103/PhysRevE.62.3167.
- [89] Gautam C. Sethia, Abhijit Sen, and Fatihcan M. Atay. Synchronous solutions and their stability in nonlocally coupled phase oscillators with propagation delays. *Physical Review E*, 81(5):056213, 2010. doi:10.1103/PhysRevE.81.056213.
- [90] Edward Ott and Thomas M. Antonsen. Low dimensional behavior of large systems of globally coupled oscillators. *Chaos*, 18(3):037113, 2008. doi:10.1063/1.2930766.
- [91] Dodla V. Ramana Reddy, Abhijit Sen, and George L. Johnston. Time delay effects on coupled limit cycle oscillators at Hopf bifurcation. *Physica D*, 129(1-2):15–34, 1999. doi:10.1016/S0167-2789(99)00004-4.
- [92] Fatihcan M. Atay. Distributed delays facilitate amplitude death of coupled oscillators. *Physical Review Letters*, 91(9):094101, 2003. doi:10.1103/PhysRevLett.91.094101.

- [93] Dodla V. Ramana Reddy, Abhijit Sen, and George L. Johnston. Phase-locked patterns and amplitude death in a ring of delay-coupled limit cycle oscillators. *Physical Review E*, 69(5):056217, 2004. doi:10.1103/PhysRevE.69.056217.
- [94] Wei Zou, Chenggui Yao, and Meng Zhan. Eliminating delay-induced oscillation death by gradient coupling. *Physical Review E*, 82(5):056203, 2010. doi:10.1103/PhysRevE.82.056203.
- [95] Junzhong Yang. Transitions to amplitude death in a regular array of nonlinear oscillators. *Physical Review E*, 76(1):016204, 2007. doi:10.1103/PhysRevE.76.016204.
- [96] Dodla V. Ramana Reddy, Abhijit Sen, and George L. Johnston. Dynamics of a limit cycle oscillator under time delayed linear and nonlinear feedbacks. *Physica D*, 144(3-4):335–357, 2000. doi:10.1016/S0167-2789(00)00086-5.
- [97] Otti D’Huys, Raul Vicente, Jan Danckaert, and Ingo Fischer. Amplitude and phase effects on the synchronization of delay-coupled oscillators. *Chaos*, 20(4):043127, 2010. doi:10.1063/1.3518363.
- [98] Louis M. Pecora and Thomas L. Carroll. Master stability functions for synchronized coupled systems. *Physical Review Letters*, 80(10):2109–2112, 1998. doi:10.1103/PhysRevLett.80.2109.
- [99] Awadhesh Prasad. Amplitude death in coupled chaotic oscillators. *Physical Review E*, 72(5):056204, 2005. doi:10.1103/PhysRevE.72.056204.
- [100] Keiji Konishi. Amplitude death in oscillators coupled by a one-way ring time-delay connection. *Physical Review E*, 70(6):066201, 2004. doi:10.1103/PhysRevE.70.066201.
- [101] Keiji Konishi. Limitation of time-delay induced amplitude death. *Physics Letters A*, 341(5-6):401–409, 2005. doi:10.1016/j.physleta.2005.04.094.
- [102] Hiroyuki Nakajima. On analytical properties of delayed feedback control of chaos. *Physics Letters A*, 232(3-4):207–210, 1997. doi:10.1016/S0375-9601(97)00362-9.
- [103] Toshiki Oguchi, Henk Nijmeijer, and Takashi Yamamoto. Synchronization in networks of chaotic systems with time-delay coupling. *Chaos*, 18(3):037108, 2008. doi:10.1063/1.2952450.
- [104] Wim Michiels and Henk Nijmeijer. Synchronization of delay-coupled nonlinear oscillators: An approach based on the stability analysis of synchronized equilibria. *Chaos*, 19(3):033110, 2009. doi:10.1063/1.3187792.

- [105] Wolfgang Kinzel, Anja Englert, Georg Reents, Meital Zigzag, and Ido Kanter. Synchronization of networks of chaotic units with time-delayed couplings. *Physical Review E*, 79(5):056207, 2009. doi:10.1103/PhysRevE.79.056207.
- [106] Kestutis Pyragas. Continuous control of chaos by self-controlling feedback. *Physics Letters A*, 170(6):421–428, 1992. doi:10.1016/0375-9601(92)90745-8.
- [107] Wolfram Just, Thomas Bernard, Matthias Ostheimer, Ekkehard Reibold, and Hartmut Benner. Mechanism of time-delayed feedback control. *Physical Review Letters*, 78(2):203–206, 1997. doi:10.1103/PhysRevLett.78.203.
- [108] Wolfram Just, Ekkehard Reibold, Hartmut Benner, Krzysztof Kacperski, Piotr Fronczak, and Janusz Holyst. Limits of time-delayed feedback control. *Physics Letters A*, 254(3-4):158–164, 1999. doi:10.1016/S0375-9601(99)00113-9.
- [109] Kestutis Pyragas. Delayed feedback control of chaos. *Philosophical Transactions of the Royal Society A*, 364(1846):2309–2334, 2006. doi:10.1098/rsta.2006.1827.
- [110] Robert Dykstra, Ding Y. Tang, and Norman R. Heckenberg. Experimental control of single-mode laser chaos by using continuous, time-delayed feedback. *Physical Review E*, 57(6):6596–6598, 1998. doi:10.1103/PhysRevE.57.6596.
- [111] Greg Kociuba and Norman R. Heckenberg. Controlling chaos in a Lorenz-like system using feedback. *Physical Review E*, 68(6):066212, 2003. doi:10.1103/PhysRevE.68.066212.
- [112] Jung-Wan Ryu, Won-Ho Kye, Soo-Young Lee, Myung-Woon Kim, Muhan Choi, Sunghwan Rim, Young-Jai Park, and Chil-Min Kim. Effects of time-delayed feedback on chaotic oscillators. *Physical Review E*, 70(3):036220, 2004. doi:10.1103/PhysRevE.70.036220.
- [113] Kestutis Pyragas. Synchronization of coupled time-delay systems: Analytical estimations. *Physical Review E*, 58(3):3067–3071, 1998. doi:10.1103/PhysRevE.58.3067.
- [114] Shangbo Zhou, Hua Li, and Zhongfu Wu. Synchronization threshold of a coupled time-delay system. *Physical Review E*, 75(3):037203, 2007. doi:10.1103/PhysRevE.75.037203.
- [115] Maoyin Chen and Jürgen Kurths. Synchronization of time-delayed systems. *Physical Review E*, 76(3):036212, 2007. doi:10.1103/PhysRevE.76.036212.
- [116] Henning U. Voss. Anticipating chaotic synchronization. *Physical Review E*, 61(5):5115–5119, 2000. doi:10.1103/PhysRevE.61.5115.

- [117] Chuandong Li, Xiaofeng Liao, and Kwok-wo Wong. Chaotic lag synchronization of coupled time-delayed systems and its applications in secure communication. *Physica D*, 194(3-4):187–202, 2004. doi:10.1016/j.physd.2004.02.005.
- [118] Meng Zhan, Xingang Wang, Xiaofeng Gong, G. W. Wei, and C.-H. Lai. Complete synchronization and generalized synchronization of one-way coupled time-delay systems. *Physical Review E*, 68(3):036208, 2003. doi:10.1103/PhysRevE.68.036208.
- [119] Elman M. Shahverdiev and K. Alan Shore. Generalized synchronization in time-delayed systems. *Physical Review E*, 71(1):016201, 2005. doi:10.1103/PhysRevE.71.016201.
- [120] Alexander Ahlborn and Ulrich Parlitz. Stabilizing unstable steady states using multiple delay feedback control. *Physical Review Letters*, 93(26):264101, 2004. doi:10.1103/PhysRevLett.93.264101.
- [121] Alexander Ahlborn and Ulrich Parlitz. Controlling dynamical systems using multiple delay feedback control. *Physical Review E*, 72(1):016206, 2005. doi:10.1103/PhysRevE.72.016206.
- [122] Keiji Konishi, Hideki Kokame, and Naoyuki Hara. Stabilization of a steady state in network oscillators by using diffusive connections with two long time delays. *Physical Review E*, 81(1):016201, 2010. doi:10.1103/PhysRevE.81.016201.
- [123] David A. Fell. Metabolic control analysis - A survey of its theoretical and experimental development. *Biochemical Journal*, 286(2):313–330, 1992. Available from: <http://www.biochemj.org/bj/286/bj2860313.htm>.
- [124] Jack K. Hale, Ettore F. Infante, and Fu-Shiang Peter Tsen. Stability in linear delay equations. *Journal of Mathematical Analysis and Applications*, 105(2):533–555, 1985. doi:10.1016/0022-247X(85)90068-X.
- [125] Leon Glass and Michael C. Mackey. *From clocks to chaos. The rhythms of life*. Princeton University Press, Princeton, 1988. doi:10.1063/1.2811091.
- [126] Richard S. Varga. *Geršgorin and his circles*. Springer, Berlin, 2004.
- [127] Serhiy Yanchuk and Przemyslaw Perlikowski. Delay and periodicity. *Physical Review E*, 79(4):046221, 2009. doi:10.1103/PhysRevE.79.046221.
- [128] Valentin Flunkert and Eckehard Schoell. Pydelay - a python tool for solving delay differential equations. 2009. arXiv:0911.1633v1.
- [129] Koen Engelborghs, Tatyana Luzyanina, and Dirk Roose. Numerical bifurcation analysis of delay differential equations. *Journal of Computational and Applied Mathematics*, 125(1-2):265–275, 2000. doi:10.1016/S0377-0427(00)00472-6.

-
- [130] Koen Engelborghs and Dirk Roose. On stability of LMS methods and characteristic roots of delay differential equations. *SIAM Journal on Numerical Analysis*, 40(2):629–650, 2002. doi:10.1137/S003614290037472X.
- [131] Tatyana Luzyanina and Dirk Roose. Numerical stability analysis and computation of Hopf bifurcation points for delay differential equations. *Journal of Computational and Applied Mathematics*, 72(2):379–392, 1996. doi:10.1016/0377-0427(96)00008-8.
- [132] Koen Verheyden, Tatyana Luzyanina, and Dirk Roose. Efficient computation of characteristic roots of delay differential equations using LMS methods. *Journal of Computational and Applied Mathematics*, 214(1):209–226, 2008. doi:10.1016/j.cam.2007.02.025.
- [133] Fan R. K. Chung. *Spectral Graph Theory*. CBMS Regional Conference Series in Mathematics Vol 92, Conference Board of the Mathematical Sciences, Washington, DC, 1997.
- [134] Illés J. Farkas, Imre Derényi, Albert-László Barabási, and Tamás Vicsek. Spectra of “real-world” graphs: Beyond the semicircle law. *Physical Review E*, 64(2):026704, 2001. doi:10.1103/PhysRevE.64.026704.
- [135] Sergey N. Dorogovtsev, Alexander V. Goltsev, José F. F. Mendes, and Alexander N. Samukhin. Spectra of complex networks. *Physical Review E*, 68(4):046109, 2003. doi:10.1103/PhysRevE.68.046109.
- [136] Christel Kamp and Kim Christensen. Spectral analysis of protein-protein interactions in drosophila melanogaster. *Physical Review E*, 71(4):041911, 2005. doi:10.1103/PhysRevE.71.041911.
- [137] Ben D. MacArthur and Rubén J. Sánchez-García. Spectral characteristics of network redundancy. *Physical Review E*, 80(2):026117, 2009. doi:10.1103/PhysRevE.80.026117.

Acknowledgements

I would like to thank everyone who supported me during the last years. First and foremost, I thank my adviser Thilo Gross for guiding my research. In particular, I have to thank him for the effort he put into teaching me scientific writing. I also would like to thank Prof. Frank Jülicher for supervising and reviewing this thesis.

Further, I thank my collaborator Gautam Sethia for the comments, remarks and discussions, which significantly improved this thesis.

I want to thank all members of the group “Dynamics of biological networks”. In particular, I want to thank Ly Do, Martin Zumsande, and Gerd Zschaler for answering all these pesky little questions about Maths, Latex, and filling formulas.

Finally, I like to thank my family and friends. In particular, I would like to thank my great-aunt for the financial support.

Versicherung

Hiermit versichere ich, dass ich die vorliegende Arbeit ohne unzulässige Hilfe Dritter und ohne Benutzung anderer als der angegebenen Hilfsmittel angefertigt habe; die aus fremden Quellen direkt oder indirekt übernommenen Gedanken sind als solche kenntlich gemacht. Die Arbeit wurde bisher weder im Inland noch im Ausland in gleicher oder ähnlicher Form einer anderen Prüfungsbehörde vorgelegt.

Die vorliegende Arbeit wurde unter der Aufsicht von Prof. Dr. Frank Jülicher am Max-Planck-Institut für Physik komplexer Systeme (Abteilung: Biologische Physik, Untergruppe: Dynamics of Biological Networks) angefertigt und von Dr. Thilo Gross betreut.

Dresden, den